Aus dem Institut für Physiologie
Universität zu Lübeck, Lübeck, Deutschland
Direktorin: Univ. Prof. Dr. rer. nat. Kristina Kusche-Vihrog
&
Department of Pharmacology and Cellular and Molecular Physiology
Yale University School of Medicine, New Haven, USA
Principle Investigator: Prof. Barbara E. Ehrlich, PhD

Neuronal Calcium Sensor 1 in Chemotherapy Induced Peripheral Neuropathy and Characterization of a Second Variant

Inauguraldissertation
zur
Erlangung der Doktorwürde der Universität zu Lübeck
-Aus der Sektion Medizin-

vorgelegt von
Göran Ramin Boeckel
aus
Westerland auf Sylt

Lübeck 2020

Alle Experimente wurden an der Yale University School of Medicine (USA) im Department of Pharmacology and Cellular and Molecular Physiology unter der Supervision von Prof. Barbara E. Ehrlich durchgeführt. Alle tierexperimentellen Versuche erfolgten in Übereinstimmung mit den Grundsätzen und Rahmenrichtlinien des Yale University's Institutional Animal Care and Use Committee (IACUC). **Animal Welfare Assurance Number: a3230-01. Yale's Assurance Number: D16-00416**

1. Berichterstatterin/Berichterstatter: Prof. Dr. med. C. de Wit

2. Berichterstatterin/Berichterstatter: Prof. Dr. rer. nat. Hendrik Ungeforeren

Tag der mündlichen Prüfung: 10.11.2020

Zum Druck genehmigt. Lübeck, den 10.11.2020

-Promotionskommission der Sektion Medizin-

三人行必有我師

—lit. if three walk together, one can be my teacher

-Confucian analects-

Table of Contents

List of abbreviations

A	adenine, deoxyadenosine
Asp	aspartate, amino acid
ATP	adenosine triphosphate
BAPTA	1,2-bis(o-aminophenoxy)ethane-N,N,N′,N′-tetraacetic acid
BCA	bicinchoninic acid
bp	base pair
c	centi-
C	cytosine, deoxycytidine
$[Ca^{2+}]$	calcium concentration
Ca^{2+}	calcium ion
Ch.	chapter
CIPN	chemotherapy induced peripheral neuropathy
dNTP	deoxyribonucleotid-triphsophate
ddNTP	dideoxyribonukleosid-triphosphate
Da	Dalton (1g / (6,022*10^23))
DMEM	Dulbecco's modified eagle's medium
DNA	deoxyribonucleic acid
DRG	dorsal root ganglion
dsDNA	double stranded DNA
EDTA	ethylenediaminetetraacetic acid
EGTA	ethylene glycol-bis(β-aminoethyl ether)-N,N,N′,N′-tetraacetic acid
e.g.	exempli gratia
ER	endoplasmic reticulum
etc	et cetera
FBS	fetal bovine serum
Fig.	figure
Frq	frequenin, Drosophila homolog of Neuronal calcium sensor-1
frq	gene name of frequenin; alias of NCS1
g	gram
G	guanine, deoxyguanosine
Glu	glutamate, amino acid
h	hour(s)
i.e.	id est
$InsP_3$	Inositol 1,4,5-trisphosphate
$InsP_3R$	inositol 1,4,5-trisphosphate receptor
ITC	isothermal titration calorimetry
HET	heterozygous, NCS-$1^{(+/-)}$
k	kilo
kb	kilobase

kg	kilogram
KO	knockout, NCS-1$^{(-/-)}$
L	liter
Mg^{2+}	magnesium ion
m	meter
m	milli-
M	molar (mol/L)
µ	micro-
min	minute(s)
mol	mol, amount of substance
n	nano-
NCS	Neuronal Calcium Sensor, protein family
NCS1	Neuronal Calcium Sensor 1, gene, mRNA
NCS-1	Neuronal Calcium Sensor 1, protein
p.	page
PTX	Paclitaxel
PDB	protein databank
PCR	polymerase chain reaction
RNA	ribonucleic acid
rpm	revolutions per minute
RyR	ryanodine receptor
s	second(s)
S.	Seite
SD	standard deviation
shRNA	short hairpin RNA
SNAP	sensory neuron action potential
Tab.	table
T_m	melting temperature
T	thymidine; deoxythymidine
TBST	Tris-buffered saline with Tween20
TDML	tail distal motor latency
TMA	tail motor amplitude
TRPV4	transient receptor potential vanilloid 4
TSNCV	tail sensory nerve conduction velocity
Var	variant
V	volt
WT	wild type, NCS-1$^{(+/+)}$
Zn^{2+}	zinc ion

1. Introduction and Theoretical Background

"In the furnaces of the stars the elements evolved from hydrogen. When oxygen and neon captured successive α particles, the element calcium was born. Roughly 10 billion years later, cell membranes began to parse the world by charge, temporarily and locally defying relentless entropy. To adapt to changing environments, cells must signal, and signaling requires messengers whose concentration varies with time. Filling this role, calcium ions (Ca^{2+}) and phosphate ions have come to rule cell signaling."— David E. Clapham in [41]

1.1 Calcium Signaling

1.1.1 Calcium homeostasis & intracellular calcium stores

Calcium (Ca^{2+}) is a divalent cation. Although approximately 99% of the human body's Ca^{2+} resides within the bones, the remaining Ca^{2+} serves essential, indispensable purposes in both extracellular and intracellular spaces. Ca^{2+}-controlled events regulate the entire life cycle of eukaryotic cells and include (among others) fertilization [64], muscle cell contraction [65], protein transcription [53], cell proliferation [33], exocytosis of neurotransmitters [140], as well as aging [104] and apoptosis [184].

At the most simple level the action of Ca^{2+} is determined merely through its presence or absence. The calcium concentration ($[Ca^{2+}]$) is therefore kept in narrow ranges of approximately 2,5 mM ± 20% for extracellular [28, 180] and around 50-100 nM for intracellular, cytosolic Ca^{2+} [73, 188], accounting for a 20000-fold difference across the plasma membrane.

An elevation of intracellular $[Ca^{2+}]$ up into the μM-range is enabled through Ca^{2+} release from internal stores such as the endoplasmic reticulum (ER) [31] or mitochondria [27] and/or from extracellular space through ion channels within the plasma membrane via influx proteins, Fig. 1, p.2 [73]. The resting $[Ca^{2+}]$ is maintained through primary and secondary active transport into those internal stores or out of the cell through proteins [73].

Depending on the cell type, specific expression of influx and efflux proteins and different patterns of signal transduction are utilized to generate different amplitudes, speed and spatio-temporal organization. This allows distinct functions to be generated, an issue of particular importance to neurons where subcompartments are known to generate unique responses [17]. Several hypotheses regarding Ca^{2+}'s dominant position (especially in comparison to other divalent cations, like Mg^{2+}) in biological systems have been proposed, and are nicely summarized in [34].

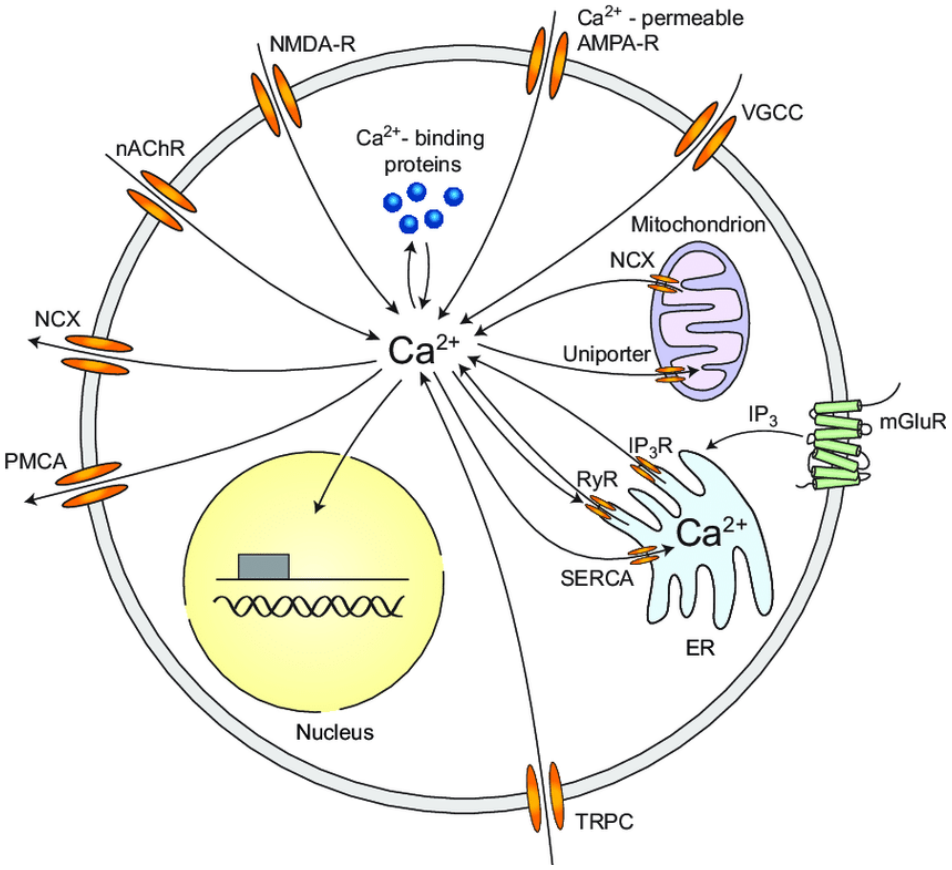

Fig. 1 **Intracellular Ca^{2+} stores and signaling enabling proteins** (adapted from [73]). ***Ca^{2+} influx.*** **AMPA-R** — α-amino-3-hydroxy-5-methyl-4-isoxazolepropionic acid-receptor (glutamate-type); **NMDA-R** — N-methyl-D-aspartate-receptor (glutamate-type); **VGCC** — voltage-gated calcium channel; **nAChR** — nicotinic acetylcholine receptors; **TRPC** — transient receptor potential channels; **IP_3R** — inositol trisphosphate receptor; **RyR** — ryanodine receptors; **mGluR** — metabotropic glutamate receptors (can generated inositol trisphosphate). ***Ca^{2+} efflux.*** **PMCA** — plasma membrane calcium ATPase; **NCX** — sodium-calcium exchanger; **SERCA** — sarco-/endoplasmic reticulum calcium ATPase

1.1.2 Calcium binding proteins

There is no consensus on the meaning of the term ‚calcium-binding protein'. In the most general sense any protein containing a specific domain to bind Ca^{2+} is a Ca^{2+}-binding protein [190]. As this definition leads to an enormous, heterogenous and unconventional group of proteins several subdivisions have been suggested; some based on the structural Ca^{2+}-binding domain (e.g. *EF-hand*, *C_2-Domain* etc. [125]) while others classify based on position relative to a membrane (*intracellular* vs *extracellular* Ca^{2+}-binding protein [169]).

A commonly used discrimination refers to the tasks performed by the proteins (other than binding Ca^{2+}), i.e. membrane-intrinsic proteins that control influx and efflux of Ca^{2+} and thus maintain and regulate the nM range of the cytosolic [Ca^{2+}] (the majority of proteins illustrated in Fig. 1, p.2) and a second group that does not

(*directly*) modify the total content of Ca^{2+} upon binding ('blue dots' in Fig. 1) [35, 73, 190]. This second group of proteins comprises a vast molecular repertoire of Ca^{2+} binding proteins that add complexity, variations and nuances to Ca^{2+} signals [17, 73]. Depending on their main function they can be further divided into Ca^{2+} buffers (1.1.2.2) and Ca^{2+} sensors (1.1.2.3), the latter of which interact with numerous target proteins and enable crosstalk with other signaling pathways [30, 77].

1.1.2.1 Ca^{2+}-binding

Both prokaryotic and eukaryotic cells have developed specialized structural motifs to bind Ca^{2+} [55]. The positively charged Ca^{2+} is often coordinated by six to seven oxygen atoms of carboxyl and/or carbonyl groups [169]. While some motifs like the *C_2-Domain* (found e.g. in protein kinase C (PKC) and synaptotagmin) are organized as so called β-sandwich consisting of β-sheets connected by loops [34], others like the *Annexin Ca^{2+}-binding Fold* are mostly organized as α-helices [71].

The most common and evolutionarily conserved Ca^{2+}-binding motif is the so called EF-hand, a helix-loop-helix motif [98]. It was first discovered in the crystalized structure of parvalbumin, a protein consisting of six α-helices (named A through F) [95]. Ca^{2+} was found to be coordinated within the 12 amino acid loop between the fifth (E) and sixth (F) α-helix, resembling a hand with a spread thumb and a pointing index finger (👆; Fig. 2, p.4) [95]. The affinity of an EF-hand to bind Ca^{2+} can change significantly depending on the amino acid residues within the binding center, as well as the side-chain packing [41]. In addition, the number of Ca^{2+}-binding motifs itself can vary among different proteins [190]. EF-hands are usually found in pairs with only few exceptions (which, however, dimerize) [102, 142]. Although EF-hands most commonly occur in (intracellular) Ca^{2+}-sensing proteins (Ch.1.1.2.3) they are not restrained to them, in that the motif has been found in the sequence of the ryanodine receptor, enabling Ca^{2+} to directly modulate a gate of its own release [189]. Regardless of the type of binding motif, several diseases have been proposed to be associated with the disruption of the ability to bind Ca^{2+} properly, including cardiovascular diseases [82], deafness [130] or subtypes of leukemia [76].

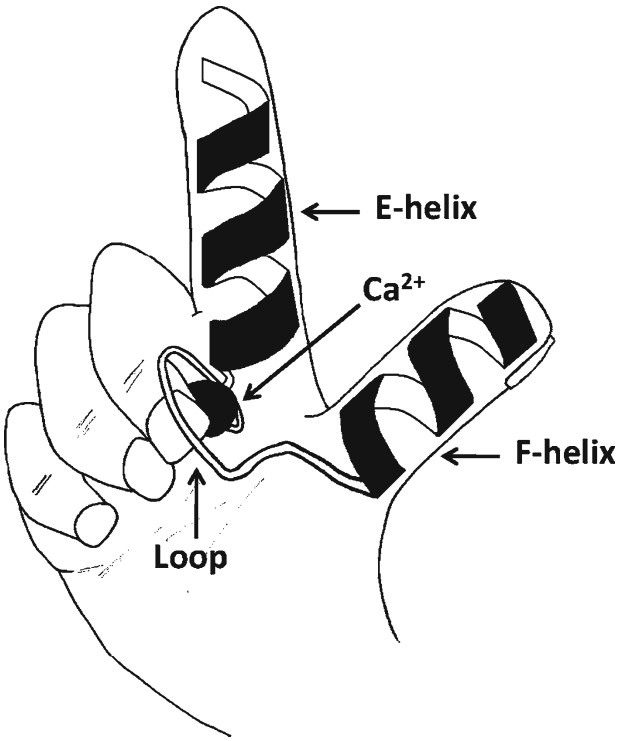

Fig. 2 **Model of the EF-hand motif** (adapted from [190]).
Ca^{2+} is bound within the loop of two α-helices, E & F.

1.1.2.2 Ca^{2+}-buffering

Exogenous (artificial) Ca^{2+}-buffers like EDTA, EGTA or BAPTA are indispensable for modern medicine and science, as they paved the way for coagulation analyses [45] and were the basis of the first generation of fluorescent Ca^{2+} indicators [73].

A specific subgroup of Ca^{2+}-binding proteins are thought to primarily bind *influxing* Ca^{2+} as endogenous Ca^{2+}-buffers. Examples of these primary Ca^{2+}-buffers are parvalbumin, calbindin and calretinin [73]. Loading and unloading of these proteins with Ca^{2+} influences not only the amplitude but also the duration of Ca^{2+}-signals [17]. Furthermore, differential expression of these proteins in certain cell types as well as within the cell helps to limit Ca^{2+}-signals to specific loci, which is the case in neurons, where localized Ca^{2+}-signals are particularly important for synapse formation and maintenance [138, 157].

Most of the ER's Ca^{2+} is bound to buffers [94]. Several Ca^{2+}-buffers within storage compartments like the ER have been identified, however, their role remains insufficiently understood [141]. A distinction between intraorganellar and cytosolic Ca^{2+}-buffers is considered to lie in their Ca^{2+}-binding characteristics; with high $[Ca^{2+}]$ in the ER (mM), its proteins show low affinity and high capacity, while the reverse is true for cytosolic Ca^{2+}-buffers, where $[Ca^{2+}]$ is low (nM) [94].

1.1.2.3 Ca^{2+}-sensing

The main difference between a Ca^{2+}-buffer protein and a Ca^{2+}-sensor protein is that upon binding Ca^{2+}-sensors undergo a conformational change that usually results in the exposure of a hydrophobic area(s) that allows their interaction with target proteins. Buffers on the other hand, merely bind (and release) Ca^{2+} without major conformational shifts and subsequent protein-protein interaction. The most common Ca^{2+}-binding domain for Ca^{2+}-sensors is the EF-hand, however, C_2-Domain-Ca^{2+}-sensors are also known to exist [135]. Several hundred Ca^{2+}-sensors are known to date, with well-known representatives like troponin C or calmodulin [190]. More recently, the distinction between Ca^{2+}-buffers and Ca^{2+}-sensors has been challenged by observations that Ca^{2+}-sensors act as (significant) buffers [109], however, for the purpose of this work it provides a useful discrimination.

1.2 Neuronal Calcium Sensor 1 (NCS-1), a Calcium-Binding Protein

1.2.1 General properties

1.2.1.1 General properties of NCS-1 (Var 1)

The superfamily of intracellular Ca^{2+}-binding proteins containing the EF-hand motif can be divided into families and subfamilies, for example the *Calmodulin Family Proteins* or the *S100 Family Proteins* [190]. Members of a family share structural aspects and are very similar in their Ca^{2+}-binding affinity.

One family whose members were found to be highly expressed in neuronal cell types (including retinal photoreceptor cells) is the *Neuronal Calcium Sensor (NCS) family*. More than 20 differently expressed human splice variants of *NCS* proteins have been identified and grouped into five classes (A-E) according to their amino acid sequence [29]. Besides containing four EF-hand motifs, of which 2-3 are functional, all members of the *NCS* family have an N-terminal myristoylation site [108]. Compared to other families, members of the *NCS* family tend to be more globular and compact [190].

NCS's most prominent member is *frequenin* (Frq), the first representative of the family to be discovered in the *Drosophila* nervous system [138]. The mammalian homolog of *frequenin* was designated *NCS-1*, Fig. 3, p.6. Beyond neuronal tissue, NCS-1 has since been shown to be expressed in heart, smooth muscle, gastrointestinal tract and endocrine tissue [72, 176]. Expression levels in human

organs and cell types differ significantly with the highest detection of NCS-1 in the cerebral cortex [38]. However, several functional aspects are probably better explained by its presence in other regions, like the hippocampus [115, 119, 152] and dorsal root ganglion (DRG) cells [8].

The interplay of structure and function is best understood if NCS-1 is considered as a two-part protein with a myristoylated N-terminal pair of EF-hands (EF1, EF2) and a C-terminal pair (EF3, EF4) which are connected by a hinge loop. Upon Ca^{2+}-binding a large positional shift of the C-terminal pair exposes a crevice that allows hydrophobic interactions with target proteins [26, 80]. Due to the lack of Ca^{2+}-coordinating amino acids (Asp or Glu) the first EF-hand does not bind Ca^{2+} [26]. The primary function of this so called *pseudo-EF-hand* is to stabilize the three functional EF-hands, as cleavage within this domain by the Ca^{2+} dependent protease calpain destabilizes the protein [18]. The detection of subtle Ca^{2+} signals enabled by this 2x2 arrangement highlights Ca^{2+}-sensing qualities over merely Ca^{2+} binding [44, 173]. It has been demonstrated that NCS-1 is capable of binding Mg^{2+} [126] and more recently Zn^{2+} has become a topic of interest [175]. The interaction between these divalent metal ions is speculated to influence conformational state, however, only little is known at this time. While N-terminal myristoylation is usually considered to play a significant role in membrane localization [4, 11], this function has lately been challenged for NCS-1, in that the presence of the myristoyl group may be required in the structural folding of the protein [97, 103].

Fig. 3 **Structural model of Ca^{2+} loaded, un-myristoylated human NCS-1** (PDB code [148]: 2lcp; deposition authors: [80]).
Three Ca^{2+} (green) are bound to the loop regions (yellow) of EF-hands 2-4; α-helices are colored in magenta; N-terminus, *the right hand side of the panel*; C-terminus, *top*.

1.2.1.2 A second frequenin in Drosophila

The evolutionary conservation of NCS-1 is underscored by homologs that have been described even in single cell organisms like yeast [3] (>60% identical [100]). In Drosophila, a second Frq-encoding gene (frq2) with 95% amino acid consensus was discovered [146]. Over- and underexpression experiments concluded distinct functions in axonal growth, bouton formation and neurotransmission [146]. Further studies by the same group elaborated specific binding between Frq2 (but not Frq1) and Ric8a, a receptor-independent activator of G-protein complexes, thereby determining a common pathway and potential pharmacological target (Tab. 1, p.8) [147]. Similarly, the first part of the present work as well as our related publication [182] focus on a second variant of human NCS-1 identified from RNA screens.

1.2.2 Molecular interactions & functions

1.2.2.1 General interactions & functions

In order to understand how a single protein can be implicated in so many different yet specific cellular functions like exocytosis [108], neurite outgrowth [87], axonal regeneration [192], and even nuclear Ca^{2+} regulation [123], it is helpful to keep in mind that most cellular functions are the result of complex protein-protein interactions, usually summed up as pathway(s). Tab. 1 (p.8) presents an overview of target proteins of NCS-1; however, these make up only a fraction, as several more have been identified using *in vitro* binding assays [30]. Some interactions depend on Ca^{2+}-bound NCS-1, while for others binding of the apo-form (NCS-1 with no bound Ca^{2+}) is required [30]. Furthermore, for some targets overlapping interactions with other Ca^{2+}-binding proteins of the calmodulin family has been shown adding further complexity [77].

While the significance of many interactions remains to be determined, some have elucidated the molecular basis of diseases such as X-linked mental retardation (XMR) (Interleukin-1 receptor accessory protein-like 1, IL1RAPL1, Tab. 1, p.8). The C-termini of NCS-1 and IL1RAPL1 have been shown to interact and co-localize at the plasma membrane with opposing effects on growth hormone release [9]. Downstream targets of IL1RAPL1 entail presynapse forming (PTPδ) as well as postsynapse forming proteins (RhoGAP2/Mcf2l & PSD-95). It has been proposed that mutations of IL1RAPL1 (several are known [112]) disrupt upstream regulation by NCS-1 leading to disrupted synaptogenesis in XMR (reviewed in further detail in [12]).

NCS-1 Interacting Protein	Abbreviation	Effect on target	Functional consequence	References
Ca^{2+}-bound state				
ADP-ribosylation factor 1	ARF1	Competes for PI4KIIIβ activation	Regulation of TGN to plasma membrane traffic	[78, 79]
α1 subunit of voltage-gated Ca^{2+} channel 2.1	$Ca_V2.1$	Activates Ca^{2+}-dependent facilitation of channel	Increases facilitation of neurotransmitter release	[161, 174]
Dopamine receptor D2	D2R	Inhibits internalisation of receptor	Promotes spatial memory formation	[88, 99, 152]
Interleukin-1 receptor accessory protein-like 1	IL1RAPL1	upstream regulation by C-terminal association	Regulates N-type channels, secretion and neurite elongation	[9, 12, 66]
Inositol 1,4,5-trisphosphate receptor	$InsP_3R$	Enhances receptor activity	Increases calcium signaling in neurons and heart	[154, 193]
Phosphatidylinositol 4-kinase IIIß	PI4KIIIß	Activates the enzyme	Regulation of TGN to plasma membrane traffic	[79, 83]
apo/unbound state				
Adenosine A2 receptor	ADORA2A	?	Increases receptor signaling	[127]
G-Protein coupled receptor Kinase 2	GRK2	Inhibits kinase activity	Inhibits receptor internalisation	[88]
Inositol 1,4,5-trisphosphate receptor	$InsP_3R$	Enhances receptor activity	Increases calcium signaling in neurons and heart	[118, 154]
Resistance to inhibitors of cholinesterase-8A/ Synembryn-A	Ric8A	?	Increases synapse number and synaptic release probability	[147]
Transient Receptor Protein 5	TRPC5	Activates channel	Retards neurite growth	[86]

AFR[78, 79], $Ca_V2.1$[161, 174], D2R[88, 99, 152], IL1RAPL[9, 12, 66], InsP3R[154, 193], PI4KIIIß[79, 83], //ADORA2A[127], GRK2[88], InsP3R[118, 154], Ric8A[147], TRPC5[86]

Tab. 1: **List of proteins that bind NCS-1** (Tab. modified from [21], originally adapted from [30]). TGN: trans-Golgi network

1.2.2.2 Interaction of NCS-1 and $InsP_3R$

For the purpose of this work the interaction between NCS-1 and the inositol 1,4,5-trisphosphate receptor ($InsP_3R$) is of great importance. By mediating the release of Ca^{2+} from the ER, the tetrameric receptor plays a pivotal role in many cellular events and malfunctions have been linked to a variety of pathological conditions ranging from epileptic seizures and ataxia [107] to bile duct obstruction [160]. Altogether, there are three known mammalian isoforms, of which the $InsP_3R$ type 1 ($InsP_3R1$) is the predominant isoform in neurons [62]. Several Ca^{2+}-binding proteins interact with the $InsP_3R$ as activators and inhibitors [90, 106, 131]. In addition to NCS-1 (Fig. 4, p.9) [154], Ca^{2+} itself can regulate channel activity [16].

NCS-1's modulation of the $InsP_3R1$ depends on $InsP_3$, since NCS-1 alone is not a direct agonist (Fig. 4, B, p.9) [154]. Furthermore the NCS-1 induced increase of ($InsP_3$-gated) channel activity is achieved through an increase of the channel's open probability. Additionally, the open probability is Ca^{2+}-dependent: High levels of [Ca^{2+}] increase the channel's open probability more than low [Ca^{2+}] (Fig. 4, D & E, p.9) [154]. The amplitude of the single-channel currents, however, remain unaltered. A NCS-1 mutant (E120Q, [187]) with reduced Ca^{2+}-binding ability through inactivation of the third EF-hand still increased the open probability of the

$InsP_3R1$. The increase (of open probability and mean open time), however, no longer depended on $[Ca^{2+}]$ (Fig. 4, F) [154].

Planar lipid bilayer experiments showed no effect of NCS-1 on the activity of the ryanodine receptor (RyR2) suggesting a specific effect on $InsP_3$ receptors [154].

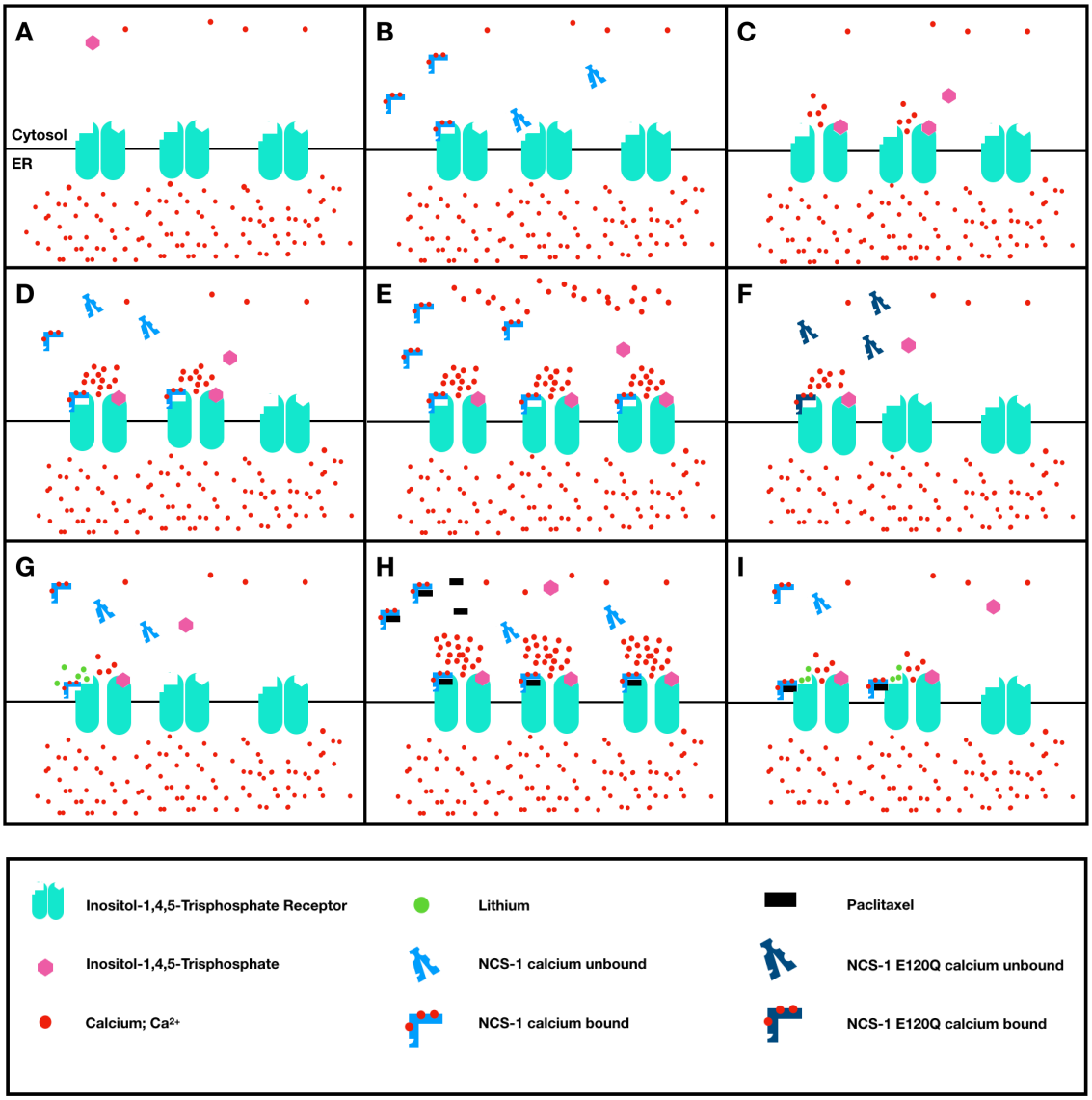

Fig. 4 **Interaction of NCS-1 and $InsP_3R$** (modified & also used in [21]).
(A) $InsP_3R1$ at rest, no Ca^{2+} flux. **(B)** NCS-1 alone does not sufficiently activate $InsP_3R$, no Ca^{2+} flux **(C)** Upon binding of $InsP_3$ $InsP_3R1$ releases Ca^{2+} from the ER **(D)** Binding of NCS-1 enhances $InsP_3$ mediated $InsP_3R1$ channel activity by increasing open probability and mean open time. The amplitude of a single-channel current remains unaltered. **(E)** Open probability and mean open time of NCS-1 mediated $InsP_3R$ activation show a Ca^{2+}-dependent increase. **(F)** The point mutation of NCS-1 (E120Q) has an unaltered Ca^{2+} -dependent conformational change, however, a reduced Ca^{2+}-binding affinity. NCS-1 E120Q increases the open probability of $InsP_3R$, but does not influence the mean open time and acts independent of the cytosolic $[Ca^{2+}]$. **(G)** Lithium offsets NCS-1 mediated enhancing effects on $InsP_3R$; immunoprecipitation remains intact. **(H)** PTX binds the hydrophobic cleft of NCS-1 in Ca^{2+}-bound state. Thereby it facilitates binding of NCS-1 to $InsP_3R$, thus inducing Ca^{2+}-oscillations. **(I)** Lithium (as well as ibudilast) inhibit PTX mediated, NCS-1 dependent increases in $InsP_3R$ channel activity, preventing Ca^{2+} oscillations.

1.3 NCS-1 in Disorders, Diseases and Development

1.3.1 Disorders & diseases

The various interactions described in Tab. 1, p.8 pose only the tip of the translational iceberg that elucidates NCS-1's contribution in diseases(Tab. 2, p.11). The majority of associated conditions is within the neuro-psychiatric spectrum, accentuating the protein's predominant expression in neuronal tissues [72].

A missense mutation of NCS-1 (R102Q) was found in a patient with autistic spectrum disorder [136] and while neither binding to IL1RAPL1 (Ch.1.2.2.1) nor Ca^{2+} were shown to be disrupted [75], disabled C-terminal dynamics were suggested to impair neuronal signaling by blocking target binding [194]. This example is rare in that the majority of the disease related changes in NCS-1 are due to changes in the magnitude of expression rather than mutations to NCS-1. NCS-1 is an integral part of pathophysiological models explaining sleep-wake disturbance symptoms in bipolar disease [49] as well as the effectiveness of lithium treatment [67]. Furthermore, elevated protein levels of NCS-1 in the prefrontal cortex of bipolar and schizophrenic patients (analyzed post mortem) suggested a quantitative aspect of NCS-1's role in disease [92]. Likewise does the finding of increased NCS1-mRNA-levels in substantia nigra neurons of patients with *Parkinson's disease* [59]. Apart from *Parkinson's disease*, NCS-1's altered regulation of dopamine receptor D2 desensitization has been used to explain the effectiveness of nicotine replacement therapy [51] and the susceptibility to cocaine addiction [114].

In oncology, recent publications have highlighted NCS-1's potential use as a prognostic and diagnostic tool. Two independent breast cancer cohorts showed a significant negative correlation of survival rates with elevation of NCS-1-levels [113]. Cell and mouse-based assays showed a correlation of NCS-1 expression and the number of distant metastases as well as prolonged cancer cell survival suggesting it as potential metastatic biomarker [6]. Aside from breast cancer, NCS-1 was shown to predict worse outcome in hepatocellular carcinoma in Asian patients [156]. Dose limiting cardiac arrhythmias under paclitaxel (PTX) treatment were attributed to altered Ca^{2+} signaling mediated through the above mentioned interaction of NCS-1 and the $InsP_3R$ [193]. Furthermore, stress tolerance in NCS-1-deficient mouse cardiomyocytes highlighted its role in survival pathways of non-neuronal tissues [120]. One of the two main focuses of the present work is to deepen the understanding of NCS-1's role in chemotherapy induced peripheral neuropathy (CIPN, Ch.1.4 & Ch.3.2).

Field of study	Disorder/ Disease	Organism	NCS-1's Role/ Observation	Reference s
Neuro-Psychiatry	Bipolar disorder & Schizophrenia	**human,** rat	>50% higher levels of NCS-1 in the PFC compared to normal controls Chronic treatment with typical or atypical antipsychotics does not change NCS-1 expression in five brain regions: prefrontal cortex, hippocampus, striatum, cortex and cerebellum Expression in leukocytes is decreased Modulation of gamma band oscillations in the PPN in a concentration-dependent manner Lithium reduces effects of over expressed NCS-1 on PPN neurons	[10, 48, 50, 92, 163, 164, 172, 177]
	Autistic spectrum disorder (ASD)	**human**	Rare missense mutation was identified in one autistic patient during study	[75, 136]
	X linked mental retardation	drosophila	Potential drug target at the NCS-1/Ric8a interface	[9, 103]
	Addiction	**human**	Genetic polymorphisms are associated with cocaine addiction in African-Americans but not European Americans Variations of the NCS-1 gene influence the efficacy of nicotine replacement therapy	[51, 114]
	ADHD	rat	Methylphenidate induces changes in expression levels in rat hippocampus, prefrontal cortex and cerebellum	[165]
	Depression/ Motivation	mouse	Deficiency appeared to result in anxiety- and depressive-like behaviors as well as in decreased willingness to work for food	[52, 128]
	Insomnia	rat	Dysregulation may lead to increased activity in PPN neurons. Potential mediated target for modulation of hyperarousal	[68]
	Parkinson's disease (PD)	**human**, mouse	Post-mortem PD brains show increased NCS-1 mRNA suggesting increased NCS-1/D2- autoreceptor signalling in PD Potential target in modulating the neuron activity and vulnerability to degeneration in PD	[59, 61]
	CNS trauma	rat	Potential intracellular target for therapeutic intervention following injury to the central nervous system; NCS-1-induced neurite sprouting	[192]
	Neuro-degeneration (ND)	in vitro	Misfolding at physiological Ca^{2+} levels suggests potential link between Ca^{2+} dysregulation, protein misfolding and ND	[81]
	Memory	mouse	Deficiency shows impaired spatial learning and memory function as well as reduced exploration Overexpression selectively in the adult murine dentate gyrus promotes a specific form of exploratory behavior Regulation of genes that are related to intrinsically motivated exploration, something considered akin to curiosity. Up regulation of expression in the hippocampus through swimming training promotes memory	[60, 115, 119, 152]
Oncology	CIPN	mouse	Prevention target through lithium pretreatment	[2, 13, 14, 18, 24, 25, 110, 139, 154, 185]
	Taxol-induced cardiac arrhythmia	rat, mouse	Increased expression in cardiomyocytes after treatment with PTX leads to an acceleration of Ca^{2+} oscillations	[193]
	Breast cancer	**human**	Outcome predictor, metastatic biomarker	[6, 113]
	Hepatocellular Carcinoma	**human**	Outcome predictor	[156]
Cardiology	Cardiac hypertrophy and stress	mouse	Increased expression in early stages of cardiac hypertrophy and potential mediator of hormone-induced progression of hypertrophy in adult hearts. Mediator of stress tolerance in cardiomyocytes; upregulation in hearts after ischemia-reperfusion	[118, 120]
Infectious Diseases	Sepsis	rat	Low expression in prefrontal cortex may be associated with the pathophysiology of cognitive impairment during sepsis	[42]
Gastro-enterology	Colitis	rat, ENS	Selective loss of NCS-1 expression after DNBS-induced colitis	[101]
Urology	Erectile dysfunction (ED)	rat, penile tissue	Potential target in the treatment of ED, upregulation after administration of tadalafil	[5]

Tab. 2: **Diseases associated with NCS-1** (modified from & also used in [21])
ADHD: attention deficit hyperactivity disorder, CNS: Central nervous system, DNBS: dinitrobenzene sulfonic acid, ENS: Enteric Nervous System, PPN: pedunculopontine nucleus

1.3.2 Developmental biology

The importance of Ca^{2+} for the initiation of life has been tracked to the primary Ca^{2+} hot spot triggered by insemination [64]. From here on the zygote passes through a complex development program and finally differentiates into highly specific cells, tissues and organs.

Not surprising, the ubiquitous NCS-1 is part of several aspects of this program. NCS-1 expression levels within mouse hearts were found to be higher during the fetal and neonatal period compared to adulthood [121]. Moreover, deletion of NCS-1 decreased survival in young mice and hormone-induced cardiac hypertrophy was largely prevented in these knockout mice [118]. NCS-1 was up-regulated in hypertrophic hearts and selective inhibition of further key players (e.g. $InsP_3R$ or calcineurin) prevented hypertrophy [118].

Tab. 3 summarizes more implications of NCS-1 in developmental biology including synaptic transmission and synaptogenesis in the rat [143] and chick [15] retina. Additionally, other sensory systems like the olfactory [173] and vestibular system [20, 134] appear to be (at least in part) regulated by NCS-1.

Sensory System	Organism	NCS-1's Role/Observation	References
Olfactory system	mouse	Expression in olfactory epithelium during development, down-regulation of axonal expression after synapse formation	[173]
Eye	chick/rat	Neuronal process outgrowth and synaptogenesis in the retina	[15, 143]
Inner ear	zebrafish	Signaling pathway for semicircular canal formation, Knockdown of NCS-1a mRNA blocked formation of semicircular canals.	[20, 134]
Heart	mouse	High expression in the heart during fetal period and decline after birth; regulator of excitation-contraction coupling in fetal and neonatal hearts through enhancement of Ca^{2+} signals	[118, 121, 122]

Tab. 3: **NCS-1's role in developmental biology** (modified from & also used in [21])

1.4 NCS-1 in Chemotherapy Induced Neuropathy

1.4.1 Paclitaxel induced neuropathy

1.4.1.1 Clinical aspects

Paclitaxel (PTX; common brand name *Taxol*) is a chemotherapeutic medication that is widely used in breast, ovarian, and lung cancer as well as Kaposi's sarcoma [186]. It was the first member of the *taxane* family to be discovered and was originally isolated from the pacific yew tree, *Taxus brevifolia* [186]. PTX's main mechanism of action is stabilization of polymerized microtubules, and thus it prevents chromosome segregation and cell division [153].

Chemotherapy induced peripheral neuropathy (CIPN) is a common and potentially dose-limiting adverse reaction to chemotherapeutic agents like PTX (but also platinum agents, vinca alkaloids, and proteasome inhibitors) [37]. A meta-analysis including 31 studies with data from more than 4000 patients reports a prevalence of more than 50% (measured in the first month after chemotherapy) [158]. CIPN in general includes a broad spectrum of most commonly sensory neuropathic symptoms, such as numbness, tingling, burning sensations; for PTX muscle weakness as a sign of motor neuropathy is possible [93].

Consensus-based recommendations within the German S3-guideline („*Supportive Therapie bei onkologischen PatientInnen*“) comprise a neurological status evaluation and anamnesis before each course of potentially neurotoxic chemotherapeutic drugs [I 1]. Furthermore, diagnosis of CIPN should include a specific pain anamnesis (CIPN specific questionnaires are suggested), motor signs (atrophies, pareses), reflexes, sensation (light touch, pain, temperature, vibration, position sense), coordination and electrophysiology (electroneurography, if necessary electromyography and/or heart rate variability assessments) [I 1]. Electrophysiology is helpful as it represents a method to objectivize and distinguish between axonal and/or demyelinating damage [I 1]. Pain is one of the main aspects of CIPN that is responsible for the poor quality of life in cancer survivors. At the same time it underlies great subjectivity which poses challenges in diagnostics and clinical practice. The variety of different assessment modalities for CIPN has recently been argued to misjudge the incidence and prevalence of CIPN [111].

There is currently no effective medication for CIPN. As the condition severely reduces the quality of life and leads to interruption or discontinuation of therapy [58], prevention strategies are needed. Discontinuation of treatment has been shown to help the process of recovery from mild forms of CIPN [149], however, the potential reduction in antineoplastic effects poses a risk that has to be carefully considered. Some prevention strategies of the last decades, including supplementation of vitamin E [7, 85] and the administration of pifithrin-μ [96, 167], have shown only limited success, so that both, German and American clinical practice guidelines, do not recommend any agent for the prevention of CIPN [I 1, 84].

This lack of evidence necessitates the identification, development and evaluation of new strategies for the prevention of one of the most devastating side effects of antineoplastic therapy at the molecular scale.

1.4.1.2 Molecular aspects

Since (peripheral) neurons do not undergo mitosis (certainly not when compared to the rate of highly proliferative cancer cells), it is reasonable to assume that PTX exerts effects other than mitotic inhibition, with regard to neurons causing CIPN. It is important to bear in mind that steady-state plasma concentrations of PTX in patients have been determined to be in the high nM-range [150]. In contrast, the early experiments used concentrations of 10 µM or higher and therefore do not reflect the situation in patients. These studies attributed PTX adverse effects primarily to an interference with microtubules [124, 151] or to effects of the solubilizer used in clinical treatment (Cremophor EL) [70].

Application of PTX to human neuroblastoma cells (SH-SY5Y) evoked an oscillatory, concentration dependent, cytosolic Ca^{2+} increase [24]. A link between PTX and deregulated Ca^{2+} had already been proposed after the observation of mitochondrial permeability transition pore opening [91]. The opening of this pore leads to intracellular [Ca^{2+}] increase and the activation of cell death pathways. PTX, however, does not bind to mitochondrial proteins. Aside from binding to ß-tubulin PTX interacts with several other proteins including the antiapoptotic protein Bcl-2 [145] and heat shock proteins [32]. In the context of CIPN the functional consequences of these interactions remain unclear [19]. Another, more interesting, binding partner of PTX being capable of initiating CIPN was found later, namely NCS-1 (Fig. 4 H, p.9) [24].

1.4.2 NCS-1 mediated CIPN - pathophysiology & prevention target

1.4.2.1 Pathophysiology

Ca^{2+} oscillations after PTX application were abrogated after knockdown of NCS-1 by shRNA [24]. Signaling through the $InsP_3R$ was still intact, because purinergic P_2Y receptor stimulation (ATP) still triggered a Ca^{2+} response [24, 179]. Furthermore, the PTX-induced Ca^{2+}-signals were $InsP_3R$ specific, as RyR inhibition did not modify them [24]. The previously established binding of NCS-1 to the $InsP_3R$ (Tab. 1, p.8) [154] was found to be enhanced in the presence of nano-molar concentrations of PTX (Fig. 4 H, p.9) [24].

Chronic exposure to low PTX concentrations attenuated Ca^{2+} signaling in SH-SY5Y and decreased NCS-1 protein levels, however, intracellular Ca^{2+} stores, cell viability and $InsP_3R$ protein integrity remained intact (Fig. 5, p.16) [25]. Importantly, an interaction between tubulin and NCS-1 could not be verified [25]. It was concluded that NCS-1 is a target of Ca^{2+} dependent protease calpain, because calpain inhibition prevented NCS-1 depletion and preserved Ca^{2+} signaling [25]. The exact cleavage site was determined to be within the pseudoEF-hand (N-terminal part of NCS-1) [18]. Upon treatment with PTX calpain activity increased in a time and concentration dependent manner [25, 185].

Transient receptor potential vanilloid 4 (TRPV4) is a Ca^{2+} channel within the plasma membrane (Fig. 1, p.2). Unlike other membrane-Ca^{2+} channels, localized increases in intracellular [Ca^{2+}] potentiate (and do not inhibit) TRPV4 activity [168]. Moreover, TRPV4 and $InsP_3R$ interact physically and co-localize partially [22]. Although TRPV4 and PTX have not been shown to interact directly, the augmentation of the intracellular [Ca^{2+}] levels through TRPV4 activity may play an important role in calpain activation. Evidence for this idea was obtained in animal models since the occurrence of CIPN was prevented by knockdown [2], or inhibition [22] of TRPV4. Other TRP-channels have also been implicated in the development of neuropathic pain [105].

These observations provide in summary a revised model for the pathophysiology of CIPN that is tubulin-independent but caused by disrupted Ca^{2+} signaling (Fig. 5, p.16):

I.) PTX augments NCS-1's activation of $InsP_3R$ [24].

II.) Active $InsP_3R$ induces Ca^{2+} oscillations [24].

III.) Ca^{2+} oscillations increase cytosolic [Ca^{2+}] [24].

IV.) Increased cytosolic [Ca^{2+}] activates Ca^{2+}-dependent TRPV4 channels [168].

V.) TRPV4 activation further increases cytosolic [Ca^{2+}] [2].

VI.) The Ca^{2+} dependent protease calpain becomes more active [2].

VII.) Calpain cleaves NCS-1 and other proteins [25].

VIII.) NCS-1 depletion leads to cessation of $InsP_3R$ mediated Ca^{2+} oscillations [25].

IX.) Impaired Ca^{2+} signaling as well as activation of calpain and caspases leads to irreversible damage and cell death [25].

This Ca^{2+} model may include an involvement of mitochondria since the excess of cytosolic Ca^{2+} may overwhelm mitochondrial storing capacity. This could further contribute to the activation of cell death pathways [91].

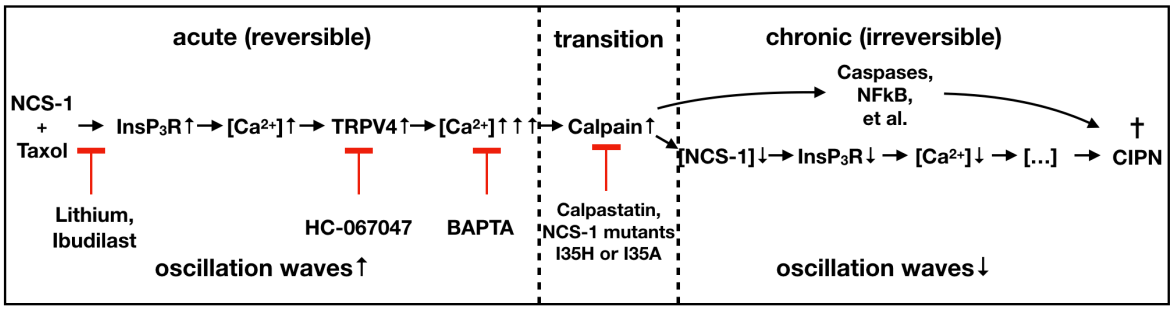

Fig. 5 **Suggested pathway for CIPN induced damage** (adapted from/also used in [21]). ***Acute (reversible).*** PTX (Taxol) facilitates binding of NCS-1 to $InsP_3R$. Binding induces Ca^{2+} oscillations from the ER. Cytosolic [Ca^{2+}] increases are further enhanced by activation of Ca^{2+} dependent TRPV4 channels. Ca^{2+} activates the Ca^{2+} dependent protease calpain, which cleaves NCS-1 and a number of other proteins. ***Chronic (irreversible).*** A negative feedback loop impairs signaling through the $InsP_3R$ leading to an attenuation of Ca^{2+} oscillations. Impaired signaling and further degradation of proteins lead to axonal damage and cell death. Lithium and ibudilast both interact with NCS-1 and prevent enhanced $InsP_3R$ activity and NCS-1 protein degradation. TRPV4 inhibitor HC-067047 reduces mechanical allodynia after PTX treatment. BAPTA and other Ca^{2+} reducing agents have been shown to interfere within this pathway. Overexpression of calpastatin, an endogenous calpain inhibitor, as well as overexpression of NCS-1 mutations (I35H or I35A) were able to protect endogenous (WT) NCS-1 from degradation in human neuroblastoma cells.

1.4.2.2 NCS-1 a feasible prevention target for CIPN

Consequently, without treatment options at hand, the molecular understanding of the pathophysiology of CIPN may help to identify molecular targets to prevent these side effects (Fig. 5). The manipulation of calpain or Ca^{2+} itself may seem reasonable, however, this approach is strongly limited due to the ubiquitous importance of both targets for cell function. In cell based assays competitive inhibitors of calpain were successfully used to prevent cleavage of native NCS-1 [13, 46, 57]. However, clinical use is limited due to the non-selectivity of (currently) existing agents [56].

According to this model another feasible target is TRPV4. TRP-channels are implicated in a variety of diseases and their pharmacological modulation is a hot topic in recent research [54]. In preclinical models, the selective antagonist of TRPV4, HC-067047 is a suitable candidate to prevent CIPN [22, 63].

The initial step in the proposed model of CIPN is the NCS-1 mediated activation of $InsP_3R$ (Fig. 4H, p.9 & Fig. 5). Treatment with lithium or ibudilast prevented enhanced Ca^{2+} signaling and subsequent NCS-1 degradation in SH-SY5Y [14]. Lithium or ibudilast neither inhibited binding of NCS-1 to PTX (Fig. 4I, p.9) nor was tubulin assembly altered [14]. The latter is of great importance as it implies that the antineoplastic activity of PTX is not impaired during co-administration. Indeed, a single prophylactic injection of either substance before PTX treatment inhibited CIPN in mice without compromising its antineoplastic effects [110].

1.5 Thesis Objectives

Neuronal Calcium Sensor 1 is a Ca^{2+}-binding protein which is expressed in most tissues and a major actor in intracellular Ca^{2+} homeostasis. The investigation of the biophysical and structural properties of NCS-1 as well as the identification of numerous molecular binding partners have delivered evidence for its important role in the regulation of various Ca^{2+}-dependent signaling pathways. From these findings models have been generated to explain diseases, disorders and ontogenesis. However, the functional implications of many interactions remain unknown. The present work focuses on two objectives:

The first objective was to characterize a second variant of human NCS-1 which was found in the National Center for Biotechnology Information (NCBI) database and compare it to the primary variant. Specific research questions involved the identification of the predominant transcript in human cell lines. Furthermore, protein stability was studied and human cells were screened for protein expression of either variant. Lastly, functional consequences of the overexpression of either protein in human cell lines were investigated.

The second objective was to elucidate NCS-1 (Var1)'s role in chemotherapy induced peripheral neuropathy in a mouse model. We hypothesize that NCS-1 is an important actor herein. To test this hypothesis we investigated nerve conduction in mice deficient for NCS-1 with or without PTX treatment and examined neuronal structures by electron microscopy.

2. Materials and Methods

2.1 Materials

2.1.1 Chemicals and Equipment

2.1.1.1 Cell culture

SH-SY5Y cell line	ATCC number CRL-2266, Homo sapiens (human), bone marrow, neuroblastoma
HEK-293 cell line	ATCC number CRL-1573, Homo sapiens (human), embryonic kidney
MB-231 cell line	ATCC number CRM-HTB-26, Homo sapiens (human), mammary gland/breast; derived from pleural effusion
Flasks	75 cm^2 tissue-culture treated polystyrene flasks, Becton Dickinson
Sterile pipettes	5mL, 10mL, 25 mL, 50mL, Falcon, Becton Dickinson
TrypLE Express	Trypsin like enzyme, Invitrogen
Penicillin-Streptomycin	stock containing 10000 μg/mL streptomycin and 10000 μg/mL penicillin, GIBCO, Invitrogen
Ham's F-12 medium	GIBCO, Invitrogen
DMEM	GIBCO, Invitrogen
heat-inactivated FBS	GIBCO, Invitrogen
MEM non-essential amino acids	GIBCO, Invitrogen
Hemocytometer	Hausser Levy Hemocytometer Chamber Set, Thermo Fisher Scientific, (Apx-Fig. 1, p.101)
Cell stain	Trypan Blue Solution, Thermo Fisher Scientific

2.1.1.2 Transfection

Glass cover slips 22mmx 22mm	Becton Dickinson
Opti-MEM	GIBCO, Invitrogen
Lipofectamine 2000	Invitrogen
Geneticin	G418 disulfate salt, Sigma-Aldrich

2.1.1.3 Cell lysis, gel electrophoresis and protein immunoblotting

BSA	Albumin bovine serum, Fraction V, Sigma-Aldrich
Dry Milk	Carnation, instant nonfat dry milk, Nestle
Electrophoresis System	Bio-Rad
Electrophoresis gels	precast polyacrylamide Tris-HCl Gel, Bio-Rad
Molecular Weight Markers	Precision Plus Protein Standards Dual Color, Bio-Rad

M-PER	Mammalian Protein Extraction Reagent, Thermo Fisher Scientific
RIPA	Lysis and Extraction Buffer, Thermo Fisher Scientific
Protease Inhibitor	Protease cocktail, Sigma-Aldrich
Protein Assay Kit	BCA Protein Assay Kit, Thermo Fisher Scientific
Protein detection kit	ECL, Super Signal West Dura Extended Duration Substrate, Thermo Fisher Scientific [I 2]
PVDF membranes	Polyvinylidene difluoride membrane, Bio-Rad
Re-blotting kit	Re-Blot Plus Kit, Millipore
Sodium orthovanadate	Na_3VO_4, Sigma-Aldrich
Tween 20	Sigma-Aldrich
X-ray Film for Western Blot Detection	Thermo Fisher Scientific
Gel Loading Buffer	BlueJuice Gel Loading Buffer, Invitrogen
Protein stain	SimplyBlue SafeStain, Invitrogen

2.1.1.4 DNA Transformation

LB (lysogeny broth) powder	Bio-Rad
Bacto Agar powder	Sigma-Aldrich
Ampicillin	stock solution 100 mg/mL (solubilized in sterilized water through a 0.22 μm filter, Qiagen)
E. coli DH5α cells	Invitrogen
SOC media	Super Optimal broth with Catabolite repression, Invitrogen
Sterile 90 mm Petri dishes	BD Biosciences

2.1.1.5 DNA/RNA Purification & Measurements

UV-Vis Spectrophotometer	NanoDrop 2000c, NanoDrop Products [I 3]
Thermocycler	7500 Fast & 7500 Real-Time PCR System, Applied Biosystems [I 4]
DNA Purification Kit	HiSpeed Mini/Midi Prep, Qiagen [I 5]
RNA Purification Kit	RNeasy Mini Kit, Qiagen [I 6], (Apx-Fig. 2, p.101)
Reverse Transcription Kit	High Capacity cDNA Reverse Transcription Kits, Applied Biosystems [I 7]
Cloning Kit	TOPO TA Cloning Kit, Invitrogen [I 8], (Apx-Fig. 3, p.102)
Genotyping Kit	REDExtract-N-Amp Tissue PCR Kit, Sigma-Aldrich [I 9]
Agarose	Sigma-Aldrich

Ethidium bromide	Thermo Fisher Scientific
DNA Gel Loading Dye	Bromophenol Blue, Thermo Fisher Scientific
1 kb Plus DNA Ladder	Invitrogen [I 10], (Apx-Fig. 4, p.97)
qPCR Master Mix	SYBR Select Master Mix, Applied Biosystems, [I 11]

2.1.1.6 Functional differences & Drug Sensitivity Assessment

IncuCyte incubator	Essen BioScience [I 12]
Paclitaxel	Sigma-Aldrich [I 13]
Cremophor EL	Sigma-Aldrich

2.1.1.7 Nerve conduction velocity measurements

Nicolet Viasys Viking Select EMG EP System	VikingQuest and VikingSelect instruments, CareFusion [I 14]
Anesthesia System	V-1 Tabletop Laboratory Animal Anesthesia System, VetEquip [I 15]
Isoflurane	Halocarbon

2.1.2 Solutions and Buffers

Growth medium SH-SY5Y	44% Ham's F-12 medium 44% DMEM (4.5%), 10% heat-inactivated FBS, 1% MEM non-essential amino acids, and 1% penicillin-streptomycin
Growth medium HEK293	88% DMEM (4.5%), 10% heat-inactivated FBS, 1% penicillin-streptomycin, 1% L-Glutamine
Growth medium MB231	88% DMEM (4.5%), 10% FBS, 1% MEM non-essential amino acids, 1% penicillin-streptomycin
Sample buffer	20% glycerol, 20% SDS, 2% 2-mercaptoethanol, 0.5 M Tris-HCl supplemented with bromophenol blue
Running buffer	25 mM TrisHCl, 192 mM glycine, 0.01% SDS
Transfer buffer	25 mM TrisHCl, 192 mM glycine, 0.01% SDS, 10% methanol
PBS	Phosphate-buffered saline; 137 mmol/L NaCl, 2.7 mmol/L KCl, 10mmol/L Na_2HPO_4, 1,8 mmol/L KH_2PO_4
TAE Buffer	0.04 M Tris, 0.04 M acetate, 1 mM EDTA, pH 8.2 to 8.4, Thermo Fisher Scientific
Blocking solution	Phosphate buffered saline with 5% non-fat dried milk powder and 0.05% Tween 20
Perfusion solution	0,9% NaCl, 0,1% $NaNO_2$, 0,1% BSA, 10mg Heparin, 5 mM TRIS
Fixation solution	200mM PBS, 4% Paraformaldehyde, 0.5% Glutaraldehyde, 1M NaOH (dropwise)

2.1.3 Oligonucleotides (Primer)

2.1.3.1 Genotyping (for details, p.35; [I 16] & [128])

Primer	Sequence 5'-3'	Product
MS66 (forward)	GTCCACCCATACCAATCACT	
MS67 (reverse) (WT)	ACAGAGAATCCAAAGCCAGC	398 bp
JH32 (reverse) (KO)	TTGTGCTGGAGAAGGGAGAG	514 bp

2.1.3.2 NCS-1 Variant Quantification (for details, p.25)

Primer	Sequence 5'-3'	Product
NCS1 Var1		
V1F (forward)	ATG GGG AAA TCC AAC AGC AAG TTG AAG CCC GAA G	
V1R (reverse)	TG GTG GGG TCT CCG AAC GGG	186bp
NCS1 Var2		
V2F (forward)	T TGA GAG ATG GCA ACG ATT ACC GAG	
V2FPC (forward)	T TGA GAG ATG GCA ACG ATT ACC GAG AAG GAG GT	193bp
V2R (reverse)	CAA TTC GCC CGT CCT TGT TTT C	193bp

2.1.4 Antibodies

Anti-NCS-1 (FL-190)	1:5000	rabbit, Santa Cruz Biotechnology
Anti-HA	1:1000	rabbit, Santa Cruz Biotechnology
Anti-FLAG	1:1000	mouse, Sigma-Aldrich
anti-rabbit	1:100000	goat, Santa Cruz Biotechnology
Anti-mouse	1:100000	goat, Santa Cruz Biotechnology

2.1.5 Mice

All animal research was performed in compliance with policies and guidelines of Yale University's Institutional Animal Care and Use Committee (IACUC). Animals were housed under conditions according to an approved Yale University protocol under a 12-h light/dark cycle. C57Bl/6 mice were used for all experiments. NCS-1 knockout mice were a kind gift from Prof. Dr. Olaf Pongs to the Ehrlich Laboratory of Molecular Hermeneutics. NCS-1 knockout mice were bred with mice obtained from Charles River Laboratories. Animals were weaned and genotyped at 3 weeks of age using the primers described in 2.1.3.1 & Fig. 7, p.35. Genotyping was carried out by digestion of mouse ear clip genomic DNA (2.2.17). Mice were fed *ad libitum* normal chow diet.

2.1.6 Software and Databanks

2.1.6.1 Databanks

Protein data bank	[148]
Ensembl genome browser 83	[47]
NCBI Nucleotide	[69]

2.1.6.2 Software

NCBI Primer-BLAST	[191]
Multalign	[43]
Image-J	[155]
qPCR analysis	[I 4]
NetPrimer	[I 17]
Reverse Complement	[I 18]
GraphPad Prism	[I 19]
EndNote	[I 20]
iWork	[I 21]
4Peaks	[I 22]

2.2 Methods

2.2.1 Cell Density Determination

Cell densities were measured with a hemocytometer (Apx-Fig. 1, p.101). Both hemocytometer and coverslip were cleaned and wiped with 70% alcohol before and after each use. Cells were loosened from culture flasks using growth medium. 20 µL of solubilized cells were transferred to an Eppendorf tube to 20 µL Trypan Blue Solution and mixed. 20 µL of the mix was pipetted between the hemocytometer and the coverslip. Each 1x1mm^2 square represents a volume of 10^{-4} mL. Cell density was calculated:

$$\text{Cells / mL} = a * d * 10^4 \text{ /mL}$$

with a = average counted squares

d = dilution factor of 2; for 20 µL Trypan Blue and 20 µL of solubilized cells

2.2.2 Measuring of DNA/RNA Concentrations

DNA concentrations were measured using a UV-Vis Spectrophotometer. Sample amounts of 1μL were measured against a corresponding blank solution (e.g. in case of a Mini/Midi Prep Mili-Q or Buffer EB). Samples were considered pure when 260nm/280nm ratio ranged between 1.8 - 2.0 (for DNA; >1.9 for RNA) as recommended by manufacturer [I 3]. Assuming the average weight of a base pair (bp) is 650 Da and that the total mass of DNA is equal to the number of copies times specific weight of a basepair bp times the total length of the template, copy numbers were calculated using the conversion formula:

n = (m * 6.022* 10^23 molecules/mol) / (l * 1 * 10^9 ng/g * 650 g/mol of bp)

units—> {copy number = (ng * number/mol) / (bp * ng/g * g/ mol of bp)}

with n = copy number
m = amount of DNA in ng (measured through NanoDrop)
l = template length in bp

2.2.3 Primer Design

NCS1 sequence was obtained online from NCBI Nucleotide [69]. Ensembl genome browser 83 [47] was used to find intron sequences. Potential primer pair candidates were identified using NCBI Primer-BLAST software [191]. Primers were designed considering the following aspects:

1). Not too long, not too short 18bp - 35bp
2). High GC content (40-60%)
3). Not more than consecutive 4 Gs or Cs
4). T_m should be similar between the two primers, ideally around 60°C.
5). Preferably end and start on a G or a C
6). Spanning a splice site to catch mRNA and not genomic DNA

Concerning dimers, hairpins and melting temperatures (T_m), primer pairs were virtually tested online using NetPrimer software [I 17]. Chosen primers were purchased from Yale Keck Foundation—Oligo Synthesis Resource. Alignment processes were facilitated using the online tool Multalin [43]. Tab. 4, p.24 & Fig. 6, p.25 give more specific insights concerning primer sequences and binding context.

Var1	Var2	Length in bp	Sequence	Primer
5' upstream sequence	5' upstream sequence	… 30	…agcgcgggcgccgcagacaaaggcgcggcc	
Exon 1 5'UTR Translated part		86	CCGGCCCGGCCCGCCCGGCCCAGCCGCTCCTG CTGGGCGCCCCAACCGGGTCCGGCCCGGGGGG GCGGGGGCCGCGGCCGCCGAGG	
		150	**ATGGGGAAATCCAACAGCAAGTTGAAGCCCGA AG**TTGTGGAGGAGCTGACCAGGAAGACCTACT	**V1F**
Intron 1-2 (28,230bp)		27,865	gtgagtgctcccagcccccagcccgcgccc … cagggccttccctgacatcccgtccccagg	
	Exon 1 5'UTR	9	GA**TTGAGAG**	**V2F(PC)**
	Translated part	10	**ATGGCAACGA**	
	Intron 1-2	346	gtaagtcttagatgttggcctgggagcaag … aaaagcctacttttctgctttctcttgcag	
Exon 2	Exon 2	25	**TTACCGAGAAGGAGGT**CCAGCAGTG	
Intron 2-3	Intron 2-3	16,849	gtgagtagctgctttttctcaaaccgtaga … accctctctggcccggtctgctgcctccag	
Exon 3	Exon 3	139	GTACAAAGGCTTCATCAAGGACTGCCCCAGTG GGCAGCTGGATGCGGCAGGCTTCCAGAAGATC TACAAGCAATTCTT**CCCGTTCGGAGACCCCAC CA**AGTTTGCCACATTTGTTTTCAACGTCTTTG AT**GAAAACAAG**	**V1R**
Intron 3-4	Intron 3-4	1,754	gtgagctggggattgatggggcctgcggca … actgaggcaatcccctctctcctgtcag	**V2R**
Exon 4	Exon 4	79	**GACGGGCGAATTG**AGTTCTCCGAGTTCATCCA GGCGCTGTCGGTGACCTCACGGGGAACC CTGGATGAGAAGCTACGGT	

Tab. 4 **NCS1 Gene sequence from ensembl genome browser [47] and NCBI Nucleotide [69] from 5' upstream sequence to exon 4 (of 8 total exons)**
Alignment of the intron and exon sequences arrangements of NCS1 Var1 and Var2. Exon sequences are shown in upper case print, intron sequences in lower case print. Only the first and last 30 bases are presented for each intron. Beginning Exon 2 the two variants share the same sequence. Primers used to detect mRNA of Var1 (V1F & V1R) are shown in purple. Primers used in qPCR to detect mRNA of Var2 (V2F & V2R) are shown in green. For plasmid construction a longer primer was used (V2FPC), the additional 8 bases are underlined. The complement of the reverse primer sequences were reverse transcribed using reverse complement software [I 18]. As Exon 1 of Var2 is within the intron sequence 1-2 of Var1 it was decided to use a non overlapping (2 Exon spanning) primer as forward primer for Var1 to maintain the greatest specificity possible. For Var2 on the other hand, an overlapping forward primer(V2F) was chosen partly due to mRNA specific amplification and partly due to the shortness (<20bp) of Exon 1 Var2.

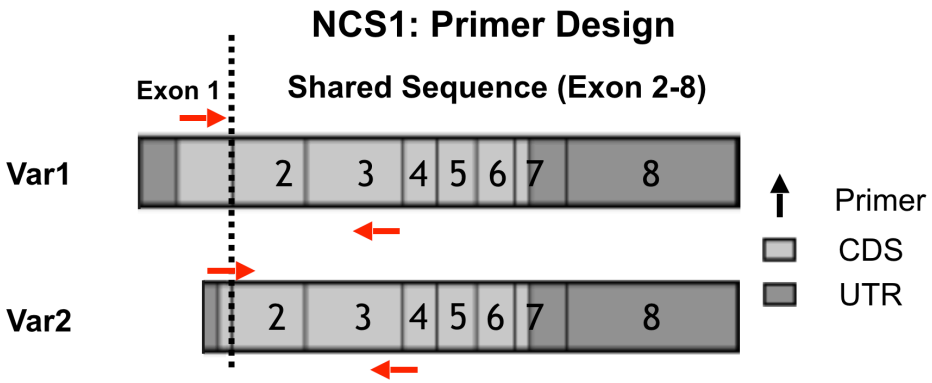

Fig. 6 **Schematic mRNA of NCS1 Var1 and Var2 and schematic primer alignment** (modified, also appeared in [182])
CDS connotes coding DNA sequence. UTR connotes untranslated region. The two variants share exon 2-8. Both primers amplify a target region of approximately 200bp (V1 186bp; V2 193bp).

2.2.4 RNA Extraction

RNA Extraction was performed using RNeasy Mini Kit (Qiagen) in accordance with manufacturer's guidelines ([I 6], (Apx-Fig. 2, p.101)).

Concept

Cells are lysed in RNases-inactivating guanidine-thiocyanate–containing buffer. Spin columns are used to get rid of contaminants and bind to RNA molecules that are longer than 200 nucleotides, thus excluding most rRNAs (e.g. 5S) and tRNAs. Ethanol provides appropriate binding conditions (Apx-Fig. 2, p.101).

Procedure

Old medium was aspirated from cell cultures of SH-SY5Y, HEK293 and MB231 75 cm^2 tissue culture flasks and cells were gently washed using ~5 mL PBS. Cells were gently displaced from surface using 5mL of fresh medium and pipetted into a 15 mL conical tube. Cell densities were determined and the volumes for $1x10^7$ cells were calculated. Cells were spun down at 300 rpm for 5 mins at 4 °C and 14 mL of supernatant was aspirated. The remaining cell pellets were solubilized through gentle pipetting and transferred into a 1.5 mL Eppendorf tube, then spun down again at 300 rpm for 5 mins at 4 °C. The remaining supernatants were completely removed and 600 μL buffer RLT for cell lysis was added. Samples were further homogenized by passing through a blunt 20-gauge needle for 10 times. After another centrifugation for 3 mins at 15,000 rpm the supernatants were transferred to 1.5 mL Eppendorf tubes and an equal volume of 70% ethanol was added to the cleared lysate and mixed. 700 µL of each sample (including precipitate, if formed) was transferred to an RNeasy column in 2 mL collection tube. Flow-through was discarded after centrifuging for 15 s at 10,000 rpm. 700 µL

of buffer RW1 was added to RNeasy spin column and centrifuged for 15 s at 10,000 rpm (flow-through again discarded). 500 µL of buffer RPE was then added to RNeasy spin column and centrifuged for 15 s at 10,000 rpm. After discarding the flow-through, 500 µL of buffer RPE was added to RNeasy spin column and centrifuged for 2 mins at 10,000 rpm. Flow-through was discarded. RNeasy spin columns were placed in new 2 mL collection tubes and centrifuged at 15,000 rpm for 1 min. RNeasy spin columns were placed in new 1.5 mL collection tubes and 40 µL RNase-free water was added to spin column membranes and centrifuged for 1 mins at 10,000 rpm. RNA yield was quantified using *NanoDrop*. Samples were stored at -80 °C.

2.2.5 Reverse Transcription

Reverse Transcription was performed using High Capacity cDNA Reverse Transcription Kit in accordance with manufacturer's protocol [I 7].

Concept

Reverse Transcription is a method used to generate DNA from RNA for downstream experiments like RT-PCR. Previously isolated and purified RNA molecules are used as templates by a reverse transcriptase which with use of (random) primers as a starting point generates complementary DNA strands (cDNA) under enzymatic consumption of added dNTPs. Since the resulting molecules are chemically indistinguishable from genomic DNA but do not contain intron sequences they represent the complementary strands to (usually) mRNA (in which the introns have been spliced out already). The convention is to call the reaction product of a reverse transcription cDNA. Due to the molecular specifics of RNA there are several approaches for an initiation point of the reverse transcription reaction (Apx-Fig. 5, p.103 & Tab. 5).

Primer	Mechanism of action	Advantage	Limitation
Oligo(dT) primers	Deoxythymidines that anneal to poly(A)tails of eukaryotic mRNA	Specific for mRNA	No detection in non-poly(A)tail RNA (e.g. prokaryotic or micro RNA)
Random primers	Random base sequences (hexamers)	Potentially universal (rRNA, tRNA etc.)	Not suitable for too long RNA templates
Gene-specific primer	Specific design for known sequence	Most specific	Extra effort to be designed and added

Tab. 5 **Advantages and limitations of primer concepts in reverse transcription**

Procedure

Kit components and RNA samples of SH-SY5Y, HEK293 and MB231 cells were thawed on ice; all pipetting steps were performed on ice. RNA samples were diluted to a working concentration of 0.1 µg/µL. Reverse transcription (RT) master mix was prepared as shown in Apx-Tab. 1, p.103. 10 µL of RNA sample was pipetted to 10 µL of RT master mix and centrifuged to get rid of air bubble and facilitate the mixing process. Reaction conditions are shown in Apx-Tab. 2, p.103. Concentration was measured using *NanoDrop*.

2.2.6 Polymerase Chain Reaction (PCR), Touchdown PCR, Gradient PCR, Colony PCR

2.2.6.1 PCR in general

Polymerase Chain Reaction (PCR) is a method used to enzymatically amplify specific DNA segments using heat stable polymerases such as *Taq*-Polymerase. *Taq*-Polymerase comes from the thermostable bacterium *Thermus aquaticus* and has an optimum working activity around 75 - 80 °C. The enzyme synthesizes a DNA strand following a complementary leading strand using desoxyribonucleotid-triphsophate molecules (dNTP; cleaving a pyrophosphate residue). To begin enzymatic activity *Taq*-Polymerase needs to bind to a short double stranded DNA segment which is provided through a specific oligonucleotide (primer) that is added to the reaction setup.

PCR reactions usually consist of three repeated steps: *denaturation*, when hydrogen bonds of double stranded DNA are disrupted because of high temperatures >90 °C; *annealing*, when primers bind to single stranded DNA (lower temperatures around 50-60 °C) and *elongation*, when *Taq*-Polymerase adds dNTPs to the free 3'-OH residue of the newly made complementary strand.

Taq-Polymerase has a nontemplate-dependent terminal transferase activity that adds a single deoxyadenosine (A) but provides no proof reading function.

2.2.6.2Touchdown PCR (TD-PCR)

The three repeated cycles during a PCR differ mainly in time (duration) and temperature during each step; there are, however, other aspects like e.g. Mg^{2+} concentration in the reaction setup. Especially the annealing temperature influences sensitivity and specificity of the PCR reaction. If the annealing temperature is too low, primer binding may be less specific and other DNA regions may be amplified as well. On the other hand an annealing temperature that is

chosen too high may result in no product at all as the energy within the reaction prevents primers from binding. As a rule of thumb annealing temperatures of 3-5 °C below primer specific melting temperature T_m (T_m is the temperature at which 50% of DNA is denatured; mainly determined through GC content of the primers) are often chosen in the beginning.

Touchdown PCR uses this theoretical concept by starting with a high annealing temperature which is gradually reduced during the following PCR steps. Thus in the beginning only the most specific binding region is amplified. Throughout the processes the amount of template of interest (correct template) grows relatively larger allowing more binding and reduced temperatures in the process. After ~10-15 cycles annealing temperature is set back to the ideal (and set) annealing temperature for the remaining cycles (20-25 cycles). The occurrence of nonspecific products is reduced. The more remaining cycles are left in the PCR reaction after touchdown the more nonspecific product may reoccur as (ideally) each step doubles the amount any given product. Touchdown PCR is especially useful if primer homology with the target sequence is unknown (DNA fingerprinting) or if products with only minor differences are investigated.

2.2.6.3 Gradient PCR

Gradient PCR is used to determine the optimum annealing temperatures for a PCR reaction. The heat block of a thermal cycler can be set to form a gradient during annealing (e.g. in a cycler with 8 sample tubes having 50 °C during annealing in the first reaction tube and 64 °C in the last and temperature gradually increases by 2 °C per tube). After setting up equal reaction volumes and visualizing PCR products using gel electrophoresis, the optimum annealing temperature can be determined (brightness of the band at the product size of interest and/or possible nonspecific amplification products; additional bands).

2.2.6.4 Colony PCR

Colony PCR is a quick method to determine the presence or absence of insert DNA in plasmid constructs in transformed bacterial colonies. After a transformation (2.2.10) a single colony can be picked using a sterile pipette tip and added to a PCR reaction setup as template. During the high temperatures of denaturation plasmids are released. Specific primers can bind to those plasmids and amplify an inserted DNA region which may be visualized on an electrophoresis gel (2.2.7 & 7.3). This, however, only shows whether or not a product of desired size is made

and not whether the sequence itself is correct. In order to rule out point mutations or verify correct insertion sequencing has to be performed (2.2.12).

Procedure

To test the designed primers for NCS1 Var2 *touchdown PCR* was performed as described in Apx-Tab. 3, p.104 & Apx-Tab. 4, p.104. Amplification products were analyzed using gel electrophoresis (Apx-Fig. 6, p.97). *Gradient PCR* was performed (conditions: Apx-Tab. 3, p.104 & Apx-Tab. 5, p.104) after which an ideal annealing temperature of 55 °C was estimated (Apx-Fig. 7, p.97).

2.2.7 DNA Gel Electrophoresis

To visualize amplified PCR products and investigate nonspecific amplification or primer dimer samples were run on an agarose gel.

Agarose gels were freshly cast using 100mL of TAE buffer and 1-3 g agarose (depending on required gel). TAE buffer and agarose were mixed in an Erlenmeyer flask and heated in a microwave. 5 μL of intercalating ethidium bromide (interestingly, originally developed to treat trypanosomiasis) was added. The gel was poured into a solidifying chamber containing a comb for well formation. Gels were allowed to solidify for 20-30 mins. Samples were run next to a 1 kb plus DNA ladder (Apx-Fig. 4, p. 97). Prior to loading, samples were visualized using DNA Gel Loading Dye. If not declared otherwise gels were run 30 mins at a current of 100V.

Limits: Detection limit of Ethidium Bromide bound to DNA is estimated to be between 0.5- 5.0 ng/band.

2.2.8 Agar Plates

500 mL molecular water, 12.5 g LB powder and 7.5 g Bacto Agar powder were mixed and autoclaved for 60 mins. Flasks were allowed to cool for 20 mins before antibiotics were added (50 mg ampicillin). 25 mL of liquid agar were poured per Petri dish and left for 30 mins to solidify. Plates were stored upside down at 4 °C.

2.2.9 Cloning

Cloning was performed using TOPO TA Cloning Kit (Apx-Fig. 3, p.102) in accordance with manufacturer's protocol [I 8].

Concept

The TOPO TA Cloning Kit contains a linearized plasmid vector (Apx-Fig. 3, p.102) with a single 3´-thymidine overhang at each end and a covalently bound Topoisomerase I. PCR products of reactions using Taq polymerase contain single

deoxyadenosine (A) at their 3´ ends due to a terminal transferase activity that is inherent to Taq. Topoisomerase I catalyzes and mediates covalent ligation between the 3′- phosphate of the plasmid vector and the 5′-hydroxyl of the original PCR product (Apx-Fig. 3, p.102).

Procedure

PCR products were made using the primer pairs for NCS-1 Var 1 (V1F and V1R; 186bp product, 2.1.3.2) and NCS-1 Var 2 (V2FPC and V2R; 193bp product, 2.1.3.2). Reaction setups were equal to those described in (Apx-Tab. 3, p.104) and cycling conditions as described in (Apx-Tab. 5, p.104) using a fixed annealing temperature of 55 °C. Products were visualized (Apx-Fig. 8, p.98). Linearized pCR2.1-TOPO plasmid vector and PCR products were gently mixed together in an Eppendorf tube and incubated for 5 mins at room temperature. Transformation was performed.

2.2.10 Transformation

Concept

A transformation is a form of horizontal gene transfer with non-viral introduction of exogenous DNA to a host organism, usually (competent) bacteria, with the intention of multiplying the inserted DNA in the course of bacterial growth.

Bacteria are plated on antibiotic containing agar plates and successfully transformed bacteria are selected through resistance genes (encoded on the transformed DNA plasmids).

Procedure

E. coli DH5α cells were thawed on ice and 45 µL aliquots were gently mixed with 40 ng of DNA plasmids and left on ice for 30 mins. Subsequently, cells were heat shocked in a 42 °C bath for 30 s and put back on ice to cool down for 2 mins. 400 µL of SOC medium was added and shaken for 1 h at 220-250 rpm at 37 °C. Bacteria were then plated on ampicillin agar plates (100 µg/mL) and incubated at 37 °C for 12-16h. A *colony PCR* (2.2.6.4) was performed to confirm the expression of plasmid DNA, as well as insertion of the correct sized fragments.

2.2.11 DNA Plasmid Amplification and Purification

Concept

Successfully transformed bacterial colonies are picked and incubated in growth medium. Bacteria are lysed and the lysate is cleared by centrifugation. DNA is

isolated by adsorption to a membrane and eluted after several washing steps. Commercial kits were used for DNA Plasmid Amplification and Purification [I 5].

Procedure

For small amounts of DNA a colony was incubated in 3 mL of LB medium and shaken at 200 rpm at 37 °C for 8 h. For larger amounts starter cultures were incubated in 150 mL of LB medium and shaken for 16 h. Purification was performed according to manufacturer's protocol [I 5].

2.2.12 DNA Sequencing

All DNA sequencing was performed as automated fluorescent sequencing with random incorporation of fluorescent dye labelled ddNTPs by the Yale School of Medicine, W.M. Keck Foundation and was fee-based [I 23]. DNA sequence files were analyzed using *4Peaks* [I 22].

2.2.13 Quantitative Polymerase Chain Reaction (qPCR)

Concept

A quantitative polymerase chain reaction (qPCR; also known as real-time polymerase chain reaction) is a method based on PCR (2.2.6) that monitors DNA amplification in real time as opposed to assessment at the end of the reaction (conventional PCR). qPCR can be used to (semi-)quantify the amount of DNA molecules within a certain probe.

Depending on the chosen method it is possible to assess absolute or relative quantification. While absolute quantification determines an absolute number of copies, relative quantification is used to detect fold changes among different samples. In absolute quantification an unknown amount of sample is compared to a standard curve and a value is extrapolated. In relative quantification results are compared to those of a housekeeping gene and a fold change is obtained.

A common method to assess the amplification is through intercalating fluorescent dyes that non-specifically bind to double-stranded DNA (dsDNA) molecules. The increase of double stranded target DNA at the end of each elongation phase correlates with the increase of fluorescence.

A melting curve analysis at the end of the experiment allows distinction between fluorescence obtained from the actual target sequence and fluorescence from nonspecific amplification or large primer dimers (both consisting of dsDNA and thus also binding the fluorescent dye). A melting curve is the graphic depiction of

detected fluorescence changes during dissociation of dsDNA during denaturation through continuous heating. A melting curve depends mainly on the length of the product as well as the GC-content within the sequence (GC = 3 hydrogen bonds; AT = 2 hydrogen bonds), making it specific for each PCR product.

Procedure

Samples of SH-SY5Y, HEK 293 and MB 231 cell line cDNA libraries were prepared (2.2.4 & 2.2.5). Primer pairs V1F and V1R were used to amplify the cDNA region spanning nucleotides 87–273 of NCS-1 Variant 1; Primer pairs V2F and V2R were used to amplify he cDNA region spanning nucleotides 3–196 of NCS-1 Variant 2 for each cDNA library sample (Fig. 6, p.25). The setup for a single 20 μL amplification reaction is shown in (Apx-Tab. 6, p.104) and was put together according to manufacturer's protocol [I 11]. A 7500 Fast & 7500 Real-Time PCR System was used for all qPCR amplifications [I 4]. The thermocycling conditions were slightly modified from manufacturer's protocol as described in (Apx-Tab. 7, p.105). Melting curves were obtained after the final elongation.

All samples were tested in triplicates. A 96-well plate layout was chosen as depicted in (Apx-Fig. 9, p.105). Standard curves for NCS1 variant 1 and NCS1 variant 2 were generated using plasmid DNA of a known amount (2.2.2) of 5000000 copies/well with a 5 fold serial dilution factor (Fig. 13, p.44). The range of each standard curve spanned six points. Confirming primer specificity the highest and lowest amount of plasmid DNA used for the standard curves were each tested against the non-corresponding primer pair, e.g. 5000000 copies/well (and 1600 copies/well) of Variant 2 plasmid DNA were put to react with V1F & V1R primers.

2.2.14 Protein Stability Assessment

2.2.14.1 Protein purification (performed by Baisheng Wang and Larry Huynh)

Protein was produced and purified as described in [18] and [182].

2.2.14.2 Stability Assessment

In order to assess protein stability at room temperature for isothermal titration calorimetry (ITC) and circular dichroism measurements 10 μL of purified NCS-1 protein (100 μM) variant 1 and variant 2 were pipetted into 2 x 13 Eppendorf tubes and left at room temperature for 0 – 12 & 24h. Before gel loading samples were stored at -80°C. After the last samples were obtained 5 μL of each sample was added to 5 μL of BlueJuice and loaded to a precast polyacrylamide gel along side

a protein ladder. The gels were run at 180 V for 1 h and washed 3 times for 5 mins. The gels were covered in *SimplyBlue SafeStain* for 1 h and kept in ultrapure distilled water overnight.

2.2.15 Western Blotting

2.2.15.1 Cell Lysis

6-well plate cultured cells were washed in ice cold PBS. One of three lysis buffers (RIPA; SDS; mPER) and protease inhibitor cocktail (1:100) were administered to the cells and shaken on a belly dancer shaker for either a short period (1 min) or a long period (5 min). Lysate was scraped off the 6-well plates and collected in Eppendorf tubes. Eppendorf tubes were either spun down at 4 °C with 14.000 rpm for 5 mins (spin) or whole cell lysate was used. In spun Eppendorf tubes supernatant was collected. 10 µL of each tube content was used to perform a BCA assay to determine the loading volume for the consecutive gel electrophoresis.

2.2.15.2 Extracting and lysing mouse tissue

Mice were anesthetized using isoflurane and sacrificed using cervical dislocation. Abdominal skin, cerebellum and kidneys were isolated and flash frozen in liquid nitrogen. Protein was later homogenized using 500 µL RIPA buffer and protease inhibitor cocktail. After homogenization samples were spun down at 4 °C with 14.000 rpm for 10 mins, supernatant was collected and BCA-assays were performed to determine protein concentrations.

2.2.15.3 Gel Electrophoresis

Sample buffer and reducing agents were added to the sample tubes and boiled at 95 °C for 10 mins. Gels were pre-run at 100 V for 10 mins. Samples and protein ladder were loaded and 180 V current was applied for 45 mins.

2.2.15.4 Transfer (wet)

Transfer-sandwich consisting of cassette, sponge, 2 filters, PVDF-membrane, gel, 2 filters, sponge, cassette was put together in transfer buffer and transfer was performed in ice at 100 V for 2 h.

2.2.15.5 Antibody Incubation

A *Ponceau* stain was performed to determine transfer efficacy and rinsed from the membrane with methanol. Depending on the observed protein the membrane was

cut, washed with PBS for 3 times and blocked with milk (blocking solution) for 1 h. Primary antibody (2.1.4) was added and shaken on a belly dancer at 4 °C overnight. Before and after incubation with secondary antibody for 2 h, membranes were washed with 5% milk in TBST 4 times for 10 mins.

2.2.15.6 Protein Detection

Super West Dura was applied according to manufacturer's protocol [I 2] and cassettes with x-ray films were exposed for different durations (1s — overnight).

2.2.16 Assessment of functional differences and Paclitaxel Sensitivity in stably transfected Cells

2.2.16.1 Stable expression of NCS-1 variants in SH-SY5Y cells (performed by Baisheng Wang)

SH-SY5Y cells were transfected with either NCS1 Var1 plasmid (+ HA-tag), NCS1 Var2 plasmid (+ Flag-tag) or an empty vector control using *Lipofectamine 2000*. Plasmids contained a resistance gene for Geneticin (G418). An optimal selection concentration of 1 mg/mL G418 was established. Cells were split after 24-48 h after transfection and colonies were picked after approximately 4 weeks. Western blot analysis was performed to check correct protein expression (Fig. 12, p.43).

2.2.16.2 Functional differences and drug sensitivity assessment (in collaboration with Baisheng Wang)

After counting stably transfected SH-SY5Y cells, they were plated to a 96-well plate and monitored in an *IncuCyte* incubator in 5% CO_2 at 37 °C. In accordance with the manufacturers' instructions [I 12] each well was monitored and four pictures were taken every 2 h. Pictures were analyzed for confluence.

In a separate experiment different amounts of PTX were added to 100 µL (single well) of the growth medium (0ng, 30ng, 70ng, 100ng, 300ng, 500ng).

2.2.17 Genotyping (PCR)

Mice were weaned 3 weeks after birth. Around the time of weaning, ears were ID tagged with metal clips (Apx-Fig. 10, p.106) and small pieces of the ears were clipped off using a sterile pair of scissors. Ear tissue was collected in labelled Eppendorf tubes and genotyping was performed through DNA extraction, amplification and gel electrophoresis.

REDExtract-N-Amp Tissue PCR Kit was used [I 9]. 50 µL of extraction buffer and 12.5 µL tissue prep were added per sample and mixed by vortexing. Extraction sat at room temperature for 10 mins and was boiled at 95 °C for 3 mins. 50 µL of neutralization buffer was added and samples were vortexed. Amplification reactions were performed using the settings according to Apx-Tab. 8, p.106 & Apx-Tab. 9, p.106. Primers (2.1.3.1) were purchased from Yale Keck Foundation—Oligo Synthesis Resource. Fig. 6 shows a schematic depiction of genomic mouse DNA, primer binding sites and Lox P sites. Electrophoretic separation after amplification generates a 514 bp band for homozygous knockout mice, a 398 bp band for wild type mice, and both bands if tissue was heterozygous [I 16]. Pictures of genotyping electrophoresis gels of all of mice used for the experiments are attached (Apx-Fig. 11, Apx-Fig. 12, & Apx-Fig. 13, pp. 98-100)

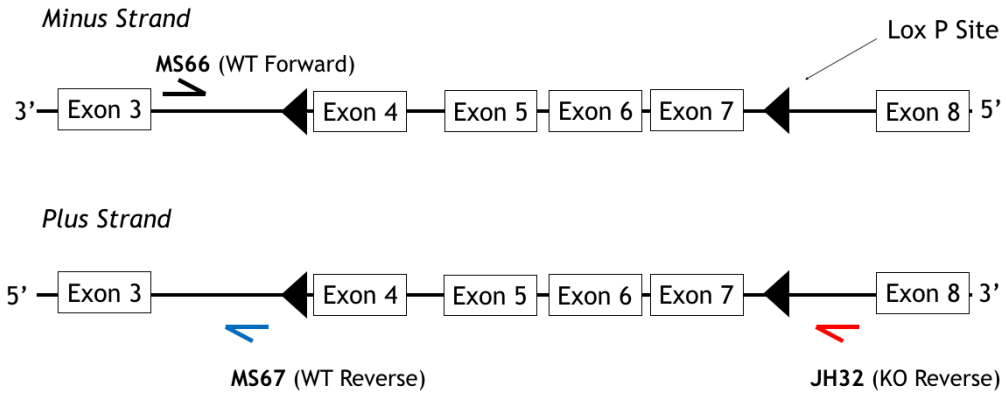

Fig. 7 **Schematic depiction of genomic mouse DNA and NCS1 primer binding** adapted from [128]
MS66 & JH32 generate a 514 bp amplification product (KO band, top, s. for example p.99). MS66 & MS67 generate a 398 bp amplification product (WT band, bottom, s. for example p.99). In heterozygous mice both bands are found after amplification. Knockout mice were generated using the CreLox-System (CRE=creates recombination; LOX P = Locus of X-over P1 Bacteriophage). (Asymmetric) Lox P sites (◀) are pointing in the same direction, indicating deletion [128] & [I 16].

2.2.18 Electrophysiology

2.2.18.1 Nerve conduction studies (NCV) at baseline

Female C57Bl/6 mice were genotyped as described in 2.2.17. Nerve conduction measurements of the tail nerves were performed with subdermal needle electrodes and a *Nicolet Viking Quest apparatus* [I 14]. Experimental setup is illustrated in Fig. 8, p.36. In total, 29 mice were investigated (WT (N=6); HET (N=15); KO (N=8)). Measurements of all mice were performed 3 separate times on

different dates by two investigators and the means and standard errors of the mean were calculated. One investigator (*Larry Huynh*) handed out the mice in random order while the other investigator (*Göran Boeckel*) performed the measurements. Parameters like age [181], weight and tail length were collected before each measurement (Tab. 6, p.50). Anesthesia was enabled with constant flow of isoflurane 2–2,5% [I 15], [129] and external body temperature was maintained with a heating pad.

Per definition, *orthodromic* refers to the physiologic conduction direction, i.e. proximal to distal for motor impulses and distal to proximal for sensory impulses. In *antidromic* conduction the electrical impulse travels in the opposite direction of normal physiologic conduction. For antidromic sensory (and orthodromic motor) measurements, the stimulating cathode (black, Fig. 8) and anode (red; Fig. 8) were placed 5 mm apart along the proximal length of the nerve. Recording and stimulating electrodes in the tail were placed 40 mm apart [137]. Needle electrodes were cleaned with 70% ethanol between animals. For sensory conduction evaluation both antidromic and orthodromic measurements were performed [178]; orthodromic measurements were carried out for motor. Impulses were delivered *supramaximally*, i.e. the current was increased to the point where action potential amplitudes no longer increased in size (+20%) (all nerve fibers excited).

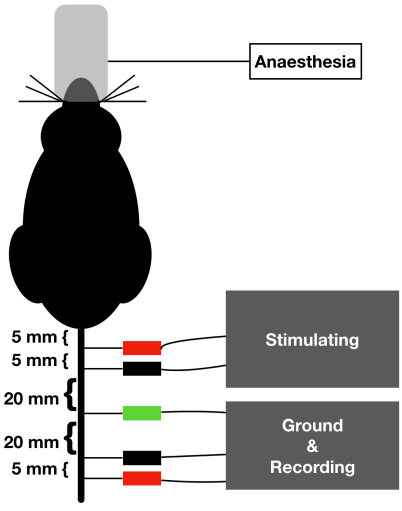

Fig. 8 **Schematic model of tail nerve conduction measurement.**
For *sensory nerves* the image represents antidromic stimulation; for motor nerves, orthodromic stimulation. For orthodromic sensory stimulation a reverse order (top to bottom) of inserted electrodes was chosen. Ground (green); stimulator cathode (black) and anode (red).

Electroneurography is sensitive to both myelin sheath and axonal changes. While the conduction velocity is largely dependent on myelination, the amplitudes of action potentials are used to determine axonal integrity. The sum of motor action potential amplitudes is called the *compound muscle action potential* (CMAP, Fig. 9), the corresponding for sensory nerve action potential (SNAP) can be determined similarly. Action potential amplitudes were measured from baseline to peak (Fig. 9) and ranged in the mV spectrum for tail motor action potentials (TMA) and in the μV spectrum for sensory. *Latency* is the time interval between an onset stimulus and the onset of response. Two latencies were recorded: peak latency and onset latency measurements [89] (Fig. 9). While onset latency represents the fasted fibers of a compound response, it is usually also more prone to artifacts than peak latency, see *Discussion*. *Tail sensory nerve conduction velocity (TSNCV)* was calculated from the obtained latencies with the formula:

***TSNCV* = d/t** [m/s], with

d = the distance between stimulus and recording electrodes (40mm) and

t = the latency, either onset latency or peak latency in [ms]

The motor conduction velocity is the speed of the conducting motor axons in the stimulated nerve. Because of the multiple parts involved in motor stimulation (i.e. axon to neuromuscular junction, neuromuscular junction transmission time and depolarization time of the muscle) it is usually assessed using two stimulation sites (instead of only one, as was done for sensory measurements). To avoid complicated or inaccurate velocity determination for motor, the tail distal motor latency (TDML) was analyzed directly (as done in [74, 170, 181]).

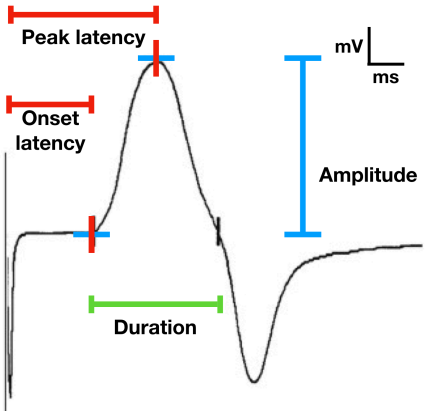

Fig. 9 **Example of an electroneurographic recording**
Latencies are time intervals between onset stimulus and the onset of response in ms (red). The amplitude (blue) is the maximal height of the (tail motor) action potential from baseline to peak (in mV or in case of sensory μV).

2.2.18.2 NCV in PTX treated mice

A total of four mice (2 KO; 2 WT, Tab. 8, p.54) were injected with PTX according to 2.2.19. NCV was repeatedly performed with the instructions described above (2.2.18.1). The first 4 NCV measurements were carried out before the start of injections and then repeated for 6 times on a weekly basis (Fig. 10).

2.2.19 Paclitaxel treatment

2.2.19.1 PTX dilutions (in collaboration with Larry Huynh)

PTX dosage and dilutions were prepared mostly following instructions in [110] as well as the PTX product information sheet [I 13]. 5 mg PTX were dissolved in 1,25 mL of ethanol. 1,25 mL of Cremophor EL were added to gain a stock solution of PTX 2mg/mL (50:50 Ethanol: Cremophor EL). 300 μL of PTX stock were dissolved in 2700 μL 0,9% saline to obtain a 0,2 mg/mL PTX solution for injection.

2.2.19.2 PTX injections (in collaboration with Larry Huynh)

2 KO and 2 WT mice were weighed each time before injections were prepared. Injections of a PTX dosage of 4,5 mg/kg body weight were administered intraperitoneally to each mouse (as done in [110]). In total, four injections were administered over 7 days (Fig. 10). Injection volumes ranged around ~420 μL depending on the weight and were rounded to one decimal place for each mouse and injection time. Mice were sacrificed 6 weeks after the first injection and dorsal root ganglia (DRG), sciatic and tibial nerves were isolated.

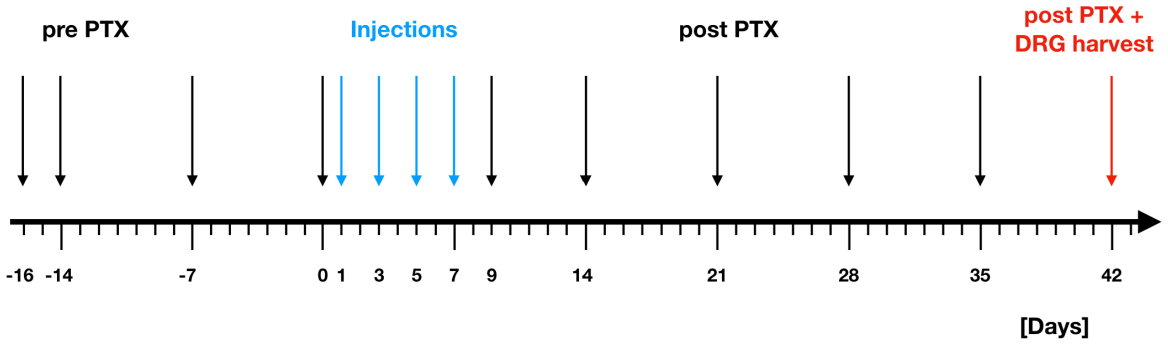

Fig. 10 **Experimental timeline for NCV and PTX injections.**
NCV measurements(vertical black arrows) were performed 4 times before and 6 times after a total of 4 PTX injections (blue arrows). On day 42 after the first injection mice were sacrificed and DRGs and sciatic nerves were harvested (red arrow).

2.2.20 DRG, Sciatic & Tibial Nerve Isolation

(in collaboration with Larry Huynh)

All tissue harvesting was performed under a hood. After the last NCV measurement, mice were anesthetized with 3% isoflurane. Ears were clipped for

consecutive protein analyses and mice were positioned on their back with spread out fixed extremities. The thoracic cavity was opened with a sterile pair of surgical scissors and access to the beating heart was dissected. A blunt needle was inserted into the left ventricle near the apex towards the aorta and the heart was perfused (~2 drops/s) with *perfusion solution* (2.1.2). After 3 mins perfusion was switched to *fixation solution* (2.1.2). Pale discoloration of liver and kidneys served as positive control for successful perfusion. Mice were doused in 70% ethanol before dissection.

2.2.20.1 Sciatic nerve and tibial nerve isolation

The skin alongside the hind leg was cut open and the sciatic nerve was identified and prepared along its distal course. Distal branches of the sciatic nerve (N. tibialis) were dissected and stored in labelled tubes. The proximal sciatic nerve was dissected and stored in labelled tubes. Procedure was repeated on the contralateral leg.

2.2.20.2 Dorsal root ganglia (DRG) isolation

The back skin was removed beginning with a small incision in the pelvic area. The head was cut at the base of the skull. The spinal column was isolated beginning with a small incision at the lateral abdominal wall and through the ribs parallel to the spinal column on both sides. The internal organs on the ventral side of the spinal column were removed. Femurs were cut and muscle and fat tissue was removed from the spinal column. The spinal canal was cut in the sagittal plane and the spinal cord was extracted. Meninges were removed and DRGs were collected in labelled tubes.

2.2.21 Transmission Electron Microscopy (TEM)

2.2.21.1 Picture generation (performed by Klara Szigeti-Buck)

DRGs and sciatic nerves were fixed and dissected as described in 2.2.20 before being embedded into blocks and sectioned for TEM analysis. The author of this work observed the process, however, all pictures were commercially and randomly generated by Klara Szigeti-Buck, who was blinded in that she was not informed about the detailed research question. Pictures were generated with AMT Camera System.

2.2.21.2 TEM image analysis

TEM pictures were analyzed using the Image-J software [155]. A minimum of 50 axons per animal and locus were analyzed, as done in similar studies [159, 183].

2371 fibers/axons were analyzed in total. Apx-Tab. 10, p.106 represents the amount of nerves that were analyzed per mouse and area. Per picture, all axons that were completely depicted were analyzed, i.e. fibers that were only partially in the picture were excluded. Fiber and axonal (minimum diameters and) perimeters were selected manually and areas measured from the enclosed pixels (by Image-J). Axon and fiber areas were then used to calculate the diameter for ideal (round) areas ($A = \pi r^2$) [23, 159]. The advantage of this approach is the more realistic estimation of (artificially) compressed fibers, where a direct measurement of diameter would underestimate the true diameter. The disadvantage of this method is the artificial skewing of data, due to an oblique projection angle of fibers. To avoid artificial skewing of data (and thus an overestimation of true diameters) minimum diameters can be analyzed directly, as done in [132, 183]. Both methods were investigated and an *area based approach* was chosen to make results more comparable to similar studies using the same approach [23]. Myelin area was calculated from fiber and axon areas [myelin area= fiber area- axon area]. Myelin sheath thickness and g-ratio were calculated from diameters [Myelin sheath thickness= (fiber diameter - axon diameter)/2]; [g ratio = axon diameter / fiber diameter].

2.2.22 Statistical analysis

Visualization of statistical results and tests were done using GraphPad Prism [I 19] and Numbers Version 5.3 (5989). To make results more comparable means ± standard error of the mean (SEM) are the default representative of analyzed data, regardless of the distribution. Medians are presented within the box-and-whisker-plots.

2.2.22.1 qPCR

Analysis was performed with the 7500 Fast & 7500 Real-Time PCR System software [I 4]. Standard curve points were generated with a 5 fold serial dilution. Each curve spanned 6 points. According to manufacturer's instructions C_T values were defined as the PCR cycle number at which the fluorescence level equaled the threshold. **C_T values** between 8 and 35 were desired (<8 too much template in the reaction; >35 amount of target in the reaction too low; background noise). **R^2 values** (correlation coefficients) were generated by the software and are defined as a measure of the closeness of fit between the regression line and the individual C_T data points of the standard reactions. A value of 1.00 indicates a perfect fit

between the regression line and the data points. An R^2 value >0.99 is desirable [I 4]. Means and standard deviations were calculated from triplicate measurements of C_T values.

2.2.22.2 Nerve Conduction Measurements Baseline

Box-and-Whisker plots are expressed in the style of Tukey, i.e. the box extends from the 25th to 75th percentiles (inter-quartile distance, IQR); whiskers are presented at 1,5 times IQR; points greater than 1,5 times IQR are plotted as individual points; analogously for the bottom 25th percentile. The median is presented as line within the box.

For the baseline measurements (no PTX treatment), all genotypes (wild type, heterozygous, and knockout) were analyzed. Structural equality of the analyzed groups was accounted for by selection (i.e. only female mice were analyzed to eliminate a potential sex confounder) and one-way ANOVA with the Holm-Sidak post-hoc test if normal distribution was assumed after a Shapiro-Wilk normality test or Bonferroni-Dunn post-hoc test for samples which failed a Shapiro-Wilk normality test. Statistical significance was considered for $p < 0,05$.

2.2.22.3 Nerve Conduction Measurements PTX treatment

Data are graphically presented as mean ± SEM. Over the course of the experiment several measurements at ten different time points were made (Fig. 10, p.38).

To facilitate analysis, different time points are summarized in three groups (baseline = the first four measurements before PTX injections; middle = measurements at days 5-7 and late= measurements at days 8-10). A Two-way ANOVA (two factor ANOVA) was performed (genotype; time). Sidak's test was used to correct for multiple comparisons (as recommended by GraphPad Prism 8).

2.2.22.4 Electron Microscopy (EM)

After failing Shapiro-Wilk normality test, knockout (KO; NCS-$1^{(-/-)}$) and wild type (WT; NCS-$1^{(+/+)}$) mice were tested using using non-parametric Mann-Whitney test. Multiple testing for dorsal root ganglion, sciatic nerve, and tibial nerve was accounted for by Bonferroni-Dunn post-hoc test. Statistical significance was considered for $p < 0,05$. Furthermore, axon diameters and myelin sheath thickness are depicted as box-and-whisker plots, expressed in the style of Tukey (*2.2.22.2*).

3. Results

3.1 Characterization of a second variant of NCS-1

3.1.1 NCS-1 variants can be identified and expressed

3.1.1.1 Identification of a second NCS-1 variant

The Ensembl genome browser [47] and the National Center for Biotechnology Information (NCBI) database [69] describe a total of three transcripts (or splice variants) for NCS-1 in humans. All transcripts are located on chromosome 9 and carry the annotation *NCS1-201*, *NCS1-202* and *NCS1-203* [47].

NCS1-202 does not code for protein. The two other transcripts, *NCS1-201* (NCS1 Var1; coding for *NCS-1 Variant 1*) and *NCS1-203* (NCS1 Var2; coding for *NCS-1 Variant 2*), consist of 8 exons, of which exons 2 – 8 are identical (Fig. 11). Exon 1 of NCS1 Var2 was identified towards the 3' end of intron 1–2 (of NCS1 Var1; specific starting point = 9:130,200,432). While exon 1 of variant 1 contains 150 bp, the alternative exon is significantly shorter with only 19 bp.

The coding sequence (CDS) of either variant, i.e. the sequence of the mRNA that is ultimately translated into protein, does not contain exon 8 and merely parts of exon 1. The resulting proteins differ in size (190 amino acids vs. 172 amino acids), as well as N-terminal sequence. Essentially, the first 22 amino acids are substituted for 4 amino acids in variant 2 (Fig. 11).

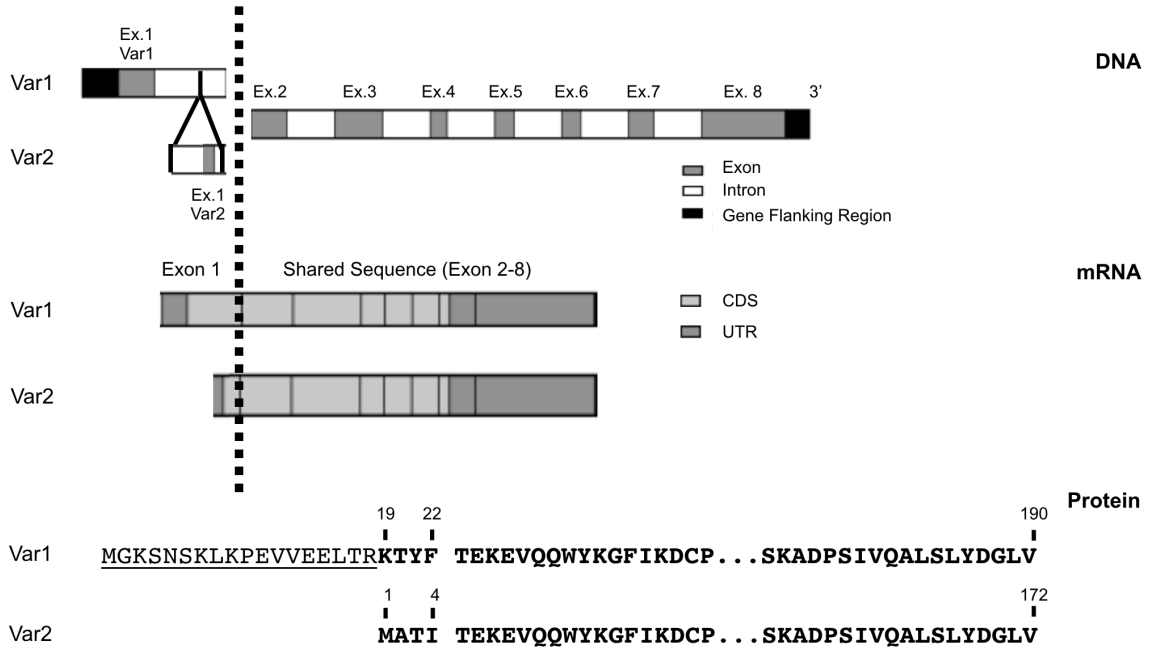

Fig. 11 **Neuronal Calcium Sensor 1 Variant Alignment**
The human NCS1 gene consists of 8 exons that code for a 190 amino acid protein. An alternative exon 1, coding for an alternative mRNA towards the 3' end of intron 1–2

(variant 1) was identified. Exon 1 differs in significantly in size (19bp vs. 150bp). Parts of exon 1 and exon 7 together with exon 2–6 are part of the coding sequence (CDS), whereas exon 8 is not translated. The 22 N-terminal amino acids of NCS-1 Var1 are substituted for four amino acids in NCS-1 Var2 (one letter code).

3.1.1.2 Expression of NCS-1 variant 1 and variant 2

Human neuroblastoma cells of the cell line SH-SY5Y were transfected with plasmids containing either NCS1 Var1 or NCS-1 Var2 as described above. Two distinct bands in western blot analysis represent the two variants (Fig. 12). For further distinguishability plasmids contained additional tags (HA for var1; Flag for Var2). Either protein variant ranges around 21kDa. The human cell line SH-SY5Y is capable of expressing both variants.

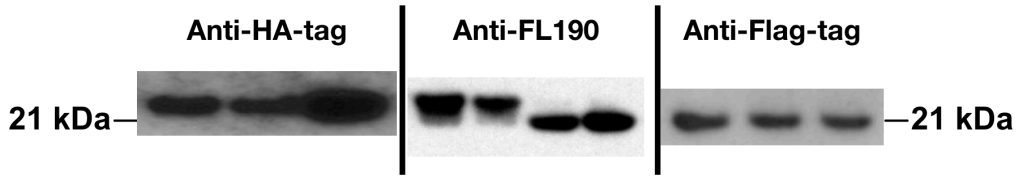

Fig. 12 **Expression and western blot detection of NCS-1 variants**
Western blots of SH-SY5Y transfected with a vector expressing NCS-1 Var1 or Var2. Each lane denotes a different SH-SY5Y clone. The panels represent different experiments. Left panel probed with anti-HA antibody (NCS-1 Var1 is HA-tagged). Right panel probed with anti-FLAG antibody (NCS-1 Var2 is FLAG-tagged). Middle panel probed with FL190, an anti-NCS-1 polyclonal antibody.

3.1.2 NCS-1 Variant 1 is the predominant transcript found in human cell lines

The high homology of both NCS1 variants' sequences necessitated primer design with emphasis on the distinctive sequence of exon 1 (2.2.3). Non-specific amplification of genomic DNA (gDNA) was avoided with *exon 1 — exon 2*-junction spanning primers; furthermore amplification products of both primers showed single sharp bands, indicating a clean amplification reaction and high specificity of each primer pair (Apx-Fig. 8, p.98). Target regions were designed in similar length (just below 200bp) to provide similar amplification efficiencies.

Standard curves were generated as described in 2.2.13 and showed a linear trend for the the log of the copy number and the cycle threshold (C_T) (Fig. 13, p.44). The closeness of fit between the regression line and individual C_T data points was considered valid as correlation coefficients (R^2) of R^2_{Var1}= 0.996 > 0.99 and R^2_{Var2}= 0.998 > 0.99, allowed quantification of the two transcripts.

The highest and lowest copy numbers of either NCS1 variant plasmid, i.e. 5000000 copies/well and 1600 copies/well, were mismatched with the non-

corresponding primer pairs: (V1F + V1R with Var2-plasmid) and vice versa (V2F +V2R with Var1 plasmid). Both cases presented C_T values which lay significantly above the highest points of either standard curve (independent points in Fig. 13). Mismatch resulted in the same amplification regardless of primer pairs and starting template amount. The variant specific amplification of the chosen primers was especially emphasized in wells with the high starting material, where at least 20 cycles lay between mismatch and primer specific amplification (right part of Fig. 13). In conclusion, the results support the specificity of the primers and allow quantitative comparisons of the two variants of NCS-1.

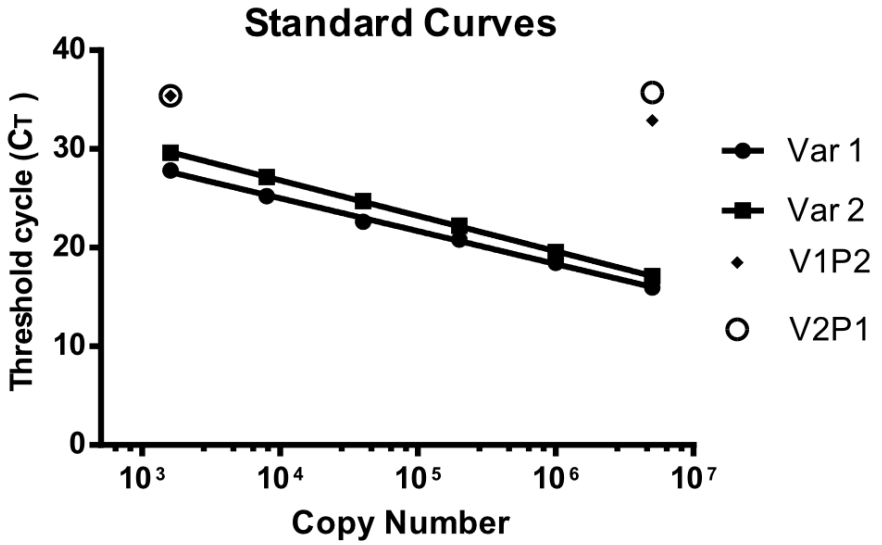

Fig. 13 **Standard curve variant quantification**
Standard curves for NCS1 Var1 and NCS1 Var2. The log of the copy number (X-axis) is shown in relation to cycle threshold (C_T) (Y-axis). Standard curves show a linear trend. Primer specificity was analyzed by mismatching templates (NCS1 plasmids) and primers, i.e. NCS1 Var1 plasmid NCS1 Var2 primers (V1P2) and vice versa (V2P1). In each case the primer mismatch cycle threshold (C_T) value lies significantly above the highest C_T value of either standard curve.

The cDNA libraries of SH-SY5Y, MB231, and HEK293 were tested using RT-PCR. All three human cell lines expressed transcripts of both NCS1 Var1 and NCS1 Var2 (Fig. 14, p.45). Furthermore, relative amounts of either NCS1 variant mRNA were compared. Limitations of mRNA detection were established through plasmid DNA controls: primer pairs matching the plasmid DNA (e.g. V1F + V1R and Var1 plasmid) were used to determine ideal amplification conditions, and thus a maximum expected expression (Fig. 14, 1st and 4th bar from left, p.45); a mismatch of primers and plasmid DNA (e.g. V1F + V1R and Var2 plasmid) was used to determine a lower limit for the detectability of the variants (Fig. 14, 2nd and 3rd bar

from left). For a reaction setup as described in Apx-Tab. 6, p.104 a lower detection limit for mRNA expression of ~100 copies/well was obtained from the mismatch control (Fig. 14, 2nd and 3rd bar from left). The C_T of these mismatch controls was >35 and independent of the amount of starting template and was thus considered background noise (2.2.22.1).

For each cell line tested, the NCS1 Var2 mRNA levels were approximately 1000 fold lower than NCS1 Var1 transcripts (Fig. 14, right bars), showing that NCS1 Var1 is the predominant transcript in the cells tested.

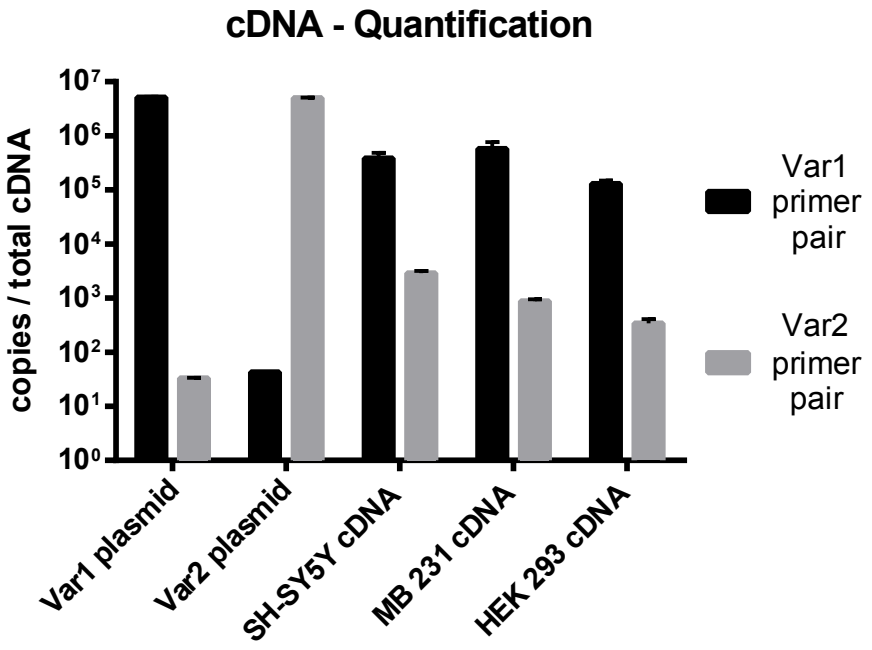

Fig. 14 **Quantification of NCS-1 variants cDNA of human cell lines**
cDNA quantification of NCS-1 in human cell lines SHSY5Y, HEK 293 & MB 231. Template DNA is depicted on the X-axis the log of copies per total cDNA is depicted on the Y-axis. Bars represent means with SD. Each point was done in triplicate. NCS1 Var1 and NCS1 Var2 differ in expression by approximately 3 log units. NCS1 Var1 plasmid and NCS1 Var2 plasmid serve as controls, the four bars on the far left show the maximum and minimum values for C_T. The mismatch primer controls give a lower limit for interpretation (second and third bar from the left).

3.1.3 Purified NCS-1 Variant 1 and Variant 2 are stable for at least 12 hours at room temperature

Some biophysical assays like e.g. isothermal titration calorimetry (ITC) require protein stability for prolonged periods of time at room temperature. It was necessary to provide evidence that purified NCS-1 variants are stable, at least for the estimated time of such assays. Thirteen samples of either variant were collected as described in 2.2.14.2 and results are shown in Fig. 15, p.46. Both

variants are stable for at least 12 hours, there was, however, some evidence of degradation for variant 2 after 24h.

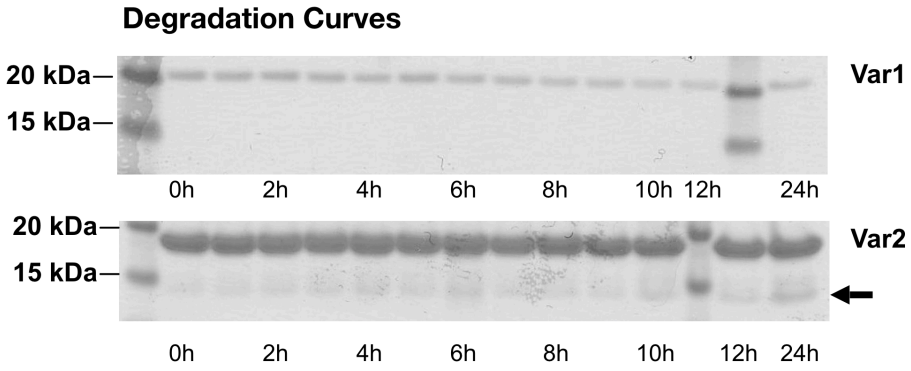

Fig. 15 **Degradation curve of either NCS-1 protein variant**
NCS-1 Var1 and NCS-1 Var2 were purified and incubated at room temperature to analyze protein stability. Lane 1 in both panels as well as lane 14 (top panel) and lane 13 (bottom panel) show molecular weight markers. Both variants are stable for at least 12 hours. There are signs of degradation of NCS-1 Var2 after 24 hours (arrow).

3.1.4 NCS-1 Variant 2 was not detected in human cell lines

Transcript amounts of either NCS1 variant showed significant differences in different cells. To evaluate NCS-1 protein quantities *in vivo*, western blot analysis was done. Known amounts of purified NCS-1 Var1 and NCS-1 Var2 were used along with positive controls and demonstrated that the polyclonal anti-NCS-1 antibody FL190 is capable of binding both isoforms (Fig. 16, p.47, first lane from left). Three human cell lines (SH-SY5Y, MB231 & HEK293) were probed as well as corresponding mouse tissues lysates (cerebellum, breast skin, kidney).

Online databases the NCBI [69] and Ensembl genome browser 83 [47] indicate the existence of a possible second variant protein only in humans (whereas tissue from other species only show a sequence that is thought to go through nonsense mediated decay). Mouse tissue lysates (Fig. 16, lane 5-7, p.47) were used as negative controls to distinguish potentially degraded (and thus presenting with a lower molecular weight) NCS-1 Var1.

NCS-1 Var1 was detected in all 3 human cell lines and all 3 mouse tissues (Fig. 16, p.47). Not surprisingly, neuronal & neuron-related cells as well as neuronal tissue expressed higher amounts of NCS-1 Var1 which is displayed through relative darkness of the cerebellar and SH-SY5Y bands (Fig. 16 lane 4 and 7, p.47). NCS-1 Var2 was not detected in either the human cells or the C57Bl/6 mouse tissue.

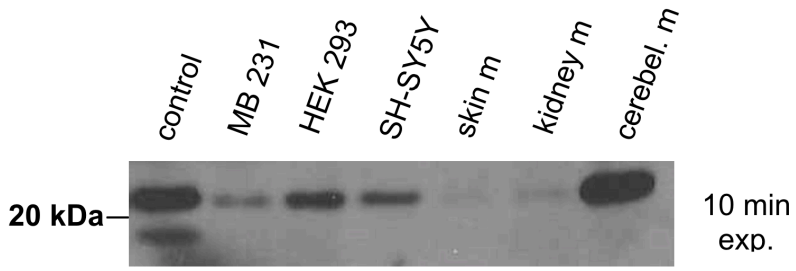

Fig. 16 **Expression of NCS-1 variants in cell lines and mouse tissue lysates**
Representative western blot of NCS-1 Var1 expression in human cell lines (SH-SY5Y, HEK 293, MB 231) and mouse tissue lysates. Polyclonal anti-NCS-1 antibody FL190 was used. Known amounts of purified NCS-1 Var1 and NCS-1 Var2 protein were used in Lane 1 as positive controls. Tissue lysates served as negative controls. Each lane was loaded with 35 µg of protein. Only NCS-1 Var1 is identified in all cell/tissue lanes.

Demonstrating that methodological factors were not responsible for loss of NCS-1 Var2, different conditions and protocol changes were tested in SH-SY5Y cells. Three different lysis buffers (RIPA, SDS, mPER) were used to investigate potential lysis mediated decay. To avoid a potential discarding of protein by spinning of lysates (membrane adherence because of myristoylation 1.2.1.1) sample preparations were altered: spun down supernatant and whole cell lysates (Fig. 17, *spin* vs *whole*) were used. Boiled at 95°C for 5 mins or unboiled (Fig. 17, *odd numbered lane* vs *even numbered lane*) were compared. Different film exposure times were chosen; 5 mins and overnight (Fig. 17 *top* vs *bottom* panel).
Even though differences concerning those variables could be identified, indicated by the relative darkness differences of NCS-1 Var1 bands, NCS-1 Var2 was not detected in SH-SY5Y cells.

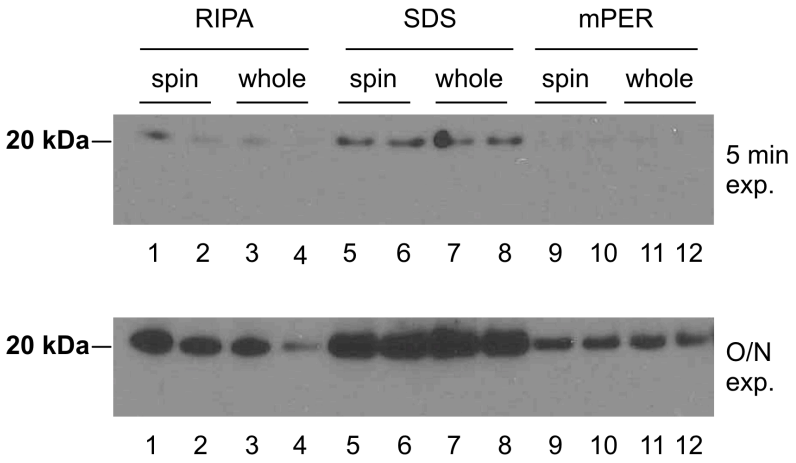

Fig. 17 **Western blot troubleshooting conditions**
Conditions tested included: three lysis buffers (*RIPA, SDS, mPER*), sample preparations (spun down supernatant collection (*spin*) or whole cell lysate (*whole*)), sample boiling at 95°C for 10 mins before loading (odd numbered lanes) or loading without boiling (even numbered lanes), and film exposure times (*5 min* or overnight (*O/N*)). NCS-1 Var2 was not detected in SHSY5Y5 cells.

3.1.5 Over-expression of either NCS-1 variant does not alter cell growth

3.1.5.1 Cell growth without PTX

Experiments related to this work found a significantly lower Ca^{2+}-binding affinity of recombinant NCS-1 Var2 compared with NCS-1 Var1 [182]. Because of the wide spectrum of cellular pathways that are affected by Ca^{2+}-signaling, functional differences were expected from overexpression of either variant. To analyze the impact of either NCS-1 variant on cell growth, SH-SY5Y stably transfected with NCS1 Var1, NCS1 Var2 or an empty vector control were monitored for cell confluence.

No difference in cell growth rate was observed (Fig. 18), suggesting either a not-significant impact of NCS-1 on alteration of intracellular Ca^{2+} required for functional differences or an insufficient level of intracellular NCS-1 concentration.

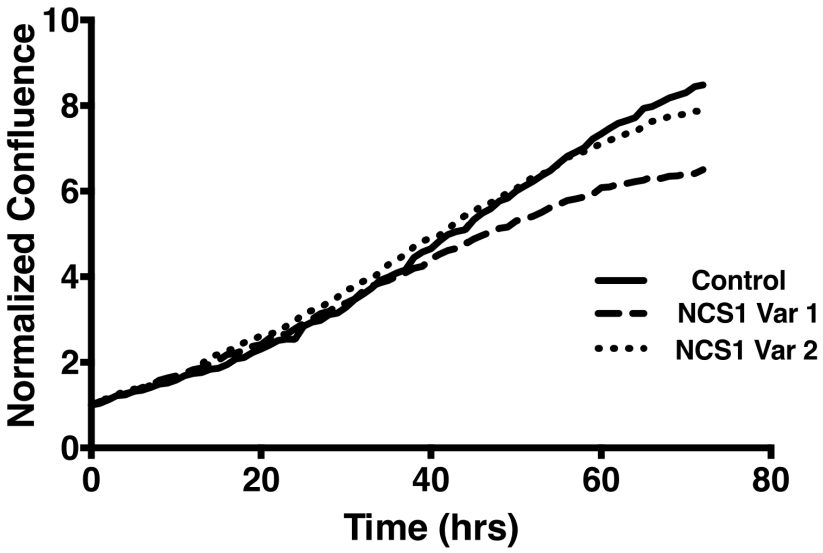

Fig. 18 **Effect of NCS-1 variant overexpression on confluence**
Confluence (% of the area occupied by cells) was monitored in cells stably expressing NCS-1 Var1, NCS-1 Var2, or a vector control. Each measurement was normalized to the starting confluence (0 hrs). No difference in cell growth rate was observed.

3.1.5.2 Cell growth in the presence of PTX

Binding of NCS-1 Var1 to PTX was shown to mediate an increased release of Ca^{2+} from the ER [24]. In a similar setup as in 3.1.5.1 stably transfected cells were incubated with different concentrations of PTX and monitored for growth arrest (Fig. 19, p.49).

A concentration dependent relationship of PTX and cell growth (measured as relative reduction of confluence [ratio of % of the area occupied by cells after and before incubation with a certain PTX concentration]) was observed. However, no

difference was found for the rate of cell growth in the presence of PTX with regard to the type of overexpressed plasmids.

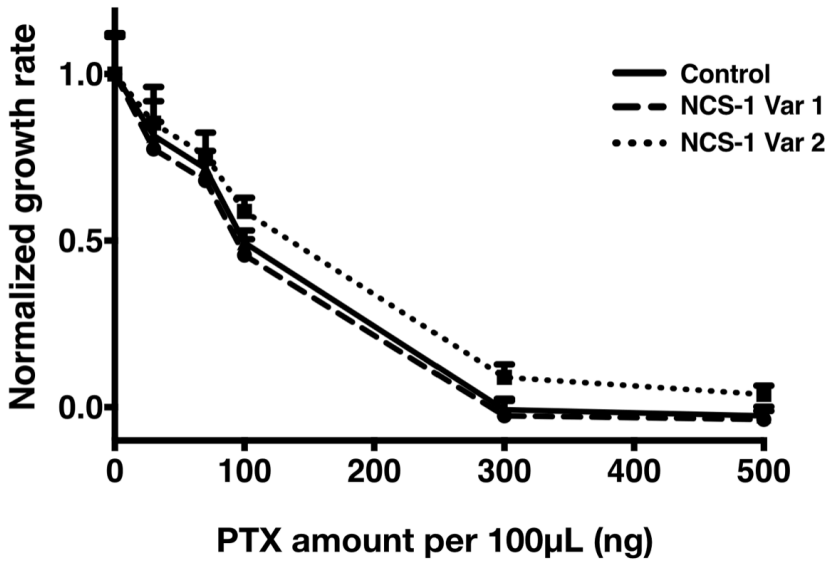

Fig. 19 **Effect of NCS-1 variant overexpression on PTX sensitivity**
Cell growth (depicted as function of normalized growth rate; ratio of % of the area occupied by cells after and before incubation with a certain PTX concentration) decreased with PTX concentration. Overexpressed NCS-1 variants did not change the cell's response to the addition of paclitaxel over the range of concentrations tested.

3.2 NCS-1's role in chemotherapy induced peripheral neuropathy

The most characteristic traits of CIPN are pain, numbness and tingling sensations. All of the above share a subjectivity that complicates objective evaluation and quantification of CIPN in patients, and even more in the mouse model. Several assays have been discussed which can be classified into electrophysiological, behavioral and histological measurements [23].

3.2.1 NCS-1 genotype does not alter nerve conduction assays at baseline

3.2.1.1 Baseline characteristics of the mice

Nerve conduction is altered in mice with CIPN after treatment with PTX [23]. PTX has been shown to mediate CIPN via an NCS-1 dependent pathway [24]. To further elucidate NCS-1's role in CIPN a total of 29 mice —NCS-1 wild-type (WT), heterozygous (HET), and knockout (KO)— were investigated using electrophysiological assays to identify potential electrophysiological alterations before PTX treatment.

The baseline characteristics of the mice are shown in Tab. 6. Nerve conduction has been shown to be age dependent in C57Bl/6 mice, however, no significant differences were detected between 4 and 20 months of age [181]. All investigated groups were structurally equal in terms of sex, age, weight, tail length and time under anesthesia.

Tab. 7, p.53 depicts the all conduction assay results presented as mean ± SEM.

Characteristic	WT (N=6)	HET (N=15)	KO (N=8)	adjusted p-value
Female sex — (%)	100	100	100	—
Age — months	7,0 ± 1,3	7,2 ± 1,1	6,3 ± 1,4	1,00 #
Weight — g	24,5 ± 2.1	23,7 ± 1,1	26,0 ± 2,5	1,00 #
Tail length — cm	8,0 ± 0,3	7,7 ± 0,1	7,7 ± 0,2	0,87 +
Time under anesthesia — min	26,9 ± 1,3	23,6 ± 1,3	25,5 ± 1,3	0,76 +

Tab. 6 **Characteristics of the mice used for nerve conduction measurements at baseline.** Female mice were grouped according to NCS-1 genotype: wild-type (WT), heterozygous (HET), and knockout (KO). Groups showed no difference in age, weight, tail length and time under anesthesia. Plus-minus values are means ± SEM. One way ANOVA with the Holm-Sidak post-hoc test (+) or Bonferroni-Dunn post-hoc test (#) was performed.

3.2.1.2 Nerve conduction velocity and latencies

Nerve conduction velocity (NCV) is the fraction of the traveled distance of a signal divided by the travel time (latency). In vertebrates NCV is highly determined by saltatory conduction which depends on myelin and by the axonal diameter. Consequently, the differently sized and differently myelinated axons result in a range of velocities, rather than a single, discrete value. To account for the range of velocities both, *onset* latencies (to investigate the fraction of fastest conducting fibers) and peak latencies (to analyze the average conducting fibers) were used to calculate tail sensory nerve conduction velocity. Evaluation of *onset* velocities is often used in clinical settings, as the fastest fibers tend to represent clinical findings (e.g. carpal tunnel syndrome) more accurately [89]. Determining the exact onset is more tricky and susceptible to artifacts than determining the peak latency. Furthermore, there are two different techniques of recording: antidromic or orthodromic [178], both of which were analyzed.

No differences were found in tail sensory nerve conduction velocities for the different NCS1 genotypes, regardless of technique (anti- or orthodromic) or analyzed latency (onset or peak) (Fig. 20).

As expected, onset latencies resulted in higher velocities than peak latencies. Furthermore, peak NCVs displayed less scattering than onset NCVs, a finding that is most likely due to the easier and more reliable identification of *peaks* rather than *onsets*.

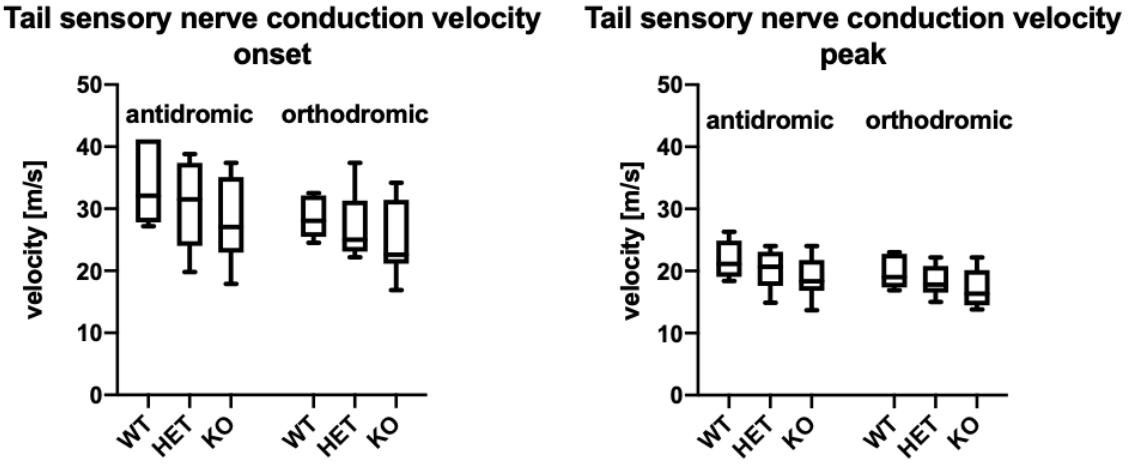

Fig. 20 **Baseline effect of NCS-1 genotype on tail sensory nerve conduction velocity (TSNCV)** Nerve conduction velocities of NCS-1 wild type (WT), heterozygous (HET) and knockout (KO) mice are presented as Tukey style box-and-whisker-plots. Take-off velocity represents the fastest conducting nerves/fibers (left panel). Peak velocity represents the average fibers (right panel). Measurements were performed antidromically and orthodromically. No statistically significant difference was observed among conduction velocities of the different genotypes. [n=6 (WT); n=15(HET); n=8 (KO)]

Due to the more complex measurements involving motor velocities, i.e. two stimulation sites are needed to calculate accurate motor nerve conduction velocity (final conduction time = proximal latency – distal latency), motor latencies were analyzed directly. Therefore, synaptic transmission is included in the measurement and times are given instead of velocities.

Again, no differences were found for tail distal motor latency (TDML) between different NCS-1 genotypes, regardless whether onset or peak latency was analyzed (Fig. 21). The tendencies derived from latencies are inverse to the velocities, i.e. the later the potential appears, the lower the velocity.

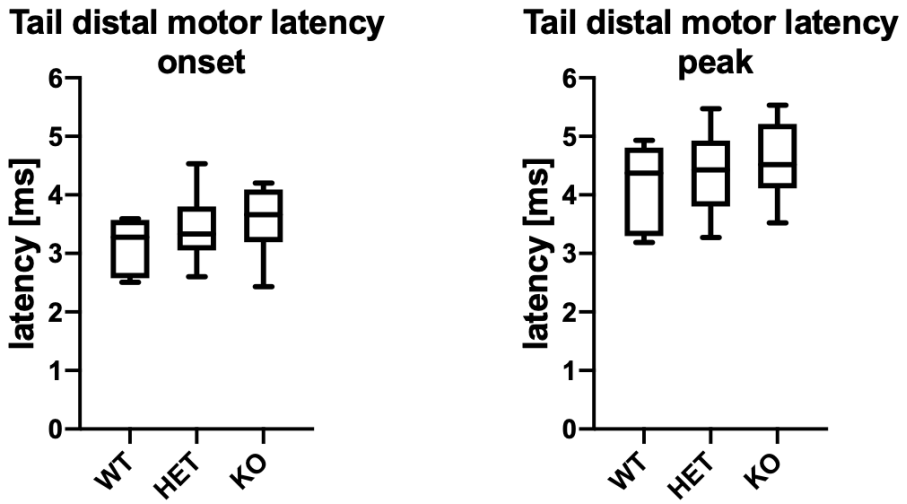

Fig. 21 **Baseline effect of NCS-1 genotype on tail distal motor latency (TDML)**
Tail distal motor latencies of NCS-1 wild type (WT), heterozygous (HET) and knockout (KO) mice are presented as Tukey style box-and-whisker-plots. Take-off latency represents the fastest conducting nerves/fibers (left panel). Peak latency represents the average fiber (right panel). Statistically significant differences were not observed among latencies of the different genotypes. [n=6 (WT); n=15(HET); n=8 (KO)]

3.2.1.3 Sensory nerve action potential & tail motor amplitude

While increases in latencies (and decreases in velocities) are indicative of demyelination, decreased amplitudes of nerve action potentials are usually associated with problems in axonal integrity. It is important to keep in mind that both sensory and tail motor amplitudes represent the summation of individual depolarizing fibers. Sensory fibers have lower thresholds to stimulation than motor fibers and while sensory responses to stimulation usually range between 1-100 μV, motor responses are substantially larger (mV range).

In the context of PTX the sensory nerve action potential (SNAP) was of special interest as axonal degeneration was observed as leading driver of PTX (and cisplatin) neuropathies [23]. No differences were found for the amplitudes of

SNAPs or compound muscle action potentials (CAMPs) between NCS1 genotypes (Fig. 22, p.53).

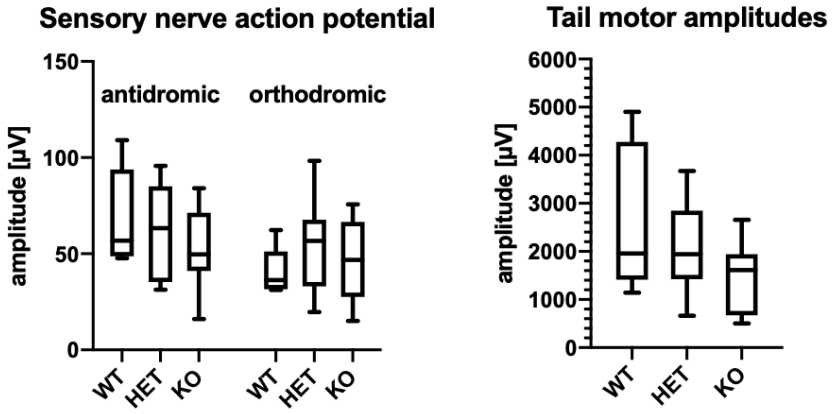

Fig. 22 **Baseline effect of NCS-1 genotype on summed action potential amplitudes**
Sensory nerve action potentials (left panel) and tail motor amplitudes (right panel) of NCS-1 wild type (WT), heterozygous (HET) and knockout (KO) mice are presented as Tukey style box-and-whisker-plots. Sensory measurements were performed antidromically and orthodromically. No statistically significant difference was observed among amplitudes of the different genotypes. [n=6 (WT); n=15(HET); n=8 (KO)]

Nerve conduction assay	WT (N=6)	HET (N=15)	KO (N=8)	adjusted p-value
Tail sensory nerve conduction velocity (onset; anti) [m/s]	28,5 ± 1,4	27,1 ± 1,2	24,9 ± 2,2	0,91
Tail sensory nerve conduction velocity (onset; ortho) [m/s]	33,6 ± 2,6	30,8 ± 1,7	28,2 ± 2,4	0,91
Tail sensory nerve conduction velocity (peak; anti) [m/s]	19,7 ± 1,1	18,5 ± 0,6	17,2 ± 1,1	0,91
Tail sensory nerve conduction velocity (peak; ortho) [m/s]	21,8 ± 1,3	20,3 ± 0,8	19,0 ± 1,2	0,91
Tail distal motor latency (onset) [ms]	3,1 ± 0,2	3,5 ± 0,1	3,6 ± 0,2	0,91
Tail distal motor latency (peak) [ms]	4,2 ± 0,3	4,4 ± 0,2	4,6 ± 0,2	0,91
Sensory nerve action potential (amplitude; anti) [μV]	68 ± 10,3	61,8 ± 6,0	51,3 ± 7,6	0,91
Sensory nerve action potential (amplitude; ortho) [μV]	40,9 ± 4,9	54,3 ± 6,0	46,1 ± 7,5	0,91
Tail motor amplitudes (amplitude) [μV]	2590 ± 632	2105 ± 224	1487 ± 262	0,73

Tab. 7 **Effect of NCS-1 genotype on nerve conduction at baseline**
Female NCS-1 were grouped according to genotype: wild-type (WT), heterozygous (HET), and knockout (KO). At baseline no differences in nerve conduction were observed, regardless of the of the method of stimulation (orthodromic=ortho vs. antidromic= anti). Onset and peak refer to the latency that was used to calculate the velocity. Values are means ± SEM, in contrast to the above Tukey style box-and-whisker-plots. One way

ANOVA with the Holm-Sidak post-hoc test (+) or Bonferroni-Dunn post-hoc test (#) was performed.

3.2.2 Nerve conduction assays failed to demonstrate a significant difference in PTX treated mice

3.2.2.1 Baseline Characteristics of PTX treated mice

To further elucidate the model of NCS-1 mediated CIPN, a 2x2 proof of concept study was conducted. Baseline characteristics of all mice used for this experiment as well as 3.2.3 are summarized in Tab. 8.

Characteristic	1343	1344	1345	1346
Genotype	WT	KO	KO	WT
Sex	female	female	female	female
Age — months	2.2	2.2	2.2	2.2
Weight — g (day 0)	16.45	21.51	21.68	20.05

Tab. 8 **Baseline Characteristics of the PTX treated mice.** Numbers in first line indicate mouse tag numbers.

3.2.2.2 Nerve conduction velocity and latencies

Tail sensory nerve conduction velocity was repeatedly measured before and after PTX injections using antidromic technique (Fig. 23). Both onset latencies and peak latencies were separately used for calculations. Regarding genotype, significant differences were not found in tail sensory nerve conduction velocity over the course of the experiment (p_{onset} = 0,99; p_{peak} = 0,93). The variation of individual mice suggests a potential problem concerning the sample size (n=2, for each genotype). Furthermore, a comparison of velocities within the genotypes suggested no effect of PTX whatsoever, which was not expected, as previous studies using similar dosing and injection schedules had reported a reduction of velocity by –8% ± 2% [23].

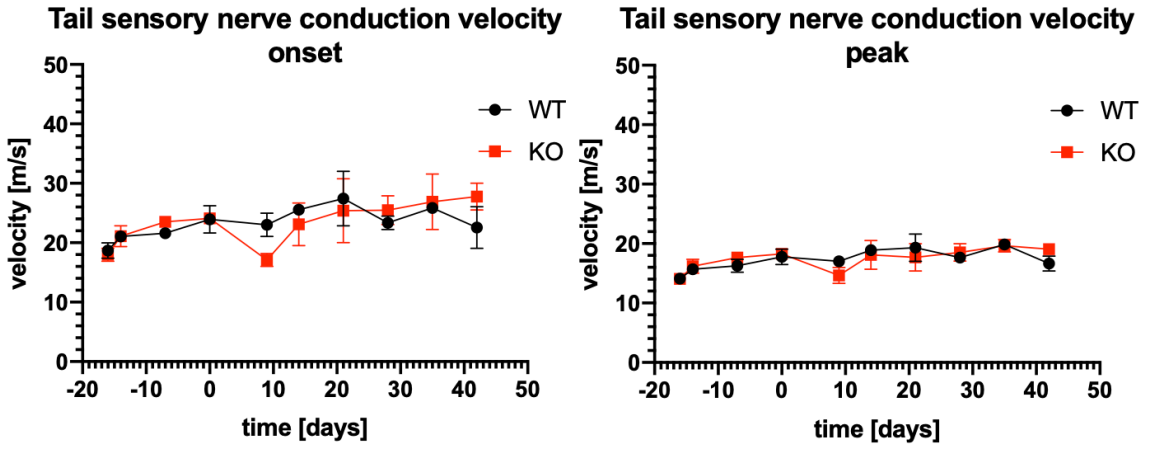

Fig. 23 **Course of TSNCV (onset & peak) before and after PTX treatment**

The TSNCV (antidromic technique) was repeatedly measured before PTX (days -16 – 0) and after PTX treatment (days 9 – 42). Injections were applied at day 1, 3, 5, and 7. Each point denotes the average TSNCV calculated either from onset latencies (left panel) or peak latencies (right panel). Whiskers represent SEM. Red (squares) = NCS-1 knockout; Black (circles) = NCS-1 wild type. [n=2, for each genotype]

Similarly, TDML was not different between genotypes over the time course (Fig. 24)(onset: *p*= 0,22; peak: *p*= 0,20). Latencies were virtually identical regardless of the target variable (onset or peak) and showed little variation before and after PTX treatment, suggesting only a subtle effect of PTX on myelination, if any, that could not be assessed in this small group of mice (n=2, for each genotype).

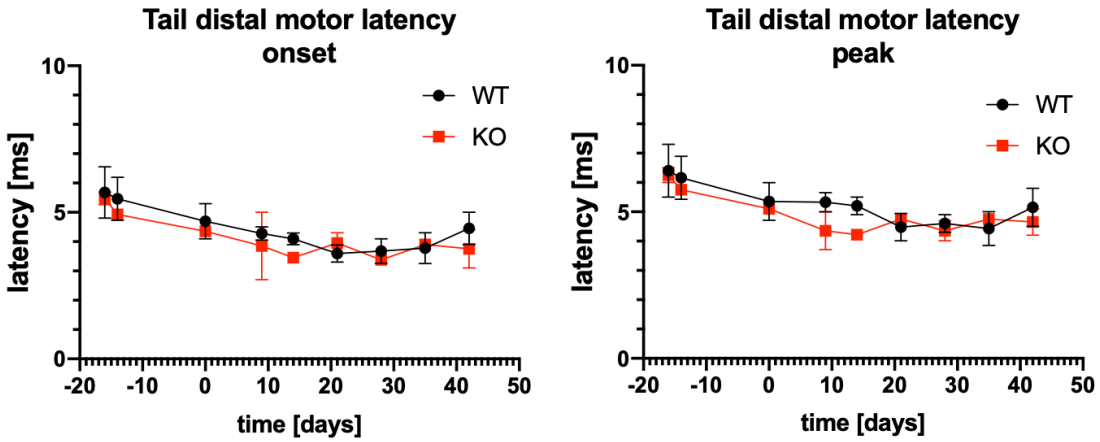

Fig. 24 **Course of TDML (onset & peak) before and after PTX treatment**
The TDML was repeatedly measured before (days -16 – 0) and after (days 9 – 42) PTX treatment. Injections were applied on days 1, 3, 5, and 7. Each point denotes mean TDML. Whiskers represent SEM. Red (squares)= NCS-1 knockout mice; Black (circles) = NCS-1 wild type mice. Time point 3 (day -7) is not presented due to a software failure.

3.2.2.3 Sensory nerve action potential & tail motor amplitude

While previous studies had found significant reductions in SNAPs over time after PTX [23], neither the amplitudes for sensory nerve action potentials nor for motor nerves changed significantly during the course of the experiment (Fig. 25, p.56) (SNAP: *p*= 0,79). TMA tended to decrease, if the first time point after the injections (day 9) is compared to day 0, (right panel, Fig. 25, p.56). However, the values recovered to control within a couple of days and did not decrease again. Differences between genotypes were not observed (TMA: *p*= 0,48).

The scattering increased after injections which suggests that potential effects of PTX may be observed with respect to action potential amplitude rather than velocities, which was more stable throughout the experiment. This is in line with previous observations of predominantly axonal pathology over demyelination. Again, the sample size is of concern and unfortunately low (n=2, each genotype).

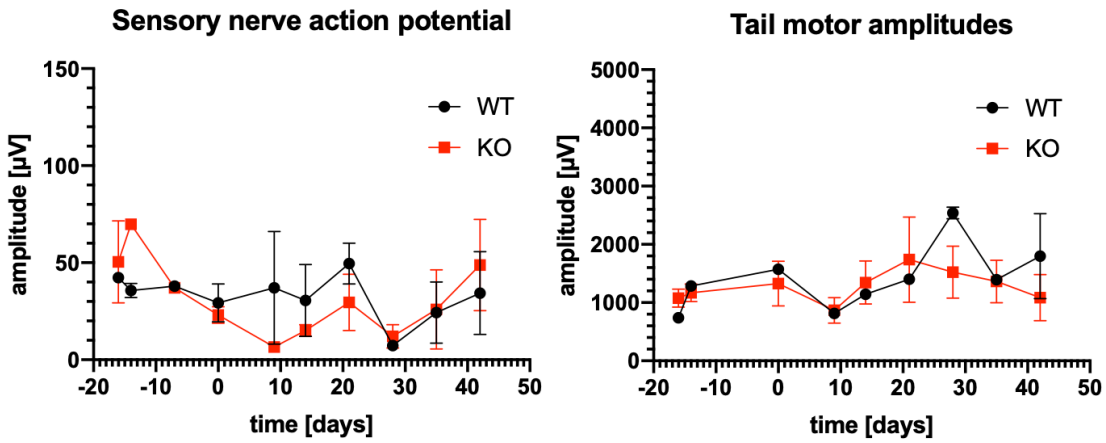

Fig. 25 **Course of SNAP & TMA before and after PTX treatment**
SNAP (left panel) and TMA (right panel) were repeatedly measured before (days -16 – 0) and after (days 9 – 42) mice were treated with PTX. Injections were applied on days 1, 3, 5, and 7. Each point denotes the mean SNAP/TMA. Whiskers represent SEM. Red(squares) = NCS-1 knockout mice; Black (circles) = NCS-1 wild type mice. Time point 3 (day -7) is not presented for motor (TMA) due to a software recording failure.

3.2.3 Electron microscopic analysis of PTX treated mice

To determine *quality* and *quantity* of ultra-structural changes after PTX treatment, animals were sacrificed and DRGs, sciatic nerves, and tibial nerves of both genotypes were harvested one month after the last PTX injection and investigated using electron microscopy (protocol: Fig. 10, p.38).

3.2.3.1 Quality of ultra-structural changes after PTX treatment

EM micrographs with various magnifications were screened for recurring signs of degeneration along the entire nerve (DRGs, sciatic and tibial nerves). Confirming previous reports [171], various stages of neuronal degeneration were observed in PTX treated mice (Fig. 26, p.57 & 107). All animals (WT & KO) showed signs of (predominantly) axonal degeneration, however, myelin decompaction and degeneration was also present. The axoplasm appeared shrunken and irregular with disintegrated amorphous granular structures. Furthermore, swollen intra-axonal mitochondria were observed (similar to previous reports [39, 40]). While in some myelinated fibers myelin seemed entirely intact, others expressed higher degrees of damage ranging from mild vacuolation to pronounced myelin decompaction and debris (Fig. 26, p.57).

3.2.3.2 Quantification of ultra-structural changes in DRGs and sciatic nerves after PTX treatment

For a *quantitative* assessment electron micrographs were analyzed using Image-J. Analogous to electrophysiological assessment (amplitude and latency/velocity) axon diameters (calculated from axon areas) as well as myelin sheath thickness

were of special interest (Fig. 27, p.57). Nerve fiber diameters (calculated from fiber areas) and g-ratios (= axon diameter / fiber diameter) were also investigated (Fig. 28 - Fig. 30, pp.58-61). G-ratio is commonly used to assess the degree (or integrity) of myelination [23, 39, 40, 183].

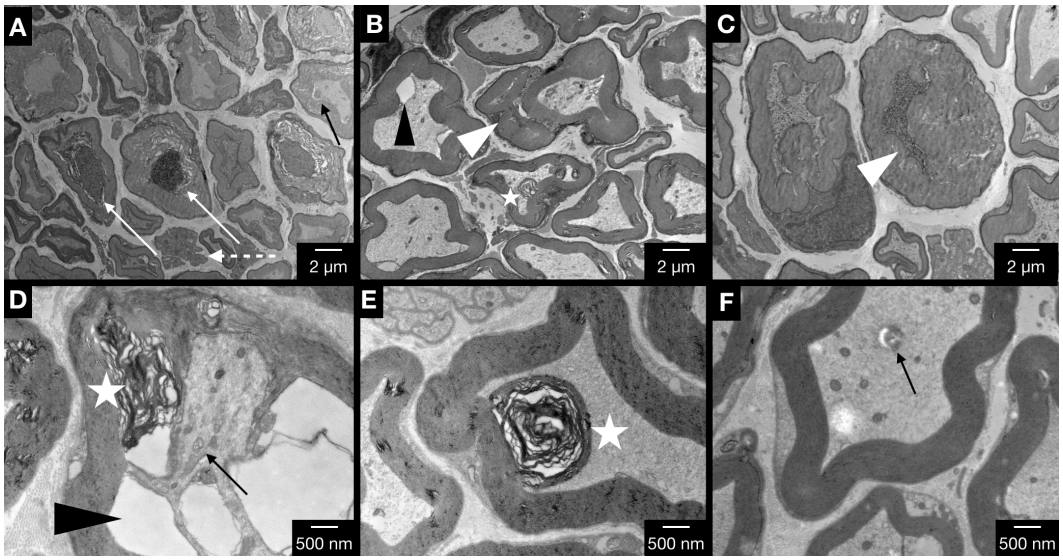

Fig. 26 **Morphologies of PTX induced neuronal degeneration (sciatic nerve)** After PTX treatment neuronal degeneration was observed in all mice, regardless of genotype. Various stages of both (predominantly) axonal degeneration and demyelination were found: **A**) Degenerated collapsing myelin profile following degeneration of axoplasm, which shows a disintegrated amorphous granular structure (white arrows). **B & C**) axoplasm has been cleared and the myelin is degenerating (white arrow head). **D**) Shrunken axon with widening of the periaxonal space, vacuolar disruption of the inner myelin layers (black arrow head; B & D). **E**) Myelin debris (white star; also found in B & D). **F**) Swollen intra-axonal mitochondria were observed (black arrow; also found in A & D). (enlarged on p. 107)

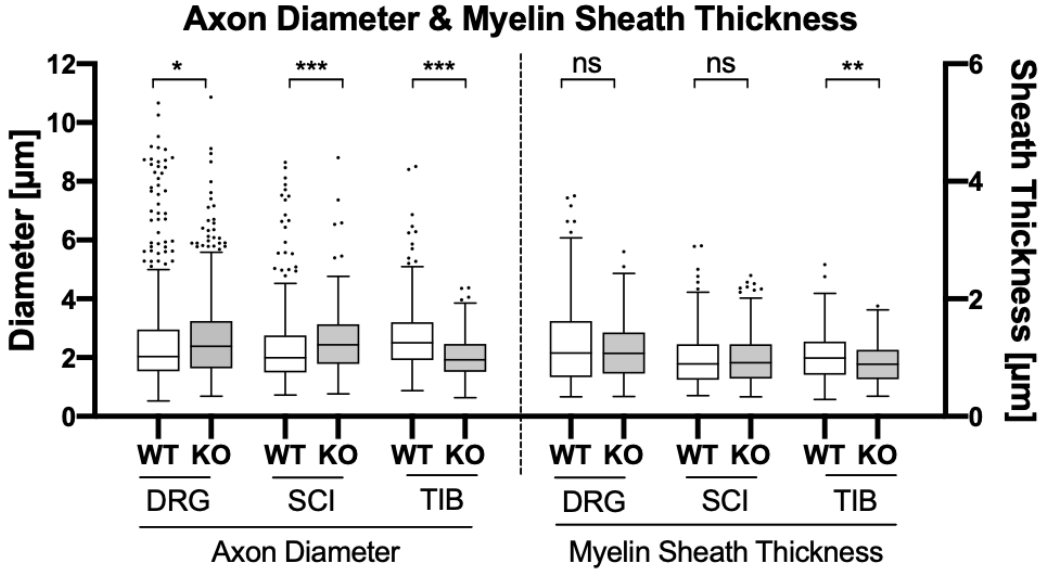

Fig. 27 **Distribution of axon diameter and myelin sheath thickness after PTX treatment** Tukey style box-and-whisker plot for axon diameter (left side) and myelin sheath thickness (right side). Wild type (=**WT**; NCS-1$^{(+/+)}$) and knockout (=**KO**; NCS-1$^{(-/-)}$) are directly compared for dorsal root ganglia (=**DRG**), sciatic nerve (=**SCI**), and tibial nerve (=**TIB**). Asterisks at the top of the figure report (adjusted) statistical significance: ns = $p > 0{,}05$; * = $p \leq 0{,}05$; ** = $p \leq 0{,}01$; *** = $p \leq 0{,}001$.

Because in the present study nerves were not obtained from untreated mice, control data were extracted from the literature [23]. Both genotypes (WT & KO) exhibited smaller axonal diameters after PTX than non-PTX treated animals. This diameter decrease was significantly larger in DRG and sciatic nerve axons of NCS-1 wild-type mice than in NCS-1 knockout mice (Fig. 27 — Fig. 29, pp.57-59). Myelin sheath thickness (and myelin area) of nerves from these regions were not different between the two genotypes.

These results are consistent with the electrophysiological findings (3.2.2) of an increased scatter of amplitudes after injections (Fig. 25, p.56) and seemingly unaffected latencies and velocities (Fig. 23, p.54 & Fig. 24, p.55). This supports the view of the predominance of axonal damage over demyelination after PTX.

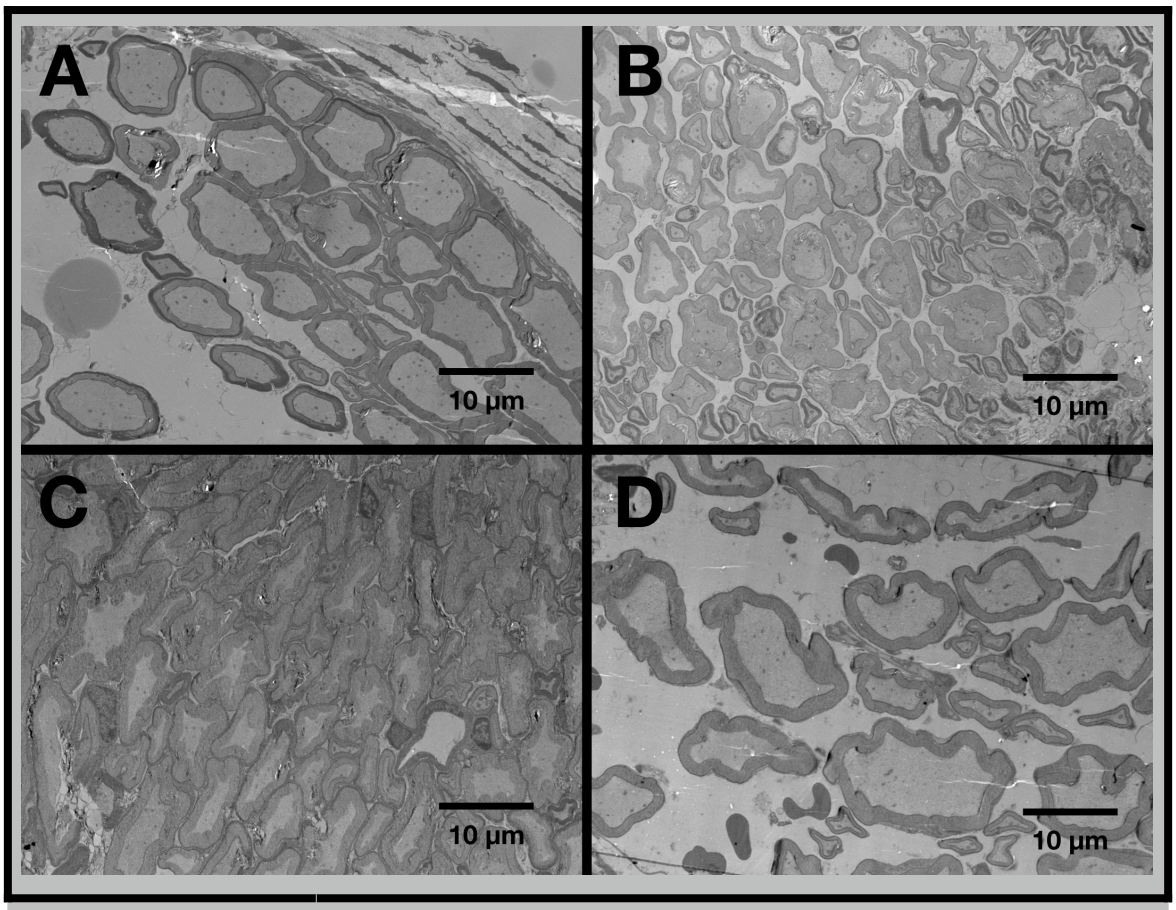

Assay	NCS-1$^{(+/+)}$ (=WT)	NCS-1$^{(-/-)}$ (=KO)	adjusted p-value
Axon diameter [μm]	2,64 ± 0,08	2,73 ± 0,08	<0,05
Axon area [μm^2]	**8,01 ± 0,61**	**7,82 ± 0,54**	
Fiber diameter [μm]	5,07 ± 0,12	4,95 ± 0,12	1,00
Fiber area [μm^2]	**25,33 ± 1,25**	**23,66 ± 1,24**	
Myelin thickness [μm]	1,22 ± 0,03	1,11 ± 0,02	0,80
Myelin area [μm^2]	17,32 ± 0,76	15,83 ± 0,74	1,00
g-ratio	0,51 ± 0,01	0,54 ± 0,004	0,02

Fig. 28 **Example and quantification of dorsal root ganglia (DRG) electron micrographs**

Top panel, A-D display each a representative TEM micrograph of a DRG of each mouse (A and B WT; C and D KO). Bottom panel shows quantification results (mean ± SEM) summarized for wild type (=WT; NCS-1$^{(+/+)}$) and knockout (=KO; NCS-1$^{(-/-)}$) as well as the adjusted (Bonferroni-Dunn) p-value. Axon areas and fiber areas were directly measured (bold print); Myelin, diameters and g-ratios were calculated from these values (*2.2.21.2*).

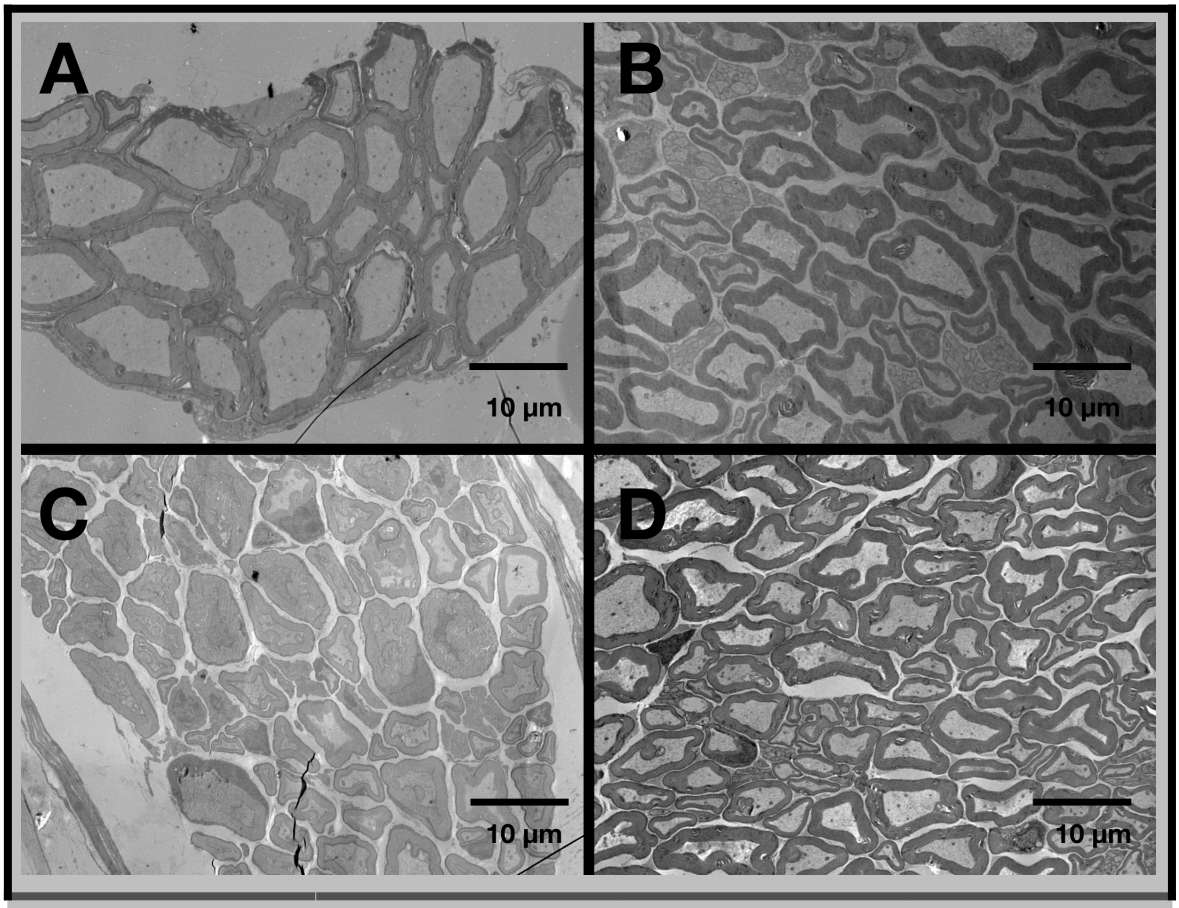

Assay	NCS-1$^{(+/+)}$ (=WT)	NCS-1$^{(-/-)}$ (=KO)	adjusted p-value
Axon diameter [μm]	2,31 ± 0,06	2,53 ± 0,06	<0,0003
Axon area [μm^2]	**5,48 ± 0,38**	**5,88 ± 0,31**	
Fiber diameter [μm]	4,26 ± 0,09	4,49 ± 0,09	0,02
Fiber area [μm^2]	**17,15 ± 0,83**	**18,17 ± 0,78**	
Myelin thickness [μm]	0,97 ± 0,02	0,98 ± 0,02	1,00
Myelin area [μm^2]	11,67 ± 0,50	12,29 ± 0,52	0,16
g-ratio	0,54 ± 0,004	0,56 ± 0,004	<0,0003

Fig. 29 **Example and quantification of sciatic nerve (SCI) electron micrographs**
Top panel, A-D display each a representative TEM micrograph of a sciatic nerve of each mouse (A and B WT; C and D KO). Bottom panel shows the quantification results (mean ± SEM) summarized for wild type (=WT; NCS-1$^{(+/+)}$) and knockout (=KO; NCS-1$^{(-/-)}$) as well as the adjusted (Bonferroni-Dunn) p-value. Axon areas and fiber areas were directly measured (bold print); Myelin, diameters and g-ratios were calculated from these values (*2.2.21.2*).

Although some previous studies found increased g-ratios after PTX treatment suggesting hypomyelination [23], others found an overall decrease of g-ratio that was significant for small fibers (axon diameter < 5μm) [39, 40]. Here too, an absolute g-ratio decrease (ideal g-ratio ≈ 0,6) was found for all regions in both genotypes (Fig. 28 - Fig. 30, pp.58-61). In DRGs and sciatic nerves of WT mice this decrease was again more pronounced (DRG: 0,51 ± 0,01 vs. 0,54 ± 0,004; p = 0,02 and SCI: 0,54 ± 0,004 vs. 0,56 ± 0,004; p < 0,0003; WT vs KO, respectively). In WT mice the g-ratio tended to be smaller in more proximal nerves (DRG: 0,51 SCI: 0,54 TIB: 0,57). This trend was not observed in NCS-1 KO animals (TIB: 0,53 SCI: 0,56 DRG: 0,54)).

Despite a measurable effect was lacking in electrophysiological assays, ultra-structural damage from PTX was visible in all treated mice. Compared with untreated animals (literature values) axon diameters were smaller confirming predominant axonal degeneration. In DRGs as well as in sciatic nerves, axon diameters were larger in NCS-1 KO mice than in WT mice suggesting that they were less affected by PTX.

3.2.3.3 Quantification of ultra-structural changes in tibial nerves after PTX treatment

CIPN initially presents with symptoms at distal sites [166]. The model of *distal-to-proximal degeneration pattern* was supported by studying a proximal and a distal segment of PTX treated mice sciatic nerves, in which a greater number of degenerated fibers were found in the distal segments [171]. Surprisingly, the most distal locus investigated here (TIB; Fig. 30) behaved opposite to the proximal parts (DRG & SCI), i.e. all parameters (axon & fiber diameter, myelin sheath thickness, and g-ratios) were significantly larger in NCS-1 WT mice than in NCS-1 KO mice.

Interestingly, when all means of the investigated parameters (axon and fiber diameters, myelin sheath thickness and g-ratios) were pooled and analyzed independent of genotype (and only with regard to location) a difference between sciatic (SCI) and tibial nerves (TIB) was not found (Tab. 9, p.61). Only the most proximal part of the investigated nerves (DRG) was significantly different from the other two locations (Tab. 9).

While the pooled means suggested no overall difference between sciatic and tibial nerves (Tab. 9), significant differences were found when genotype specific subgroups were analyzed (Fig. 27, p. 57; Fig. 29 & Fig. 30) in these loci, suggesting NCS-1's potential role to differentially affect these parameters.

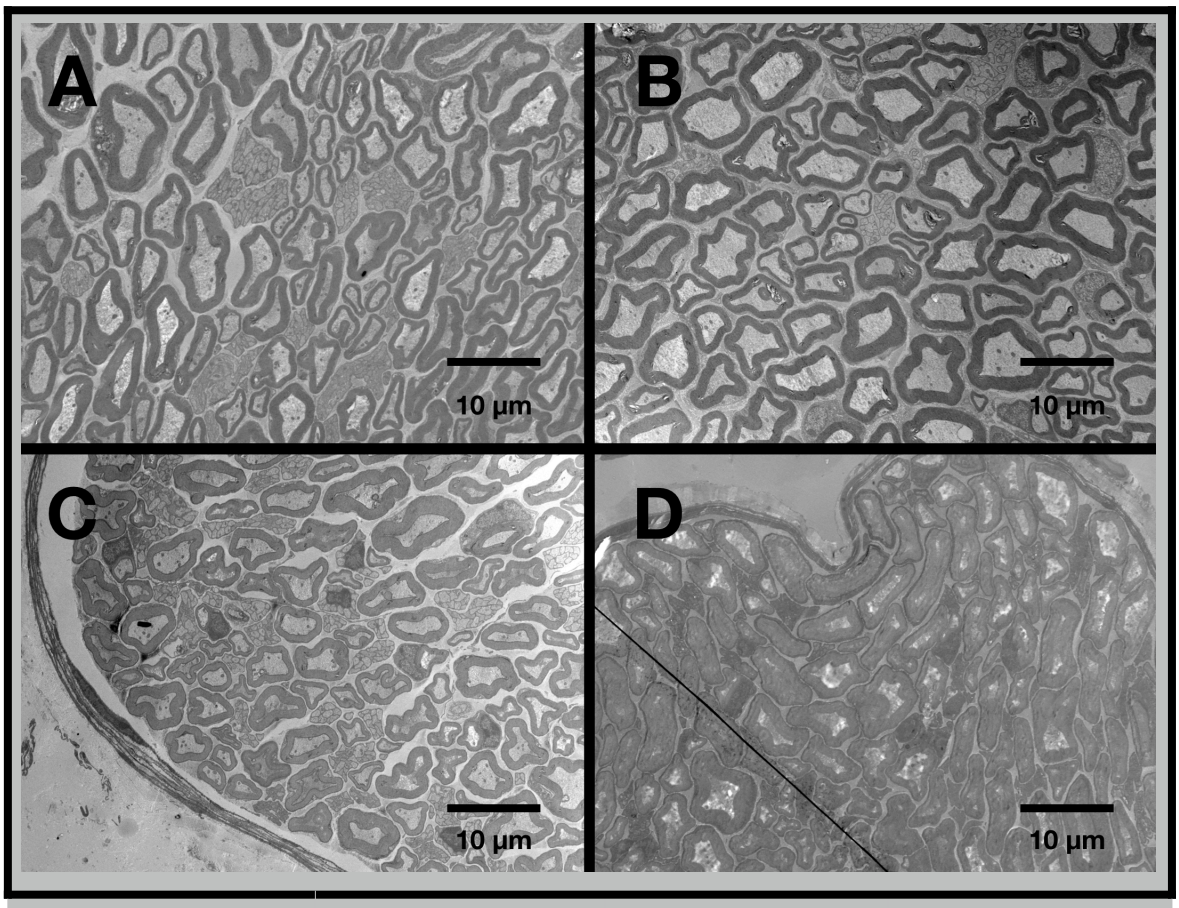

Assay	NCS-1$^{(+/+)}$ (=WT)	NCS-1$^{(-/-)}$ (=KO)	adjusted p-value
Axon diameter [μm]	2,68 ± 0,05	2,03 ± 0,04	<0,0003
Axon area [μm^2]	**6,55 ± 0,28**	**3,58 ± 0,15**	
Fiber diameter [μm]	4,69 ± 0,08	3,84 ± 0,07	<0,0003
Fiber area [μm^2]	**19,40 ± 0,69**	**12,70 ± 0,47**	
Myelin thickness [μm]	1,00 ± 0,02	0,91 ± 0,02	0,0021
Myelin area [μm^2]	12,85 ± 0,44	9,11 ± 0,34	<0,0003
g-ratio	0,57 ± 0,004	0,53 ± 0,004	<0,0003

Fig. 30 **Example and quantification of tibial nerve (TIB) electron micrographs**
Top panel, A-D display each a representative TEM micrograph of tibial nerve of each mouse (A and B WT; C and D KO). Bottom panel, quantification results (mean ± SEM) summarized for wild type (=WT) and knockout (=KO) as well as the adjusted p-value. Axon areas and fiber areas were directly measured (bold print); Myelin, diameters and g-ratios were calculated from these values (*2.2.21.2*).

Assay	DRG	SCI	TIB
Axon Diameter [μm]	2,68 ± 0,19	2,41 ± 0,16	2,43 ± 0,04
Fiber Diameter [μm]	5,02 ± 0,43	4,36 ± 0,43	4,37 ± 0,06
Myelin sheath thickness [μm]	1,17 ± 0,02	0,98 ± 0,01	0,97 ± 0,01
g-ratio	0,52 ± 0,004	0,55 ± 0,003	0,55 ± 0,003

Tab. 9 **Locus dependent PTX effect (regardless of genotype)**
Pooled wild-type and knockout results for the different nerve loci. DRG = dorsal root ganglion (most proximal); SCI= sciatic nerve; TIB= tibial nerve (most distal)

4. Discussion

4.1 Characterization of a second variant of NCS-1

The first part of the present work was dedicated to identifying, characterizing and comparing functional differences of two NCS-1 variants. Quantitive deviations [59, 92] as well as qualitative differences (i.e. mutations and single nucleotide polymorphisms) [75, 114] have been linked to alterations in Ca^{2+}-signaling which have been identified as drivers and contributors to human diseases including schizophrenia, bipolar disorder, addiction, chemotherapy induced peripheral neuropathy and many more (Tab. 2, p.11).

All previous (human) reports that linked NCS-1 dependent alterations in cell functions to disease did not acknowledge that there could be NCS-1 variants. For the Drosophila homolog of NCS-1, *Frequenin*, a second variant was discovered [146]. Despite a 95% amino acid consensus distinct functions in mediated G-protein regulation were identified for *Frequenin 2* (1.2.1.2). Analogously to the findings in Drosophila, a distinct functional role for the human NCS-1 Var2 was hypothesized.

An analysis of online databases led to the identification of an alternative start (Exon1 NCS-1 Var2) within the sequence of intron 1-2 of NCS-1 Var1 (Fig. 11, p.42). The predicted protein from this alternative mRNA is significantly shorter, with an N-terminal substitution of the first 22 amino acids for 4 different amino acids (leading to a total of Var2: 172aa vs. Var1: 190aa).

Primary interest lay in quantifying mRNA levels for either variant in three different human cell lines (SH-SY5Y [neuroblastoma]; MB231 [breast cancer]; HEK293 [embryonic kidney]). Both, NCS-1 variant 1 and NCS-1 variant 2, were identified in all cell lines and showed an approximate ratio of 1000:1 (Var1: Var2), regardless of the cell type, indicating that NCS-1 Var1 is the predominant variant in human cells (Fig. 14, p.45).

Recombinant protein was cloned and purified from the known sequence of both NCS-1 variants and it was demonstrated that either protein variant can be expressed by human cells (Fig. 12, p.43). The observation that the (recombinant) protein is stable over 12 hours provided by this study (Fig. 15, p.46) is critical for understanding properties of this Ca^{2+}-binding that are not part of the present work, however, published alongside in [182]. Among these properties are the thermodynamic parameters from isothermal titration calorimetry of NCS-1 Var1

and Var2 that show a 100 times higher Ca^{2+}-binding affinity of NCS-1 Var1 compared to NCS-1 Var2 (Apx-Fig. 14 & Apx-Tab. 11, p.108). The different Ca^{2+}-binding affinities are interesting for at least two reasons: Firstly, they are the basis for potential involvement in the regulation of distinct Ca^{2+}-pathways or in distinct Ca^{2+}-dependent cellular states. This finding adds further nuances to a network of Ca^{2+}-binding proteins with many different Ca^{2+}-binding affinities ranging from high affinity like NCS-1 Var1 and visinin-like protein 1 (VILIP-1) to low affinity proteins like synaptotagmin.

Secondly, NCS-1 Var2 can be looked at as an intermediate between NCS-1 Var1 in its native state and after cleavage by calpain. After full cleavage of NCS-1 Var1 the first 36 amino acids are removed, leaving a truncated protein, that no longer binds Ca^{2+} [18]. It was previously assumed that removal of the pseudoEF-hand disrupts protein stability [18]. NCS-1 Var2 is essentially a version lacking the N-terminal 18 amino acids (+ 4 exchanged amnio acids in the N-terminus). NCS-1 Var2 enables an understanding that partial removal of the N-terminus (of NCS-1 Var1), as it might occur during temporary activation of calpain during PTX treatment [14, 25], leaves a protein that is still able to bind Ca^{2+}, however, at much lower affinity and therefore being insufficient to regulate Ca^{2+} effectively.

After examining mRNA levels and *in vitro* protein properties the protein expression levels were investigated in cell culture by western blot analysis. Although mRNA levels suggested a low but relevant amount, NCS-1 Var2 was not detected at the protein level in SH-SY5Y, MB231 or HEK293 cells (Fig. 16, p.47). Despite investigation under various different conditions the protein was not detected (Fig. 17, p.47) and it is concluded that NCS-1 Var2 is either not expressed, expressed and rapidly degraded or expressed in amounts beyond the detection limits of western blot analysis (usually in the low picogram to mid femtogram range).

The different expression levels as well as the distinct biophysical properties of the NCS-1 variants raised the question about functional implications in cellular physiology and pathophysiology. Calpain (and possibly other proteases) mediated decay of NCS-1 Var1 is an integral part of the pathophysiological model of CIPN that depends on an intact Ca^{2+}-homeostasis (Fig. 5, p.16). It was therefore expected that (over-)expression of NCS-1 Var2, with a Ca^{2+}-binding affinity two orders of magnitude lower than NCS-1 Var1, would result in detectable changes concerning confluence in the absence and/or presence of PTX.

However, cell confluence was neither in the absence (Fig. 18, p.48) nor in the presence of PTX (Fig. 19, p.49) significantly different between cells expressing the two NCS-1 variants.

PTX acts antineoplastically through inhibition of the depolymerization of tubulin [117] and also binds to NCS-1 [24]. The efficacy of PTX to alter cell growth could have been diminished by flooding the cells with an alternative binding partner (NCS-1 instead of tubulin) through overexpression of either variant. Excess NCS-1 could have bound most of the available PTX, thus preventing its effect on cell growth (brought about via tubulin binding). However, the comparison with an *empty plasmid* control suggests that overexpression of NCS-1 does not impair tubulin binding of PTX (assessed through the confluence study), since the empty plasmid control which exhibits normal NCS-1 levels demonstrated the same PTX sensitivity as the cells overexpressing either variant.

If any changes whatsoever had emerged in the incucyte-based analyses between the two variants and controls, a consecutive deeper analysis would have followed. For instance, caspase assays might have shed light on the potential role of apoptosis. An MTT (3-(4,5-dimethylthiazol-2-yl)-2,5-diphenyltetrazolium bromide)-assay may have been used, since it detects rapidly dividing cells which can exhibit high rates of MTT reduction, potentially pinpointing effects on metabolic activity. However, this aspect was not the primary highlighted point at this stage of the investigation. In case of differences would have been detetcted other confounders would have been analyzed as well such as the formation of „giant cells“, which may develop in the presence of PTX.

NCS-1 binds and modulates the $InsP_3R$ in an $InsP_3$ dependent manner (Fig. 4, p. 9) [154]. To demonstrate an immediate functional consequence, live cell Ca^{2+}-imaging was performed in SH-SY5Y cells that were transfected with either NCS-1 Var1 plasmids or NCS-1 Var2 plasmids (Apx-Fig. 15, p.109). It was hypothesized that reduced Ca^{2+}-binding of NCS-1 Var2 resulted in a weaker interaction with $InsP_3R$ and in diminished Ca^{2+}-responses (fluorescence change) upon stimulation with ATP that induces Ca^{2+}-release from $InsP_3R$ through activation of its receptor (P_2Y). Unfortunately, the results from this experiment were inconsistent and reproducible results were not achieved. Several conditions including different cell lines, stable vs. transient transfection, transfection agents, Ca^{2+} indicator application time, stimulus perfusion velocity, coverslip coating agents were tested. Although the experimental setup was reasonable for the research question even more troubleshooting needs to be done for more consistency and reproducibility. Apx-Fig. 15 shows a successful representative live cell imaging experiment.

In conclusion, a second human variant of NCS-1 (NCS-1 Var2) was characterized using common biochemical and physiological assays. Despite (low level) detection of mRNA NCS-1 Var2 protein expression was not detected. Purified (recombinant) protein was stable in biophysical assays and a lower Ca^{2+}-binding affinity for NCS-1 Var2 compared with NCS-1 Var1 was found. The results from functional cell based assays in combination with the undetectable, low expression level and Ca^{2+}-binding affinity make it unlikely that NCS-1 Var2 plays a major regulatory role in human cells. These results suggest that NCS-1 Var1 is the critical protein variant for human disorders, diseases and development.

4.2 NCS-1's role in chemotherapy induced peripheral neuropathy

The second part of the present work was dedicated to further elucidate NCS-1 (Var1)'s role in chemotherapy induced peripheral neuropathy in a mouse model. Nerve conduction measurements were performed in NCS-1 knockout, heterozygous and wild-type C57Bl/6 mice at baseline and in a 2x2 proof of principle trial in the course of PTX treatment. Genotype dependent ultrastructural changes after PTX treatment were quantified in three different peripheral nerve loci using electron microscopy.

In general, conduction velocity is largely dependent on myelination, while the amplitudes of action potentials are a measure for axonal integrity. Depending on the stimulation site and current, motor and sensory nerves can be investigated independently. Electroneurography is thus sensitive to both myelin sheath and axonal changes for motor and sensory nerves. While CIPN has been demonstrated to affect both categories (velocities and amplitudes) a predominant pattern of axonal damage (amplitude reduction) was expected for PTX treated mice from previous reports. At baseline no difference was expected. Indeed, differences in nerve conduction were not found for untreated NCS-1 knockout or heterozygous mice compared to wild-type mice. Technical (*antidromic* vs *orthodromic* measurements) and analysis specific (*onset* vs *peak* latency) variations confirmed previously reported nuances that necessitate a precise and detailed description of the methodology. However, regardless of analyzed

parameter such as latencies, velocities, and action potential amplitudes all were similar in the different NCS-1 genotypes (Fig. 20, Fig. 21 & Fig. 22, pp. 51 - 53).

Electrophysiology is one important facet of CIPN evaluation used in both research and clinical practice [23] & [I 1]. It is objective and relatively easy to perform, however, to allow comparison from different studies, a precise description of the technique is essential. While onset latencies represent the fastest fibers and may arguably be the most relevant for clinical evaluation, they are indeed more tricky to detect than peak latencies (at least with a system where latencies are manually picked from a recording, 2.1.1.7). The data presented here reflect this aspect by the scatter which is larger for onset than for peak derived conduction parameters (Fig. 20, p.51).

The different techniques to detect nerve conduction velocity can also be used to control internal validity of data points. While velocities should be virtually identical, SNAP amplitudes are larger for stimulated antidromical than for orthodromic stimulation [178]. The data presented here confirms this aspect (Fig. 22, p.53).

Concerning *absolute* values, the data presented here are in line with those examining untreated, wild-type mice in other experimental studies that used such electrophysiological assays (many of which investigate diabetic neuropathy). For example, the (onset) TSNCV found here ranged from 25-34m/s, similar to velocities found in healthy control animals in a (diabetes related) study (25m/s [116]) and velocities amount to 28-35m/s in another study (investigating age impact) [181]. Other studies avoided absolute values entirely and relied on relative changes to compare the results of different treatment groups [23].

In the NCS-1 dependent model of CIPN pathophysiology, the neuropathy is mediated through altered Ca^{2+}-signaling that is set in motion by PTX induced NCS-1 dependent $InsP_3R$ Ca^{2+} release (Fig. 5, p.16). Without PTX treatment nerve conduction studies in mice should give identical values in different NCS-1 genotypes as was found in Fig. 20, Fig. 21 and Fig. 22. Confirming this electrophysiological equality at baseline for NCS-1 knockout (and heterozygous) mice does not only lay the foundation for investigations in the context of CIPN, but also characterizes the phenotype of these mice for other (nerve conduction-related) studies in the huge context of NCS-1 related diseases (Tab. 2, p.11).

In the next step a proof of principle study was conducted and 2x2 mice were treated with PTX. From the model of CIPN described in 1.4.2.1 it was hypothesized that absence of NCS-1 prevents PTX induced $InsP_3R$ signaling

enhancement and thus protects from impairment in nerve conduction. Unexpectedly, significant differences between NCS-1 knockout and NCS-1 wild-type mice were not observed for TSNCV, TDML, and sensory as well as motor action potential amplitudes after PTX treatment (Fig. 23, Fig. 24 & Fig. 25; pp. 54-56). Despite close-meshed investigation for up to 6 weeks after the last injection of PTX velocities and latencies remained stable. An increased scatter of points for the amplitudes of the action potentials was observed, which may reflect axonal neuropathy, however, the 2x2 setup failed to reach statistical significance.

Nerve conduction studies in the tail nerve have been used previously as outcome parameter in animals developing CIPN [23, 36]. While an early study used very high doses of PTX (60mg/kg i.v. on 3 days) [185], the treatment schedule administered here was considerably lower (4,5mg/kg i.p. on 4 alternating days, Fig. 10, p.38) and was also applied more recently [39, 40, 110]. There are reports of even lower dosing protocols (cumulative dose 4mg/kg i.p. [23, 162]; 6mg/kg once i.p. [1]), that were also sufficient to induce CIPN as indicated by mechanical allodynia, thermal hyperalgesia and in nerve conduction parameter reductions (SNAP amplitude > velocity) in those studies. Dose remains one of the most important issues and some reports suggest 30 mg/kg i.v. 3 times a week for 2 weeks for reliable induction of nerve degeneration [171].

In the present study, none of the animals died from PTX injections and their weight remained stable throughout the experiment which was also observed in previous studies [23]. While this study [23] found significant reduction of SNAPs and a temporary decrease in TSNCV (normalized after one week), the data presented here did not reveal significant changes in either parameter after PTX treatment.

As with any evaluation method, nerve conduction studies have limitations and confounders. Specifically for research purposes it is important to keep in mind, that conduction velocities are temperature dependent and that the body temperature in an anesthetized mouse quickly drops, unless care is taken to maintain body temperature. Furthermore, age was found to be a confounder in electro-physiological assessment, as NCV was found to decline in mice [181] and humans [144] with age. Considering the (usually) advanced age of patients receiving chemotherapy and the various metabolic, anatomic and systemic alterations associated with age, older mice may provide a better suited model for studies on side effects of chemotherapeutic drugs. The mice used in this study for baseline measurements were 7 months old which corresponds to a human equivalent of

around 30-38 years [I 24] considering the total life span. In the 2x2 design, in which mice were treated with PTX, their age was merely 2.2 months. Other studies investigating PTX effects used even younger mice at the age of 9 weeks [23], 7 weeks [39], and 6 weeks [40].

Concerning neuropathies in general, it is useful to keep in mind that routine electrophysiological measurements overrepresent the largest and fastest neurons. Large diameter fibers tend to have the most myelin and the least electrical resistance, thus they make up a large percentage of the summed action potentials and conduction velocities. Neuropathies that mostly affect small fibers may not be revealed using this method. However, for C57Bl/6 mice, distinct patterns of neuropathies affecting different electrophysiological aspects have been shown for several chemotherapeutics beyond PTX [23], validating this method for this type of studies.

In summary, the failure to reproduce a detrimental effect of PTX on electrophysiological parameters is most likely related to the small number of mice used in this study (2 KO and 2 WT). Other considerable explanations may lie in the multiple confounders mentioned above. The scatter of data of SNAPs and CMAPs after PTX injections might be smaller in a larger group using the same experimental setup and thereby a seizable difference between NCS-1 genotypes may also be uncovered.

Ultrastructural analysis may reveal damages induced by PTX before electrophysiological (or behavioral) assays are able to detect them. Indeed, transmission electron microscopy revealed various stages of neuronal degeneration. PTX affected axons predominantly, but myelin degeneration was also present (Fig. 26, p.57 &107). The complex architecture of neurons needs to be considered when histological or ultrastructural analyses are performed. Three different (peripheral nerve) loci were investigated, namely DRG, sciatic nerve, and tibial nerve. A quantitative analysis of axon diameters in DRGs and sciatic nerves revealed significantly larger diameters in NCS-1 KO animals (with preserved myelin sheath thickness). This suggests that NCS-1 has a detrimental role in CIPN. The absence of NCS-1 and thereby reduced PTX induced alteration of $InsP_3R$ signaling may be involved in the protection of neurons and their axons leading to preserved axonal diameters in NCS-1 deficient mice compared to those of wild-type animals after PTX treatment. However, this was not found in the most distal part of the neurons (tibial nerve) in which, surprisingly, the inverse was observed, i.e. smaller axon

diameters in NCS-1 KO mice. The mean difference in overall fiber diameters for the tibial nerve were more pronounced than compared with the other loci (WT≈4,7μm vs. KO≈3,8μm, Fig. 30, p.61). This finding may result from spatially asymmetric effects of PTX. If PTX is more detrimental in peripheral parts (of peripheral nerves) smaller neurons (especially in WT mice) may have been cleared after decay thus leaving only larger neurons for the analysis (selection bias). The more distal areas are distinct in terms of perfusion, micro nutrition, temperature etc. Spatial (and temporal) differences in protein distribution and neuronal architecture are thus possible explanations for these discrepant findings which require further validation.

Lastly, even though more than 2000 fibers were analyzed it is important to keep in mind that the data is based on a 2x2 proof of principle design (2.2.19.2). Statistical validity based on high *n-number* of many axons should not be confused with biological generalizability. The analysis of all fibers (and axons) of a single mouse can be considered as a single experiment and provide useful insights to the action of PTX on an electron microscopical scale. It may help to generate hypotheses, yet larger cohorts (with more than 2 mice) are needed to proof if these hypotheses are supported by reproducible experimental data and, are indeed biologically relevant. For example, a mean difference of 1μm in fiber diameter may be statistically significant, however, the biological relevance of this finding needs to be challenged and accounted for.

With regard to NCS-1's significance, other groups suggest alternative hypotheses for the development of CIPN. While this study [133] did find an $InsP_3R$-dependent axon degeneration they reported unchanged NCS-1 protein levels upon treatment with PTX, a finding conflicting with results from other investigators [25]. The electron microscopic findings in DRGs and sciatic nerves presented here are compatible with previous findings that explain CIPN prevention by lithium pretreatment [110], because the lack of NCS-1 (the key player for the initial Ca^{2+} oscillations) seemed to have a protective effect in preserving axonal integrity. However, careful attention has to be paid to the anatomical location in future studies, because spatial and architectural aspects of neurons may have a larger impact in the development of CIPN than previously assumed.

In conclusion, the present study investigated nerve conduction in C57Bl/6 mice expressing NCS-1 or lacking this protein. Tail nerve action potential amplitudes and tail sensory nerve conduction velocities were similar in all genotypes which

suggests that NCS-1 does not exert a functional effect on these parameters. The experimental design examining PTX toxicity failed to demonstrate significant differences in electro-physiology between genotypes after PTX treatment, however, ultrastructural assays revealed a predominantly axonal neuropathy with distinct patterns in different loci arguing for a more nuanced consideration of anatomical sites for understanding of the effect of PTX on neurons and for the development of strategies to protect from CIPN.

4.3 Conclusions

All previous (human) reports that linked NCS-1 to alterations in cell functions in disease did not acknowledge that distinct NCS-1 variants in human tissues may exist. A second human variant of NCS-1 (NCS-1 Var2) was characterized using common biochemical and physiological assays. The results from functional cell based assays in combination with very low protein expression levels (below the detection limit) and much lower Ca^{2+}-binding affinity suggest that NCS-1 Var2 does not exert a significant regulatory role in human cells. Thus, NCS-1 Var1 is most likely the critical protein variant for human disorders, diseases and development.

Concerning the role of NCS-1 in chemotherapy-induced peripheral neuropathy, the study evaluated initially the role of NCS-1 in action potential conduction in nerves using NCS-1 deficient mice. Tail nerve action potential amplitudes and tail sensory nerve conduction velocities were similar in all genotypes investigated (WT, HET, KO). A 2x2 proof of principle design failed to demonstrate significant differences in nerve conduction in mice after PTX treatment independent of the presence of NCS-1. However, ultrastructural assays revealed a predominant axonal neuropathy with distinct patterns in different anatomical loci arguing for a role of NCS-1 in the pathophysiology of PTX damages in certain nerve fibers. Thus, NCS-1 remains a worthwhile target in the investigation and the design of strategies directed against CIPN.

5. Summary

5.1 English

Introduction & Aims: Neuronal calcium sensor 1 (NCS-1) is a Ca^{2+} binding protein which is expressed in most tissues and a main player in intracellular Ca^{2+} homeostasis. The present work focused on two objectives: Firstly, a second variant of human NCS-1 was characterized (NCS-1 Var2). Secondly, NCS-1's role in chemotherapy induced peripheral neuropathy (CIPN) upon paclitaxel (PTX) was investigated in the mouse model, since an interaction of NCS-1 by its interaction with the inositol trisphosphate receptor ($InsP_3R$) was previously suggested.

Methods: In the first part cDNA libraries from three human cell lines were generated via mRNA extraction and reverse transcription. Specific primers to distinguish either isoform were designed using online resources and databanks. Plasmids containing either NCS-1 variant were cloned and semiquantitative assessment of the cDNA libraries was performed using quantitative PCR with the standard curve method. Recombinant protein of both variants was analyzed for stability at room temperature. Western blot analysis with variations in several parameters was used to determine protein quantities of both NCS-1 variants in three human cell lines and mouse tissues. Neuroblastoma cells (SH-SY5Y) expressing either NCS-1 Var1, NCS-1 Var2, or empty plasmids were studied for cell growth by analyzing cell confluence with and without addition of different PTX concentrations. In the second part tail nerve conduction studies were performed on a total of 29 C57Bl/6 mice expressing distinct levels of NCS-1 expression (6 NCS-1(+/+); 15 NCS-1(+/-); 8 NCS-1(-/-)). Tail sensory nerve conduction velocity, tail distal motor latencies, sensory nerve action potentials and compound muscle action potentials were analyzed. In a proof of principle design trial two NCS-1(-/-) and two NCS-1(+/+) mice received PTX treatment (4,5mg/kg i.p. on 4 alternating days). Neural electrophysiology parameters were recorded before and after injections. Finally, mice were sacrificed and dorsal root ganglia (DRG), sciatic nerves and tibial nerves were harvested and analyzed qualitatively and quantitatively by electron microscopy.

Results: A transcript for a second human variant of NCS-1 (NCS-1 Var2) was identified in the NCBI library with an alternative exon 1 within the intron 1-2 sequence of NCS-1 Var1 resulting in a protein in wich the N-terminal 22 amino

acids are substituted by 4 amino acids after genetic transfer. SH-SY5Y are capable of expressing both NCS-1 variants. Purified NCS-1 Var1 and Var2 proteins are stable for at least 12 hours at room temperature. NCS-1 Var2 mRNA levels are approximately 1000 fold lower than NCS1 Var1 in human cell lines. Despite measurable transcript levels, even after considerable variation NCS-1 Variant 2 protein was not detected in human cell lines. (Over-)expression of either NCS-1 variant did not alter cell growth or death in live cell analysis assays.

In the mouse studies, it was demonstrated that the nerve conduction (velocity, latency, amplitudes) was not altered in mice deficient for NCS-1 at untreated control conditions. In a 2x2 proof of principle design an affection of nerve conduction was not found after PTX treatment independent of the presence of NCS-1. Ultrastructural analysis showed (predominantly) axonal degeneration in both genotypes after PTX. In DRGs and sciatic nerves, axon diameters were significantly smaller in wild-type mice than in NCS-1 knockout mice. However, this was not found in tibial nerves, in fact, the axon diameters were reversed in these more distal nerves.

Discussion: The functional cell based assays in junction with the very low expression level (below detection limit) and reduced Ca^{2+}-binding affinity suggest that NCS-1 Var2 does not exert a significant regulatory role in human cells. This finding is different from the results from NCS-1's Drosophila homolog Frequenin, as a second isoform of frequenin was demonstrated to interact with other proteins and thereby modulate specific cellular functions. Deficiency of NCS-1 did not affect nerve conduction assessed in the anesthetized mouse suggesting that this protein is not required for nerve conduction physiology. Technical and analysis specific variations necessitate a precise and detailed description of the methodology to make results of different studies comparable. A larger repetition of the same experimental setup might yield in a seizable difference in PTX-induced nerve damage that depends on NCS-1 genotype. Locus specific ultrastructural patterns of (axonal) neuropathy should be validated in a larger trials and considered in future hypothesis generation.

Conclusion: Human NCS-1 has two variants, of which NCS-1 Var1 is suggested to be the critical protein. NCS-1 has been implicated in several diseases and disorders. It has no function in nerve conduction physiology but may be implicated in the development of CIPN. NCS-1 may thus be a feasible target for the investigation and design of strategies against CIPN.

5.2 German

Einleitung: Kalzium (Ca^{2+}) ist ein divalentes Kation, das zahlreiche zelluläre Funktionen und Prozesse, wie Fertilisation, Muskelzellkontraktion, Exozytose und Apoptose ermöglicht und reguliert. Ein 20000-facher Gradient über die Zellmembran sowie ein riesiges Arsenal von exprimierten zellulären und subzellulären, hoch-spezifischen Ca^{2+}-Bindungsproteinen ermöglichen die zunächst paradox anmutende Regulierung entgegengesetzter Prozesse (Zelltod vs Überleben) als auch ein *fine tuning* von Signalkaskaden durch ein und dasselbe Ion unter Bildung von subzellulär regulierten Kompartimenten. Mit Ca^{2+} interagierende Proteine lassen sich in zwei große Gruppen einteilen: Solche, die mittels In- und Efflux die *Absolutmenge* an zytosolischem Ca^{2+} verändern (z.B. SERCA oder $InsP_3R$) und solche, welche die Gesamtkonzentration von Ca^{2+} nicht beeinflussen (Fig. 1, S.2). Vertreter der letztgenannten Gruppe binden freies, zytosolisches Ca^{2+} an spezifische Domänen (z.B. C_2-Domain oder EF-hand), erfahren dabei eine Konformationsänderung und können so mit anderen Proteinen interagieren.

Die Superfamilie der intrazellulären EF-hand-Ca^{2+}-Bindungsproteine kann in Unterfamilien eingeteilt werden, deren Vertreter strukturell ähnlich aufgebaut sind und eine ähnliche Affinität zu Ca^{2+} aufweisen (z.B. *Calmodulin Proteinfamilie*). Vertreter der anderen Gruppe sind z.B. die evolutionär hochkonservierten *Neuronal Calcium Sensor Proteinfamilie*, die besonders in neuronalen Zellen exprimiert werden. Der bedeutendste Vertreter ist der Neuronale Calcium Sensor 1 (NCS-1; Fig. 3, S.6) bzw. sein *Drosophila* Homolog, *Frequenin* (FREQ1). In Drosophila wurde gezeigt, dass eine Isoform von Frequenin, Frequenin 2, trotz einer Aminosäuresequenz-Übereinstimmung von 95% durch variantenspezifische Interaktion differente Signalwege beeinflusst.

NCS-1 besitzt einen 2x2-Aufbau, d.h. insgesamt vier EF-Hand-Domänen, von denen die ersten beiden (EF1, EF2) über einen *hinge loop* mit den Domänen EF3 und EF4 verbunden sind. Der ersten EF-Hand fehlen wichtige Ca^{2+}-koordinierende Aminosäurereste, weshalb nur die zweite bis vierte EF-Hand Ca^{2+} binden. Nach Ca^{2+} Bindung, kommt es zu einer Verlagerung des C-terminalen EF-Hand Paars und zur Freilegung einer hydrophoben Spalte, die Protein-Interaktionen ermöglicht. Zahlreiche Zielproteine für NCS-1 wurden gefunden (Tab. 1, S.8). Für etwa 10 dieser Interaktionen sind bisher funktionelle, physiologische Konsequenzen beschrieben, die mit einer Vielzahl von Erkrankungen assoziiert wurden (Tab. 2, S.11). Ein

Großteil dieser Erkrankungen ist dem neuro-psychiatrischen Spektrum zuzuordnen, jedoch wurden auch u.a. onkologische und kardiologische Phänomene mit NCS-1 assoziiert, was die ubiquitäre Expression widerspiegelt.

Für die vorliegende Arbeit war vor allem die Interaktion von NCS-1 und dem Inositoltrisphosphat-Rezeptor ($InsP_3R$) relevant, da diese über ein gestörtes Ca^{2+}-Signaling als Treiber für Chemotherapie-induzierte periphere Neuropathie (CIPN) beschrieben wurde (Fig. 4, S.9). CIPN ist eine häufige und zuweilen dosis-limitierende Nebenwirkung von zytostatischen Medikamenten unterschiedlicher Gruppen wie den Taxanen (z.B. Paclitaxel (PTX)), aber auch von Platinderivaten (z.B. Cisplatin), Vincaalkaloiden (z.B. Vincristin) und Proteasom-Inhibitoren (z.B. Bortezomib). Klinisch imponiert die Nebenwirkung mit neuropathischen Schmerzen in Form von Taubheit, Kribbeln und/oder Brennen, aber auch Muskelschwächen als Ausdruck einer Motoneuropathie. Aufgrund der Subjektivität des Leitsymptoms (Schmerz) ergibt sich diagnostisch, evaluatorisch sowie wissenschaftlich eine größere Herausforderung als bei anderen dosislimitierenden, leichter quantifizierbaren Nebenwirkungen (z.B. Agranulozytose). Die S3-Leitlinie („Supportive Therapie bei onkologischen PatientInnen“) empfiehlt neben Anamnese und Neurostatus auch spezifische Schmerzfragebögen und ggf. elektro-physiologische Untersuchungen (ENG, EMG). Derzeit gibt es keine effektive Therapie für CIPN. Da sowohl Lebensqualität als auch u.U. das Gesamtüberleben negativ beeinflusst werden und die Zahl der Krebserkrankungen (und damit Chemotherapien) steigt, liegt die Dringlichkeit für die Entwicklung von effektiven Präventionsstrategien für CIPN auf der Hand.

Für Paclitaxel (PTX), dessen antineoplastische Wirkung über Mitosehemmung durch eine Interaktion mit Mikrotubuli zustande kommt, erschließt sich die Entstehung einer Neuropathie nicht unmittelbar, da Neurone im Gegensatz zu neoplastischen Zellen keine Mitose durchlaufen. Das NCS-1 abhängige Modell zur Entstehung von CIPN basiert molekular auf einer gestörten Ca^{2+}-Homöostase (Fig. 5, S.16): PTX bindet NCS-1 und induziert Ca^{2+}-Oszillationen am $InsP_3R$. Eine dadurch verursachte Erhöhung der intrazellulären Ca^{2+}-Konzentration führt zur Aktivierung von Calpain, einer Ca^{2+}-abhängigen Protease, welche NCS-1 (und weitere Proteine) spaltet, was zu weiterer Dysregulation im Ca^{2+}-Signaling, Aktivierung von Caspasen und schließlich neuronalem Zelltod führt. Da sich die molekularen Mechanismen des antineoplastischen Effekts und der Entwicklung von CIPN in diesem Modell unterscheiden, stellen die einzelnen zur CIPN führenden Schritte potenzielle

Angriffspunkte zur Prävention dieser unerwünschten Wirkung dar. Ein besseres Verständnis der Rolle von NCS-1 könnte somit die molekularen Grundlagen der CIPN entschlüsseln und zur Entwicklung einer effektiven Prävention führen.

Fragestellungen: In der vorliegenden Dissertation wurde der Neuronale Calcium Sensor 1 (NCS-1) unter zwei wesentlichen Gesichtspunkten untersucht: Erstens wurde eine zweite—bisher nicht beachtete—(menschliche) Variante von NCS-1 (NCS-1 Var2) charakterisiert. Spezifische Fragestellungen umfassten das Verhältnis beider NCS-1 Varianten (Var1 und Var2) auf mRNA- und Proteinebene, Stabilitätsprüfung von rekombinantem NCS-1 Var2 Protein, sowie funktionelle Unterschiede zur (Über-)expression beider Varianten in menschlichen Zelllinien.

Zweitens wurde die Rolle von NCS-1 in der Chemotherapie-induzierten peripheren Neuropathie (CIPN) im Mausmodell näher untersucht. Hierzu wurde die nervale Funktion mittels Elektrophysiologie in Tieren, die NCS-1 exprimieren oder nicht, vor und nach Behandlung mit Paclitaxel (PTX) sowie NCS-1 Genotyp abhängige strukturelle Unterschiede entlang peripherer Nerven nach PTX Behandlung mittels Elektronenmikroskopie untersucht.

Methoden: Für den ersten Teil (Charakterisierung der zweiten Variante von NCS-1) wurden cDNA Bibliotheken von insgesamt drei menschlichen Zelllinien (SH-SY5Y = Neuroblastom; HEK 293 = Embryonale Nierenzellen; MB 231 = Brustkrebs, Adenokarzinom) erstellt. Hierfür wurde mithilfe von kommerziell erworbenen Kits RNA extrahiert, aufgereinigt und in cDNA (revers-)transkribiert. DNA/RNA Messungen erfolgten mittels UV-Spektrophotometer; Zellzahlen wurden mittels Hämozytometer bestimmt.

Unter Zuhilfenahme von Online-Datenbanken (NCBI Nucleotide; Ensembl genome browser 83 & NCBI Primer-BLAST) wurden Isoform-spezifische Primer-Paare entworfen und virtuell (NetPrimer) und anschließend praktisch (PCR) getestet. Amplifikationsprodukte wurde mittels Gelelektrophorese und Ethidiumbromid visualisiert. Der amplifizierte, Isoform-spezifische Abschnitt jedes Primer-Paars wurde anschließend mittels TOPO TA Cloning Kit in ein Plasmid geklont. Kompetente E. coli DH5α wurden mit den Plasmiden transformiert und mittels selektiver Agar-Platten selektioniert. Korrekte Expression von Plasmid-DNA wurde mittels Kolonie-PCR und anschließender Sequenzierung verifiziert. Plasmid-Amplifikation und Purifikation wurde mit kommerziellen Kits (QIAprep® Miniprep/ Midiprep) durchgeführt. Relative Transkript-Expression der beiden NCS-1 Varianten in den cDNA Bibliotheken wurde mittels qPCR semiquantitativ erfasst. Dazu wurden

mithilfe der Isoform-spezifischen Plasmide über Verdünnungsreihen zwei Standardkurven erstellt. Mismatch-Primer-Kontrollen wurden als unteres Detektionslimit definiert.

Purifiziertes, rekombinant hergestelltes Protein von beiden NCS-1 Varianten wurde dankenswerterweise von Baisheng Wang and Larry Huynh zur Verfügung gestellt. Zur Bestimmung der Proteinstabilität wurden Proben des Proteins in Eppendorf-Gefäße pipettiert und bei Raumtemperatur unterschiedlich lange gelagert (0 - 24h). Proben wurden mithilfe eines Polyacrylamidgels aufgetrennt und visualisiert.

Zur Bestimmung der Protein-Expression wurden Western Blots durchgeführt. Die drei oben genannten Zelllinien wurden untersucht, wobei rekombinantes NCS-1 Protein beider Isoformen als Positiv-Kontrolle verwendet wurde und zum Vergleich sowie als Negativ-Kontrolle Protein aus Mausgewebe (Cerebellum, Niere, Haut) genutzt wurde. Nach der Lyse wurden die Zelllysate gekocht und Proteine mittels Polyacrylamid-Gelelektrophorese separiert. Es erfolgte anschließend ein (feuchter) Transfer auf eine PVDF-Membran und eine Blockierung der Membran mit 5% Milch in TBST. Anschließend erfolgte eine Übernacht-Inkubation mit Primärantikörper (u.a. FL-190; polyklonal) und nach Applikation von Sekundärantikörper die Detektion mittels *Super West Dura* und Röntgenfilmen. Protokollbedingungen wurden für die Parameter Lyse-Puffer, Antikörper-Konzentrationen, Lysat-Präparation und Expositionszeiten variiert.

Konfluenz- und Paclitaxel-Sensitivitätsassays wurden mithilfe eines *IncuCyte Live-Cell Analysis System* Inkubators durchgeführt. Hierfür wurden mit NCS-1 Var1, NCS-1 Var2 oder leeren Plasmiden stabil transfizierte SH-SY5Y Zellen (bereitgestellt durch Baisheng Wang) gezählt und auf 96-well-Platten pipettiert. Anschließend wurde die Konfluenzänderung der Zellen mittels Fotoaufnahmen über die Zeit ermittelt. In einem separaten Experiment wurden zusätzlich zum Medium unterschiedliche Mengen PTX hinzugefügt.

Für den zweiten Teil (Rolle von NCS-1 für CIPN im Mausmodell) wurden NCS-1 knockout (KO; erhalten von Prof. Dr. Olaf Pongs), heterozygote (HET) und Wildtyp (WT) C57Bl/6 Mäuse gezüchtet. Im Alter von ca. 3 Wochen wurde eine Genotypisierung der Tiere mittels REDExtract-N-Amp Tissue PCR Kit durchgeführt.

Elektrophysiologische Untersuchungen wurden mit subdermalen Nadelelektroden eines Nicolet Viking Quest Apparats im Schwanz durchgeführt. Zwischen 2 Mäusen wurden die Elektroden mit 70% Ethanol gereinigt. Alle Messungen erfolgten unter Isofluran-Narkose. Die Körpertemperatur der Mäuse wurde mittels Hitzekissen

konstant gehalten. Parameter wie Alter, Schwanzlänge, Gewicht und Narkosezeiten wurden dokumentiert. Zunächst wurden an drei verschiedenen Tagen in zufälliger Reihenfolge (randomisiert durch Larry Huynh) insgesamt 29 Mäuse (WT (n=6); HET (n=15); KO (n=8)) untersucht. Messmethoden (antidrome vs orthodrome Stimulation) wurden variiert und gesondert dokumentiert. Untersucht wurden sensible Nervenleitgeschwindigkeit, motorische Latenzzeit, Motoramplitude (Summenaktionspotential; CMAP) und Amplitude von sensiblen (Schwanz-)Nerven (SNAP). Weiterhin wurden onset (Beginn des Aktionpotentials; schnellste Fasern) und peak (Zenith des Aktionspotentials; „Durchschnittsfaser“) unterschieden.

Außerdem erhielten in einer Ministudie zwei Knockout-Mäuse und zwei Wildtyp-Mäuse jeweils über 8 Tage an jedem 2. Tag eine intraperitoneale Injektion von 4,5 mg/kgKG PTX, so dass insgesamt 4 Injektionen verabreicht wurden. Die Nervenleitgeschwindigkeit wurde, wie oben beschrieben, an insgesamt vier Tagen vor und einmal wöchentlich für sechs Wochen nach der Behandlung durchgeführt. Am Tag der letzten Messung wurden die Mäuse anästhesiert und über intraventrikuläre Applikation von Fixationslösung fixiert und anschließend Spinalganglien (DRG), Nervus ischiadicus (SCI) und Nervus tibialis (TIB) extrahiert. Von Klara Szigeti-Buck wurden Bilder der Dissektate mittels Transmission-Elektronenmikroskop angefertigt. Die Mikrographien wurden anschließend mithilfe der Software Image J qualitativ und quantitativ analysiert.

Die Visualisierung aller statistischer Ergebnisse erfolgte mithilfe der Software GraphPad Prism. Ergebnisse der quantitativen PCR wurden als Mittelwerte und Standardabweichungen dargestellt (jede Messung wurde 3-fach wiederholt). Durch die 7500 Fast & 7500 Real-Time PCR System Software wurden darüberhinaus R^2 values (Korrelationskoeffizienten) für die Standardkurven bestimmt (1.00 entspricht perfekter Übereinstimmung). Elektrophysiologische Ergebnisse wurden als Tukey-Box-and-Whisker plots dargestellt, wobei die Box sich über die 25. - 75. Perzentile erstreckt und die Whisker das 1,5-fache des Interquartilenabstandes beschreiben. Datenpunkte außerhalb der Whisker wurden als individuelle Punkte aufgetragen. Darüberhinaus wurden die Daten als Mittelwert ± Standardfehler des Mittelwertes dargestellt. Für die nicht mit PTX behandelten Mäuse wurden one-way ANOVAs mit Holm-Sidak (normalverteilt) oder Bonferroni-Dunn (nicht-normalverteilt) post-hoc Tests durchgeführt. Statistische Signifikanz wurde bei $p < 0,05$ angenommen. Two-way ANOVA wurde bei PTX Behandlung verwendet. Sidak’s Test wurde für die Korrektur nach multiplem Testen verwendet. Ergebnisse der Auswertung der

elektronenmikroskopischen Bilder wurden mittels Mann-Whitney Test analysiert (nach Durchführung eines Shapiro-Wilk Tests).

Ergebnisse: Mit Hilfe des Ensembl genome browser und der NCBI Datenbank wurde das Transkript einer zweiten Isoform von NCS-1 identifiziert (NCS1 Var2; Fig. 11, S.42). NCS1 Var1 und Var2 unterscheiden sich durch ein alternatives Exon1, welches sich (für NCS1 Var2) zwischen dem Intron 1-2 von NCS-1 Var1 befindet. Da das alternative Exon1 deutlich kürzer ist, resultiert auch ein am N-Terminus verkürztes Protein (172 Aminosäuren vs 190 Aminosäuren). Mit zusätzlichen Markern (Flag und HA) in Plasmide geklont, wurde gezeigt, dass beide Protein-Isoformen in SH-SY5Y Zellen exprimiert werden können (Fig. 12, S.43).

Für biophysikalische Analysen wie die isotherme Titrationskalorimetrie (ITC) war es notwendig die Stabilität der zu untersuchenden Proteine bei Raumtemperatur nachzuweisen. Purifiziertes Protein beider NCS-1 Varianten war für mindestens 12 Stunden bei Raumtemperatur stabil. Nach 24 Stunden waren allerdings deutliche Zeichen einer beginnenden Degradation zu erkennen (Fig. 15, S.46).

Obgleich Unterschiede bezüglich der Transkriptmenge in einzelnen Zelllinien bestanden, war in allen untersuchten Zelllinien die mRNA von NCS1 Var2 um den Faktor 1000 niedriger exprimiert als die mRNA von NCS1 Var1 (Fig. 14, S.45). Aufgrund der hohen Sequenzhomologie der Varianten wurde eine Mismatch-Primer Kontrolle (z.B. Var2-Primer mit Var1-Plamiden) als unteres Detektionslimit definiert, so dass ausgeschlossen wurde, dass unspezifische (und damit weniger effektive) Amplifikation von Var1 als NCS1 Var2-mRNA identifiziert wurde. Die Transkript-menge von NCS1 Var2 unterschied sich deutlich von der Mismatch-Kontrolle.

Um die auf mRNA-Ebene festgestellten Unterschiede zwischen NCS1 Var1 und Var2 auch auf Proteinebene darzustellen, wurden Western Blots von Lysaten der drei oben genannten Zelllinien durchgeführt. Trotz Variation verschiedener methodischer Parameter wurde NCS-1 Var2 in keiner der Zelllinien nachgewiesen und konnte lediglich in der Positivkontrolle (rekombinantes Protein) nachgewiesen werden (Fig. 16 & Fig. 17, S.47).

Ergebnisse von isothermen Titrationskalorimetrie-Analysen (ITC) hatten eine deutlich niedrigere Ca^{2+}-Bindungsaffinität der NCS-1 Var2 im Vergleich zu NCS-1 Var1 gezeigt (Apx-Fig. 14, S.108). Dieser Unterschied lässt über ein verändertes Signaling auch funktionelle Konsequenzen für die Zelle vermuten. Stabil mit NCS-1 Var1, NCS-1 Var2 oder leeren Plasmiden transfizierte SH-SY5Y Zellen wurden daher mit Hilfe eines IncuCyte-Inkubators auf ihr Wachstumsverhalten hin

untersucht. Die Wachstumsraten waren aber in allen Gruppen ähnlich. Die Zugabe von PTX zeigte zwar eine Reduktion der Zellen in Abhängigkeit von der PTX-Konzentration, jedoch wurden keine Unterschiede in den verschiedenen Gruppen von Zellen beobachtet.

Um die Rolle von NCS-1 in Chemotherapie-induzierter peripherer Neuropathie im Mausmodell näher zu charakterisieren, wurden zunächst elektrophysiologische Messungen am Schwanz von 29 C57Bl/6 Mäusen unterschiedlichen NCS1-Genotyps durchgeführt. Für alle untersuchten Parameter (motorische Latenzzeit, sensible Nervenleitgeschwindigkeit und Amplituden von motorischen und sensiblen Summenaktionspotentialen) wurden keine Unterschiede zwischen Tieren, die WT, HET oder KO für NCS-1 waren, festgestellt (Fig. 20 - Fig. 22, S.51 - 53). Dies galt unabhängig von Messmethode (antidrom vs orthodrom) oder Auswertung (onset vs peak). Wie in anderen Studien zuvor beschrieben ist, wurde eine insgesamt verminderte Streuung der Daten beobachtet, wenn peak statt onset-Werte zur Bestimmung der Leitgeschwindigkeit unterschiedlicher Fasern analysiert wurden.

Die im Rahmen einer Ministudie mit PTX behandelten Mäuse zeigten neurographisch keine Unterschiede zwischen NCS-1 Knockout und Wildtyp. Während Nervenleitgeschwindigkeit und motorische Latenzzeiten über den Verlauf des Experiments konstant blieben (Fig. 23, S.54 & Fig. 24, S.55), zeigte sich bereits früh nach Abschluss der PTX-Injektionen eine deutliche Streuung der Messergebnisse in der Amplitude der Potentiale (Fig. 25, S.56). Ein möglicher Effekt (axonale Neuropathie) konnte jedoch v.a. aufgrund der zu niedrigen Zahl der untersuchten Tiere weder nachgewiesen noch wirklich ausgeschlossen werden.

Neben der Neurographie wurden auch ultrastrukturelle Veränderungen der peripheren Nerven nach PTX-Administration untersucht. Hierzu wurden elektronenmikroskopische Bilder der Spinalganglien und der Querschnitte des Nervus ischiadicus und Nervus tibialis analysiert. Sämtliche Bilder zeigten verschiedene Stadien neuronaler Degeneration. Vordergründig wurden axonale Schäden beobachtet, aber auch Myelin-Veränderungen waren sichtbar (Fig. 26, S.57). Quantitativ zeigte sich im Wildtyp sowohl in den Spinalganglien, wie auch im Nervus ischiadicus eine deutliche Reduktion der Axondurchmesser im Vergleich zu NCS-1 KO Tieren, während die Myelinscheidendicke bei beiden Genotypen (NCS-1 WT & KO) vergleichbar war (Fig. 27, S.57). Überraschend zeigte sich eine Umkehrung im Nervus tibialis, denn hier waren die Axone aus NCS-1 KO Tieren signifikant kleiner als die aus WT Mäusen. Im Bereich des Nervus tibialis fand sich

zudem eine signifikant kleinere Myelinscheidendicke in NCS-1 KO im Vergleich zu NCS-1 WT.

Diskussion: Der erste Teil dieser Arbeit widmete sich der Identifikation und Charakterisierung einer zweiten menschlichen Variante des Neuronalen Calcium Sensor 1. Für das *Drosophila* Homolog von NCS-1, Frequenin 1, ist (in der Literatur) eine Isoform beschrieben (Frequenin 2), die über spezifische Protein-Interaktionen in verschiedene Signalwege des Frq1 eingreift. Da die Übereinstimmung der Sequenzen beider Formen in Drosophila mit 95% deutlich höher ist als im menschlichen NCS-1, wurde vermutet, dass funktionelle Unterschiede zwischen den beiden Isoformen im menschlichen NCS-1 noch deutlicher sein könnten. In drei menschlichen Zelllinien existiert das Transkript einer NCS1 Isoform (NCS1 Var2), jedoch in etwa um den Faktor 1000 geringerer Konzentration im Vergleich zu NCS1 Var1. Auf Proteinebene konnte endogenes NCS-1 Var2 mit den hier verwendeten Methoden nicht nachgewiesen werden. Da alle Positiv- und Negativkontrollen der Western Blots die erwarteten Ergebnisse lieferten und der Nachweis des Proteins also funktionell intakt war, ergeben sich folgende Möglichkeiten: 1. NCS-1 Var2 Protein wird physiologisch nicht exprimiert, 2. NCS-1 Var2 Protein wird nach Expression sehr schnell degradiert oder 3. NCS-1 Var2 Protein wird exprimiert, wobei die Konzentration jedoch unterhalb des Detektionslimits vom Western Blot liegt (Piko- bis Femtogramm-Bereich). Der erhebliche quantitative Unterschied auf mRNA-Ebene und die fehlende Nachweisbarkeit auf Proteinebene sprechen für eine allenfalls untergeordnete Rolle von NCS-1 Var2.

Transfizierte Zellen exprimieren zwar beide Isoformen, jedoch wurden nach Transfektion der beiden Varianten keine funktionellen Unterschiede im Zellwachstum gefunden. Aufgereinigtes, rekombinant hergestelltes Protein beider Isoformen war für mindestens 12 Stunden stabil, was die Voraussetzung für biophysikalische Untersuchungen mittels isothermer Titrationskalorimetrie ist (Apx-Fig. 14, S.108; nicht primär Teil dieser Arbeit).

Neben dem deutlichen quantitativen Unterschied der Expression beider Varianten zeigten ITC-Ergebnisse weiterhin eine um den Faktor 100 niedrigere Ca^{2+}-Affinität von NCS-1 Var2 gegenüber NCS-1 Var1. Da gerade diese Eigenschaft für die Funktion entscheidend ist, lassen sich Unterschiede der jeweiligen Varianten für Ca^{2+}-abhängige Signalwege vermuten. Das Zellwachstum unterschied sich jedoch weder in Abwesenheit (Fig. 18, S.48) noch in Gegenwart von PTX (Fig. 19, S.49) bei

Zellen, die die eine oder die andere NCS-1 Variante (nach experimenteller Induktion) exprimierten.

Eine unmittelbare Konsequenz der Funktion von NCS-1 ist die Regulation des intrazellulären Ca^{2+}. So ist bekannt, dass NCS-1 den Ca^{2+}-Efflux aus dem ER via $InsP_3R$ verstärkt. Daher wurde intrazelluläres Ca^{2+} mittels Ca^{2+}-imaging nach Rezeptorstimulation mit ATP in mit NCS-1 transfizierten SH-SY5Y Zellen gemessen. ATP aktiviert $InsP_3R$ über den P_2Y-Rezeptor und erhöht intrazelluläres Ca^{2+} möglicherweise unterschiedlich in Abhängigkeit von der transfizierten NCS-1 Variante (Apx-Fig. 15, S.109). Leider war es trotz Variation verschiedener Parameter (unterschiedlich alte (Teilungsgeneration) Zellen, stabile vs transiente Transfektion, verschiedene Transfektionswirkstoffe, Indikatorapplikationszeiten, Deckglasbehandlung) nicht möglich, reproduzierbare Ergebnisse zu erreichen. Dennoch ist dieser experimentelle Ansatz grundsätzlich sinnvoll, um die funktionelle Bedeutung der beiden NCS-1 Varianten *in vivo* zu beurteilen.

Im zweiten Teil dieser Arbeit wurde die Rolle von NCS-1 bei Chemotherapie-induzierter peripherer Neuropathie im Mausmodell untersucht. Es wurde zunächst gezeigt, dass der NCS-1 Genotyp a priori keinen Einfluss auf die gemessenen Parameter der nervalen Funktion hat. Dies ist ein wichtiges Ergebnis, da die elektrophysiologische (neben der behavioralen) Phänotypisierung der NCS-1-Knockout Maus die experimentelle Grundlage bildet, auf der mögliche durch PTX verursachte Veränderungen der NCS-1 abhängigen Hypothese der Neurotoxizität zugeordnet werden können. Auch im Hinblick auf die verschiedenen weiteren Erkrankungen in denen NCS-1 eine Rolle spielt (Tab. 2, S.11), kann dieses Ergebnis von Bedeutung sein. Deutlich wurde zudem, dass für die Vergleichbarkeit von verschieden Studien, eine exakte Angabe der Methoden wichtig ist, da die Absolutwerte der Ergebnisse von der verwendeten Methodik abhingen (z.B. antidrom/orthodrom; onset/peak).

Eine Protektion vor PTX induzierter Schädigung konnte in der Ministudie mit der Neurographie nicht nachgewiesen werden. Als Grund hierfür ist vor allem das Studiendesign anzunehmen, das lediglich bei sehr starken Effekten einen erkennbaren Unterschied angezeigt hätte. Weder bei den Wildtyp- noch bei den Knockout-Mäusen konnte eine ausreichend starke Neuropathie induziert werden, die neurographische Veränderungen zeigte. Gründe können zum einen die applizierte PTX-Dosis, zum anderen auch der Zeitpunkt der Messung (zu früh oder zu spät) sein. In der Literatur sind Protokolle mit deutlich niedrigeren Dosen beschrieben, die ausreichend waren, um eine CIPN auszulösen. Auch die Messzeitpunkte waren

engmaschiger als in anderen Studien. Schließlich fiel auf, dass nach Abschluss der Injektionen die Streuung der Daten für die sensible Amplitude zunahm. Da insbesondere eine Reduktion dieses Parameter Ausdruck einer axonalen Neuropathie ist, könnte die hier beobachtete Streuung dahingehend interpretiert werden, dass bei einer Studie mit einer größeren Beobachtungsgruppe deutliche Unterschiede zwischen den Genotypen erkennbar werden würden.

Obwohl neurographisch keine Alteration der nervalen Parameter erkennbar waren, zeigten sich deutliche neuronale Schädigungsmuster auf elektronenmikroskopischer Ebene. Quantitativ zeigte sich im Bereich der Spinalganglien und des Nervus ischiadicus eine signifikant stärkere Reduktion der Axondurchmesser von Wildtyp-Mäuse im Vergleich zu den NCS-1 Knockout Tieren (bei gleicher Myelinscheidendicke). Dieses Ergebnis lässt vermuten, dass das Fehlen von NCS-1 (Fig. 5, S.16) eine neuronale Protektion bewirkt. Es sollte berücksichtigt werden, dass das auf etwa 1000 Axonen basierende, statistisch signifikante Ergebnis (ebenso wie die elektrophysiologischen Ergebnisse) biologisch nur auf jeweils 2 Tieren (2x2 Design) basiert. Überraschend war zudem, dass dieser Befund im Bereich des Nervus tibialis umgekehrt war. Anders als in den weiter proximal gelegenen Arealen waren hier jedoch auch die Myelinschichtdicken reduziert. Gründe für diese deutlichen Unterschiede könnten zum einen in der spezifischen Anatomie der Neurone liegen, aber auch die Neuron umgebenden Faktoren (Perfusion, Mikronutrition, Temperatur) unterscheiden sich entlang der proximal-distal-Achse. Strukturelle Unterschiede wurden entlang der Nerven bereits zuvor in anderen Studien festgestellt.

Fazit: NCS-1 Var1 ist die relevante Proteinvariante im Menschen. NCS-1 Var2 spielt allenfalls eine untergeordnete Rolle, kann jedoch als Zwischenprodukt von degradiertem NCS-1 Var1 und nicht-degradiertem NCS-1 Var1 nützliche Erkenntnisse liefern. Der NCS-1 Genotyp hat keinen Einfluss auf die elektroneurographischen Parameter in C57Bl/6 Mäusen ohne PTX Behandlung. In einer 2x2 Ministudie konnten NCS-1-Genotyp-abhängige, ultrastrukturelle Unterschiede in Hinblick auf die Schädigung durch PTX auf die Axondicke festgestellt werden, die abhängig von der betrachteten Lokalisation entlang des Nerven waren. NCS-1 ist ein vielversprechender Angriffspunkt für das Verständnis der Pathogenese und die Entwicklung von Präventionsstrategien bei CIPN.

6. Bibliography

6.1 Original Works

1 Alessandri-Haber, N., et al., Interaction of transient receptor potential vanilloid 4, integrin, and SRC tyrosine kinase in mechanical hyperalgesia. J Neurosci, 2008. **28**(5): p. 1046-57.

2 Alessandri-Haber, N., et al., Transient receptor potential vanilloid 4 is essential in chemotherapy-induced neuropathic pain in the rat. J Neurosci, 2004. **24**(18): p. 4444-52.

3 Ames, J.B., et al., Structure and calcium-binding properties of Frq1, a novel calcium sensor in the yeast Saccharomyces cerevisiae. Biochemistry, 2000. **39**(40): p. 12149-61.

4 Ames, J.B., et al., Portrait of a myristoyl switch protein. Curr Opin Struct Biol, 1996. **6**(4): p. 432-8.

5 Andrade, E., et al., cDNA microarray analysis of differentially expressed genes in penile tissue after treatment with tadalafil. BJU Int, 2008. **101**(4): p. 508-12.

6 Apasu, J.E., et al., Neuronal calcium sensor 1 (NCS1) promotes motility and metastatic spread of breast cancer cells in vitro and in vivo. Faseb j, 2018: p. fj201802004R.

7 Argyriou, A.A. and H.P. Kalofonos, Vitamin E for preventing chemotherapy-induced peripheral neuropathy. Support Care Cancer, 2011. **19**(5): p. 725-6; author reply 727-8.

8 Averill, S., et al., Neuronal calcium sensor-1 is expressed by dorsal root ganglion cells, is axonally transported to central and peripheral terminals, and is concentrated at nodes. Neuroscience, 2004. **123**(2): p. 419-27.

9 Bahi, N., et al., IL1 receptor accessory protein like, a protein involved in X-linked mental retardation, interacts with Neuronal Calcium Sensor-1 and regulates exocytosis. Hum Mol Genet, 2003. **12**(12): p. 1415-25.

10 Bai, J., et al., Abnormalities in the dopamine system in schizophrenia may lie in altered levels of dopamine receptor-interacting proteins. Biol Psychiatry, 2004. **56**(6): p. 427-40.

11 Baksheeva, V.E., et al., Ca2+ -myristoyl switch in neuronal calcium sensor-1: a role of C-terminal segment. CNS Neurol Disord Drug Targets, 2015. **14**(4): p. 437-51.

12 Bandura, J. and Z.P. Feng, Current Understanding of the Role of Neuronal Calcium Sensor 1 in Neurological Disorders. Mol Neurobiol, 2019.

13 Benbow, J.H., B. DeGray, and B.E. Ehrlich, Protection of neuronal calcium sensor 1 protein in cells treated with paclitaxel. J Biol Chem, 2011. **286**(40): p. 34575-82.

14 Benbow, J.H., et al., Inhibition of paclitaxel-induced decreases in calcium signaling. J Biol Chem, 2012. **287**(45): p. 37907-16.

15 Bergmann, M., et al., Differential expression of neuronal calcium sensor-1 in the developing chick retina. J Comp Neurol, 2002. **449**(3): p. 231-40.

16 Berridge, M.J., M.D. Bootman, and H.L. Roderick, Calcium signalling: dynamics, homeostasis and remodelling. Nat Rev Mol Cell Biol, 2003. **4**(7): p. 517-29.

17 Berridge, M.J., P. Lipp, and M.D. Bootman, The versatility and universality of calcium signalling. Nat Rev Mol Cell Biol, 2000. **1**(1): p. 11-21.

18 Blachford, C., et al., Discrete proteolysis of neuronal calcium sensor-1 (NCS-1) by mu-calpain disrupts calcium binding. Cell Calcium, 2009. **46**(4): p. 257-62.

19 Blagosklonny, M.V. and T. Fojo, Molecular effects of paclitaxel: myths and reality (a critical review). Int J Cancer, 1999. **83**(2): p. 151-6.

20 Blasiole, B., et al., Neuronal calcium sensor-1 gene ncs-1a is essential for semicircular canal formation in zebrafish inner ear. J Neurobiol, 2005. **64**(3): p. 285-97.

21 Boeckel, G.R. and B.E. Ehrlich, NCS-1 is a regulator of calcium signaling in health and disease. Biochim Biophys Acta, 2018.

22 Boehmerle, W., et al., TRPV4 inhibition prevents paclitaxel-induced neurotoxicity in preclinical models. Exp Neurol, 2018. **306**: p. 64-75.

23 Boehmerle, W., et al., Electrophysiological, behavioral and histological characterization of paclitaxel, cisplatin, vincristine and bortezomib-induced neuropathy in C57Bl/6 mice. Sci Rep, 2014. **4**: p. 6370.

24 Boehmerle, W., et al., Paclitaxel induces calcium oscillations via an inositol 1,4,5-trisphosphate receptor and neuronal calcium sensor 1-dependent mechanism. Proc Natl Acad Sci U S A, 2006. **103**(48): p. 18356-61.

25 Boehmerle, W., et al., Chronic exposure to paclitaxel diminishes phosphoinositide signaling by calpain-mediated neuronal calcium sensor-1 degradation. Proc Natl Acad Sci U S A, 2007. **104**(26): p. 11103-8.

26 Bourne, Y., et al., Immunocytochemical localization and crystal structure of human frequenin (neuronal calcium sensor 1). J Biol Chem, 2001. **276**(15): p. 11949-55.

27 Bravo-Sagua, R., et al., Calcium Transport and Signaling in Mitochondria. Compr Physiol, 2017. **7**(2): p. 623-634.

28 Bronner, F., Extracellular and intracellular regulation of calcium homeostasis. ScientificWorldJournal, 2001. **1**: p. 919-25.

29 Burgoyne, R.D., Neuronal calcium sensor proteins: generating diversity in neuronal Ca2+ signalling. Nat Rev Neurosci, 2007. **8**(3): p. 182-93.

30 Burgoyne, R.D. and L.P. Haynes, Sense and specificity in neuronal calcium signalling. Biochim Biophys Acta, 2015. **1853**(9): p. 1921-32.

31 Burgoyne, T., S. Patel, and E.R. Eden, Calcium signaling at ER membrane contact sites. Biochim Biophys Acta, 2015. **1853**(9): p. 2012-7.

32 Byrd, C.A., et al., Heat shock protein 90 mediates macrophage activation by Taxol and bacterial lipopolysaccharide. Proc Natl Acad Sci U S A, 1999. **96**(10): p. 5645-50.

33 Capiod, T., Extracellular Calcium Has Multiple Targets to Control Cell Proliferation. Adv Exp Med Biol, 2016. **898**: p. 133-56.

34 Carafoli, E. and J. Krebs, Why Calcium? How Calcium Became the Best Communicator. J Biol Chem, 2016. **291**(40): p. 20849-20857.

35 Carafoli, E., et al., Generation, control, and processing of cellular calcium signals. Crit Rev Biochem Mol Biol, 2001. **36**(2): p. 107-260.

36 Carozzi, V.A., et al., Neurophysiological and neuropathological characterization of new murine models of chemotherapy-induced chronic peripheral neuropathies. Exp Neurol, 2010. **226**(2): p. 301-9.

37 Cavaletti, G., P. Alberti, and P. Marmiroli, Chemotherapy-induced peripheral neurotoxicity in the era of pharmacogenomics. Lancet Oncol, 2011. **12**(12): p. 1151-61.

38 Chen, C., et al., Human neuronal calcium sensor-1 shows the highest expression level in cerebral cortex. Neurosci Lett, 2002. **319**(2): p. 67-70.

39 Chen, L.H., et al., Integrating Image-Based High-Content Screening with Mouse Models Identifies 5-Hydroxydecanoate as a Neuroprotective Drug for Paclitaxel-Induced Neuropathy. Mol Cancer Ther, 2015. **14**(10): p. 2206-14.

40 Chen, Y.F., et al., Minoxidil is a potential neuroprotective drug for paclitaxel-induced peripheral neuropathy. Sci Rep, 2017. **7**: p. 45366.

41 Clapham, D.E., *Calcium signaling.* Cell, 2007. **131**(6): p. 1047-58.

42 Comim, C.M., et al., Evaluation of NCS-1, DARPP-32, and neurotrophins in hippocampus and prefrontal cortex in rats submitted to sepsis. Synapse, 2014. **68**(10): p. 474-9.

43 Corpet, F., Multiple sequence alignment with hierarchical clustering. Nucleic Acids Res, 1988. **16**(22): p. 10881-90.

44 Cox, J.A., et al., Cation binding and conformational changes in VILIP and NCS-1, two neuron-specific calcium-binding proteins. J Biol Chem, 1994. **269**(52): p. 32807-13.

45 Crist, R.A., et al., Effects of EDTA on routine and specialized coagulation testing and an easy method to distinguish EDTA-treated from citrated plasma samples. Lab Hematol, 2009. **15**(4): p. 45-8.

46 Cuerrier, D., T. Moldoveanu, and P.L. Davies, Determination of peptide substrate specificity for mu-calpain by a peptide library-based approach: the importance of primed side interactions. J Biol Chem, 2005. **280**(49): p. 40632-41.

47 Cunningham, F., et al., *Ensembl 2015.* Nucleic Acids Research, 2015. **43**(D1): p. D662-D669.

48 D'Onofrio, S., J. Hyde, and E. Garcia-Rill, Interaction between neuronal calcium sensor protein 1 and lithium in pedunculopontine neurons. Physiol Rep, 2017. **5**(7).

49 D'Onofrio, S., S. Mahaffey, and E. Garcia-Rill, *Role of calcium channels in bipolar disorder.* Curr Psychopharmacol, 2017. **6**(2): p. 122-135.

50 D'Onofrio, S., et al., Lithium decreases the effects of neuronal calcium sensor protein 1 in pedunculopontine neurons. Physiol Rep, 2016. **4**(6).

51 Dahl, J.P., et al., Interaction between variation in the D2 dopamine receptor (DRD2) and the neuronal calcium sensor-1 (FREQ) genes in predicting response to nicotine replacement therapy for tobacco dependence. Pharmacogenomics J, 2006. **6**(3): p. 194-9.

52 de Rezende, V.B., et al., NCS-1 deficiency causes anxiety and depressive-like behavior with impaired non-aversive memory in mice. Physiol Behav, 2014. **130**: p. 91-8.

53 Dewenter, M., et al., Calcium Signaling and Transcriptional Regulation in Cardiomyocytes. Circ Res, 2017. **121**(8): p. 1000-1020.

54 Dietrich, A., Modulators of Transient Receptor Potential (TRP) Channels as Therapeutic Options in Lung Disease. Pharmaceuticals (Basel), 2019. **12**(1).

55 Dominguez, D.C., M. Guragain, and M. Patrauchan, Calcium binding proteins and calcium signaling in prokaryotes. Cell Calcium, 2015. **57**(3): p. 151-65.

56 Donkor, I.O., An updated patent review of calpain inhibitors (2012 - 2014). Expert Opin Ther Pat, 2015. **25**(1): p. 17-31.

57 Donkor, I.O. and R. Korukonda, Synthesis and calpain inhibitory activity of peptidomimetic compounds with constrained amino acids at the P2 position. Bioorg Med Chem Lett, 2008. **18**(17): p. 4806-8.

58 58. Dougherty, P.M., et al., Taxol-induced sensory disturbance is characterized by preferential impairment of myelinated fiber function in cancer patients. Pain, 2004. **109**(1-2): p. 132-42.

59 Dragicevic, E., et al., Cav1.3 channels control D2-autoreceptor responses via NCS-1 in substantia nigra dopamine neurons. Brain, 2014. **137**(Pt 8): p. 2287-302.

60 Drumond, L.E., et al., Differential effects of swimming training on neuronal calcium sensor-1 expression in rat hippocampus/cortex and in object recognition memory tasks. Brain Res Bull, 2012. **88**(4): p. 385-91.

61 Duda, J., C. Potschke, and B. Liss, Converging roles of ion channels, calcium, metabolic stress, and activity pattern of Substantia nigra dopaminergic neurons in health and Parkinson's disease. J Neurochem, 2016. **139 Suppl 1**: p. 156-178.

62 Egorova, P.A. and I.B. Bezprozvanny, Inositol 1,4,5-trisphosphate receptors and neurodegenerative disorders. Febs j, 2018. **285**(19): p. 3547-3565.

63 Everaerts, W., et al., Inhibition of the cation channel TRPV4 improves bladder function in mice and rats with cyclophosphamide-induced cystitis. Proc Natl Acad Sci U S A, 2010. **107**(44): p. 19084-9.

64 Fees, C.P. and B.J. Stith, Insemination or phosphatidic acid induces an outwardly spiraling disk of elevated Ca(2+) to produce the Ca(2+) wave during Xenopus laevis fertilization. Dev Biol, 2019.

65 Gambardella, J., et al., New Insights in Cardiac Calcium Handling and Excitation-Contraction Coupling. Adv Exp Med Biol, 2018. **1067**: p. 373-385.

66 Gambino, F., et al., IL1-receptor accessory protein-like 1 (IL1RAPL1), a protein involved in cognitive functions, regulates N-type Ca2+-channel and neurite elongation. Proc Natl Acad Sci U S A, 2007. **104**(21): p. 9063-8.

67 Garcia-Rill, E., et al., Implications of gamma band activity in the pedunculopontine nucleus. J Neural Transm (Vienna), 2016. **123**(7): p. 655-665.

68 Garcia-Rill, E., et al., Pedunculopontine arousal system physiology - Implications for insomnia. Sleep Sci, 2015. **8**(2): p. 92-9.

69 Geer, L.Y., et al., The NCBI BioSystems database. Nucleic Acids Res, 2010. **38**(Database issue): p. D492-6.

70 Gelderblom, H., et al., Cremophor EL: the drawbacks and advantages of vehicle selection for drug formulation. Eur J Cancer, 2001. **37**(13): p. 1590-8.

71 Gerke, V. and S.E. Moss, Annexins: from structure to function. Physiol Rev, 2002. **82**(2): p. 331-71.

72 Gierke, P., et al., Expression analysis of members of the neuronal calcium sensor protein family: combining bioinformatics and Western blot analysis. Biochem Biophys Res Commun, 2004. **323**(1): p. 38-43.

73 Grienberger, C. and A. Konnerth, *Imaging calcium in neurons.* Neuron, 2012. **73**(5): p. 862-85.

74 Hamilton, R.T., et al., Elevated protein carbonylation, and misfolding in sciatic nerve from db/db and Sod1(-/-) mice: plausible link between oxidative stress and demyelination. PLoS One, 2013. **8**(6): p. e65725.

75 Handley, M.T., et al., Structural and functional deficits in a neuronal calcium sensor-1 mutant identified in a case of autistic spectrum disorder. PLoS One, 2010. **5**(5): p. e10534.

76 Hayes, M.J., et al., *Annexinopathies.* Subcell Biochem, 2007. **45**: p. 1-28.

77 Haynes, L.P., et al., Analysis of the interacting partners of the neuronal calcium-binding proteins L-CaBP1, hippocalcin, NCS-1 and neurocalcin delta. Proteomics, 2006. **6**(6): p. 1822-32.

78 Haynes, L.P., et al., Specificity, promiscuity and localization of ARF protein interactions with NCS-1 and phosphatidylinositol-4 kinase-III beta. Traffic, 2007. **8**(8): p. 1080-92.

79 Haynes, L.P., G.M. Thomas, and R.D. Burgoyne, Interaction of neuronal calcium sensor-1 and ADP-ribosylation factor 1 allows bidirectional control of phosphatidylinositol 4-kinase beta and trans-Golgi network-plasma membrane traffic. J Biol Chem, 2005. **280**(7): p. 6047-54.

80 Heidarsson, P.O., et al., The C-terminal tail of human neuronal calcium sensor 1 regulates the conformational stability of the Ca(2)(+)(-) activated state. J Mol Biol, 2012. **417**(1-2): p. 51-64.

81 Heidarsson, P.O., et al., Direct single-molecule observation of calcium-dependent misfolding in human neuronal calcium sensor-1. Proc Natl Acad Sci U S A, 2014. **111**(36): p. 13069-74.

82 Heizmann, C.W., Ca(2+)-Binding Proteins of the EF-Hand Superfamily: Diagnostic and Prognostic Biomarkers and Novel Therapeutic Targets. Methods Mol Biol, 2019. **1929**: p. 157-186.

83 Hendricks, K.B., et al., Yeast homologue of neuronal frequenin is a regulator of phosphatidylinositol-4-OH kinase. Nat Cell Biol, 1999. **1**(4): p. 234-41.

84 Hershman, D.L., et al., Prevention and management of chemotherapy-induced peripheral neuropathy in survivors of adult cancers: American Society of Clinical Oncology clinical practice guideline. J Clin Oncol, 2014. **32**(18): p. 1941-67.

85 Huang, H., et al., Vitamin E does not decrease the incidence of chemotherapy-induced peripheral neuropathy: a meta-analysis. Contemp Oncol (Pozn), 2016. **20**(3): p. 237-41.

86 Hui, H., et al., Calcium-sensing mechanism in TRPC5 channels contributing to retardation of neurite outgrowth. J Physiol, 2006. **572**(Pt 1): p. 165-72.

87 Hui, K., et al., Neuronal calcium sensor-1 modulation of optimal calcium level for neurite outgrowth. Development, 2007. **134**(24): p. 4479-89.

88 Kabbani, N., et al., Interaction with neuronal calcium sensor NCS-1 mediates desensitization of the D2 dopamine receptor. J Neurosci, 2002. **22**(19): p. 8476-86.

89 Kasius, K.M., et al., Comparison of peak versus onset latency measurements in electrodiagnostic tests for carpal tunnel syndrome. J Clin Neurophysiol, 2014. **31**(4): p. 382-6.

90 Kasri, N.N., et al., Regulation of InsP3 receptor activity by neuronal Ca2+-binding proteins. Embo j, 2004. **23**(2): p. 312-21.

91 Kidd, J.F., et al., Paclitaxel affects cytosolic calcium signals by opening the mitochondrial permeability transition pore. J Biol Chem, 2002. **277**(8): p. 6504-10.

92 Koh, P.O., et al., Up-regulation of neuronal calcium sensor-1 (NCS-1) in the prefrontal cortex of schizophrenic and bipolar patients. Proc Natl Acad Sci U S A, 2003. **100**(1): p. 313-7.

93 Kramer, R., et al., Neurotoxic 1-deoxysphingolipids and paclitaxel-induced peripheral neuropathy. Faseb j, 2015. **29**(11): p. 4461-72.

94 Krebs, J., L.B. Agellon, and M. Michalak, Ca(2+) homeostasis and endoplasmic reticulum (ER) stress: An integrated view of calcium signaling. Biochem Biophys Res Commun, 2015. **460**(1): p. 114-21.

95 Kretsinger, R.H. and C.E. Nockolds, Carp muscle calcium-binding protein. II. Structure determination and general description. J Biol Chem, 1973. **248**(9): p. 3313-26.

96 Krukowski, K., et al., Prevention of chemotherapy-induced peripheral neuropathy by the small-molecule inhibitor pifithrin-mu. Pain, 2015. **156**(11): p. 2184-92.

97 Lemire, S., A. Jeromin, and E. Boisselier, Membrane binding of Neuronal Calcium Sensor-1 (NCS1). Colloids Surf B Biointerfaces, 2016. **139**: p. 138-47.

98 Lewit-Bentley, A. and S. Rety, *EF-hand calcium-binding proteins.* Curr Opin Struct Biol, 2000. **10**(6): p. 637-43.

99 Lian, L.Y., et al., Characterisation of the interaction of the C-terminus of the dopamine D2 receptor with neuronal calcium sensor-1. PLoS One, 2011. **6**(11): p. e27779.

100 Lim, S., et al., Structure of a Ca2+-myristoyl switch protein that controls activation of a phosphatidylinositol 4-kinase in fission yeast. J Biol Chem, 2011. **286**(14): p. 12565-77.

101 Lourenssen, S., et al., Intestinal inflammation modulates expression of the synaptic vesicle protein neuronal calcium sensor-1. Am J Physiol Gastrointest Liver Physiol, 2002. **282**(6): p. G1097-104.

102 Maki, M., et al., Structures, functions and molecular evolution of the penta-EF-hand Ca2+-binding proteins. Biochim Biophys Acta, 2002. **1600**(1-2): p. 51-60.

103 Mansilla, A., et al., Interference of the complex between NCS-1 and Ric8a with phenothiazines regulates synaptic function and is an approach for fragile X syndrome. Proc Natl Acad Sci U S A, 2017. **114**(6): p. E999-e1008.

104 Martin, N. and D. Bernard, Calcium signaling and cellular senescence. Cell Calcium, 2018. **70**: p. 16-23.

105 Materazzi, S., et al., TRPA1 and TRPV4 mediate paclitaxel-induced peripheral neuropathy in mice via a glutathione-sensitive mechanism. Pflugers Arch, 2012. **463**(4): p. 561-9.

106 Matifat, F., et al., Regulation of InsP3-mediated Ca2+ release by CaMKII in Xenopus oocytes. Pflugers Arch, 2001. **441**(6): p. 796-801.

107 Matsumoto, M., et al., Ataxia and epileptic seizures in mice lacking type 1 inositol 1,4,5-trisphosphate receptor. Nature, 1996. **379**(6561): p. 168-71.

108 McFerran, B.W., M.E. Graham, and R.D. Burgoyne, Neuronal Ca2+ sensor 1, the mammalian homologue of frequenin, is expressed in chromaffin and PC12 cells and regulates neurosecretion from dense-core granules. J Biol Chem, 1998. **273**(35): p. 22768-72.

109 McMahon, S.M. and M.B. Jackson, An Inconvenient Truth: Calcium Sensors Are Calcium Buffers. Trends Neurosci, 2018. **41**(12): p. 880-884.

110 Mo, M., et al., Prevention of paclitaxel-induced peripheral neuropathy by lithium pretreatment. FASEB J, 2012. **26**(11): p. 4696-709.

111 Molassiotis, A., et al., Are we mis-estimating chemotherapy-induced peripheral neuropathy? Analysis of assessment methodologies from a prospective, multinational, longitudinal cohort study of patients receiving neurotoxic chemotherapy. BMC Cancer, 2019. **19**(1): p. 132.

112 Montani, C., et al., The Synaptic and Neuronal Functions of the X-Linked Intellectual Disability Protein Interleukin-1 Receptor Accessory Protein Like 1 (IL1RAPL1). Dev Neurobiol, 2019. **79**(1): p. 85-95.

113 Moore, L.M., et al., Calcium Sensor, NCS-1, Promotes Tumor Aggressiveness and Predicts Patient Survival. Mol Cancer Res, 2017. **15**(7): p. 942-952.

114 Multani, P.K., et al., Neuronal calcium sensor-1 and cocaine addiction: a genetic association study in African-Americans and European Americans. Neurosci Lett, 2012. **531**(1): p. 46-51.

115 Mun, H.S., et al., Self-directed exploration provides a Ncs1-dependent learning bonus. Sci Rep, 2015. **5**: p. 17697.

116 Murakami, T., et al., Development of sensory neuropathy in streptozotocin-induced diabetic mice. Brain Behav, 2013. **3**(1): p. 35-41.

117 Naaz, F., et al., Anti-tubulin agents of natural origin: Targeting taxol, vinca, and colchicine binding domains. Eur J Med Chem, 2019. **171**: p. 310-331.

118 Nakamura, T.Y., et al., Neuronal calcium sensor-1 promotes immature heart function and hypertrophy by enhancing Ca2+ signals. Circ Res, 2011. **109**(5): p. 512-23.

119 Nakamura, T.Y., et al., Possible Signaling Pathways Mediating Neuronal Calcium Sensor-1-Dependent Spatial Learning and Memory in Mice. PLoS One, 2017. **12**(1): p. e0170829.

120 Nakamura, T.Y., S. Nakao, and S. Wakabayashi, Neuronal Ca(2+) sensor-1 contributes to stress tolerance in cardiomyocytes via activation of mitochondrial detoxification pathways. J Mol Cell Cardiol, 2016. **99**: p. 23-34.

121 Nakamura, T.Y., et al., Developmental expression of NCS-1 (frequenin), a regulator of Kv4 K+ channels, in mouse heart. Pediatr Res, 2003. **53**(4): p. 554-7.

122 Nakamura, T.Y. and S. Wakabayashi, Role of neuronal calcium sensor-1 in the cardiovascular system. Trends Cardiovasc Med, 2012. **22**(1): p. 12-7.

123 Nakao, S., S. Wakabayashi, and T.Y. Nakamura, Stimulus-dependent regulation of nuclear Ca2+ signaling in cardiomyocytes: a role of neuronal calcium sensor-1. PLoS One, 2015. **10**(4): p. e0125050.

124 Nakata, T. and H. Yorifuji, Morphological evidence of the inhibitory effect of taxol on the fast axonal transport. Neurosci Res, 1999. **35**(2): p. 113-22.

125 Nalefski, E.A. and J.J. Falke, The C2 domain calcium-binding motif: structural and functional diversity. Protein Sci, 1996. **5**(12): p. 2375-90.

126 Naqvi, M.M., et al., Single-molecule folding mechanisms of the apo- and Mg(2+)-bound states of human neuronal calcium sensor-1. Biophys J, 2015. **109**(1): p. 113-23.

127 Navarro, G., et al., NCS-1 associates with adenosine A(2A) receptors and modulates receptor function. Front Mol Neurosci, 2012. **5**: p. 53.

128 Ng, E., et al., Neuronal calcium sensor-1 deletion in the mouse decreases motivation and dopamine release in the nucleus accumbens. Behav Brain Res, 2016. **301**: p. 213-25.

129 Oh, S.S., et al., The effects of anesthesia on measures of nerve conduction velocity in male C57Bl6/J mice. Neurosci Lett, 2010. **483**(2): p. 127-31.

130 Pangrsic, T., E. Reisinger, and T. Moser, Otoferlin: a multi-C2 domain protein essential for hearing. Trends Neurosci, 2012. **35**(11): p. 671-80.

131 Patel, S., et al., Ca2+-independent inhibition of inositol trisphosphate receptors by calmodulin: redistribution of calmodulin as a possible means of regulating Ca2+ mobilization. Proc Natl Acad Sci U S A, 1997. **94**(21): p. 11627-32.

132 Payne, S.C., et al., Myelin sheath decompaction, axon swelling, and functional loss during chronic secondary degeneration in rat optic nerve. Invest Ophthalmol Vis Sci, 2012. **53**(10): p. 6093-101.

133 Pease-Raissi, S.E., et al., Paclitaxel Reduces Axonal Bclw to Initiate IP3R1-Dependent Axon Degeneration. Neuron, 2017. **96**(2): p. 373-386.e6.

134 Petko, J.A., et al., Proteomic and functional analysis of NCS-1 binding proteins reveals novel signaling pathways required for inner ear development in zebrafish. BMC Neurosci, 2009. **10**: p. 27.

135 Pinheiro, P.S., S. Houy, and J.B. Sorensen, C2-domain containing calcium sensors in neuroendocrine secretion. J Neurochem, 2016. **139**(6): p. 943-958.

136 Piton, A., et al., Mutations in the calcium-related gene IL1RAPL1 are associated with autism. Hum Mol Genet, 2008. **17**(24): p. 3965-74.

137 Plastaras, C.T., et al., Effect of interelectrode distance on sural nerve action potential parameters. Am J Phys Med Rehabil, 2008. **87**(3): p. 183-8.

138 Pongs, O., et al., Frequenin--a novel calcium-binding protein that modulates synaptic efficacy in the Drosophila nervous system. Neuron, 1993. **11**(1): p. 15-28.

139 Pourmohammadi, N., et al., Lithium attenuates peripheral neuropathy induced by paclitaxel in rats. Basic Clin Pharmacol Toxicol, 2012. **110**(3): p. 231-7.

140 Pozzi, D., I. Corradini, and M. Matteoli, The Control of Neuronal Calcium Homeostasis by SNAP-25 and its Impact on Neurotransmitter Release. Neuroscience, 2018.

141 Prins, D. and M. Michalak, *Organellar calcium buffers.* Cold Spring Harb Perspect Biol, 2011. **3**(3).

142 Rayl, M., et al., Penta-EF-Hand Protein Peflin Is a Negative Regulator of ER-To-Golgi Transport. PLoS One, 2016. **11**(6): p. e0157227.

143 Reynolds, A.J., S.E. Bartlett, and C. Morgans, The distribution of neuronal calcium sensor-1 protein in the developing and adult rat retina. Neuroreport, 2001. **12**(4): p. 725-8.

144 Rivner, M.H., T.R. Swift, and K. Malik, Influence of age and height on nerve conduction. Muscle Nerve, 2001. **24**(9): p. 1134-41.

145 Rodi, D.J., et al., Screening of a library of phage-displayed peptides identifies human bcl-2 as a taxol-binding protein. J Mol Biol, 1999. **285**(1): p. 197-203.

146 Romero-Pozuelo, J., et al., Chronic and acute alterations in the functional levels of Frequenins 1 and 2 reveal their roles in synaptic transmission and axon terminal morphology. Eur J Neurosci, 2007. **26**(9): p. 2428-43.

147 Romero-Pozuelo, J., et al., The guanine-exchange factor Ric8a binds to the Ca(2)(+) sensor NCS-1 to regulate synapse number and neurotransmitter release. J Cell Sci, 2014. **127**(Pt 19): p. 4246-59.

148 Rose, A.S., et al., NGL viewer: web-based molecular graphics for large complexes. Bioinformatics, 2018. **34**(21): p. 3755-3758.

149 Rowinsky, E.K., et al., *Neurotoxicity of Taxol.* J Natl Cancer Inst Monogr, 1993(15): p. 107-15.

150 Rowinsky, E.K., et al., Paclitaxel steady-state plasma concentration as a determinant of disease outcome and toxicity in lung cancer patients treated with paclitaxel and cisplatin. Clin Cancer Res, 1999. **5**(4): p. 767-74.

151 Roytta, M. and C.S. Raine, Taxol-induced neuropathy: further ultrastructural studies of nerve fibre changes in situ. J Neurocytol, 1985. **14**(1): p. 157-75.

152 Saab, B.J., et al., NCS-1 in the dentate gyrus promotes exploration, synaptic plasticity, and rapid acquisition of spatial memory. Neuron, 2009. **63**(5): p. 643-56.

153 Schiff, P.B., J. Fant, and S.B. Horwitz, Promotion of microtubule assembly in vitro by taxol. Nature, 1979. **277**(5698): p. 665-7.

154 Schlecker, C., et al., Neuronal calcium sensor-1 enhancement of InsP3 receptor activity is inhibited by therapeutic levels of lithium. J Clin Invest, 2006. **116**(6): p. 1668-74.

155 Schneider, C.A., W.S. Rasband, and K.W. Eliceiri, *NIH Image to ImageJ: 25 years of image analysis.* Nat Methods, 2012. **9**(7): p. 671-5.

156 Schuette, D., et al., Hepatocellular Carcinoma Outcome Is Predicted by Expression of Neuronal Calcium Sensor 1. Cancer Epidemiol Biomarkers Prev, 2018. **27**(9): p. 1091-1100.

157 Seress, L., et al., Distribution, morphological features, and synaptic connections of parvalbumin- and calbindin D28k-immunoreactive neurons in the human hippocampal formation. J Comp Neurol, 1993. **337**(2): p. 208-30.

158 Seretny, M., et al., Incidence, prevalence, and predictors of chemotherapy-induced peripheral neuropathy: A systematic review and meta-analysis. Pain, 2014. **155**(12): p. 2461-70.

159 Sherman, D.L., et al., Arrest of myelination and reduced axon growth when Schwann cells lack mTOR. J Neurosci, 2012. **32**(5): p. 1817-25.

160 Shibao, K., et al., Loss of inositol 1,4,5-trisphosphate receptors from bile duct epithelia is a common event in cholestasis. Gastroenterology, 2003. **125**(4): p. 1175-87.

161 Sippy, T., et al., Acute changes in short-term plasticity at synapses with elevated levels of neuronal calcium sensor-1. Nat Neurosci, 2003. **6**(10): p. 1031-8.

162 Smith, S.B., S.E. Crager, and J.S. Mogil, Paclitaxel-induced neuropathic hypersensitivity in mice: responses in 10 inbred mouse strains. Life Sci, 2004. **74**(21): p. 2593-604.

163 Souza, B.R., et al., DARPP-32 and NCS-1 expression is not altered in brains of rats treated with typical or atypical antipsychotics. Neurochem Res, 2008. **33**(3): p. 533-8.

164 Souza, B.R., et al., Lack of effects of typical and atypical antipsychotics in DARPP-32 and NCS-1 levels in PC12 cells overexpressing NCS-1. J Negat Results Biomed, 2010. **9**: p. 4.

165 Souza, R.P., et al., Methylphenidate alters NCS-1 expression in rat brain. Neurochem Int, 2008. **53**(1-2): p. 12-6.

166 Starobova, H. and I. Vetter, Pathophysiology of Chemotherapy-Induced Peripheral Neuropathy. Front Mol Neurosci, 2017. **10**: p. 174.

167 Strom, E., et al., Small-molecule inhibitor of p53 binding to mitochondria protects mice from gamma radiation. Nat Chem Biol, 2006. **2**(9): p. 474-9.

168 Strotmann, R., G. Schultz, and T.D. Plant, Ca2+-dependent potentiation of the nonselective cation channel TRPV4 is mediated by a C-terminal calmodulin binding site. J Biol Chem, 2003. **278**(29): p. 26541-9.

169 Strynadka, N.C. and M.N. James, Crystal structures of the helix-loop-helix calcium-binding proteins. Annu Rev Biochem, 1989. **58**: p. 951-98.

170 Sullivan, K.A., et al., Mouse models of diabetic neuropathy. Neurobiol Dis, 2007. **28**(3): p. 276-85.

171 Tasnim, A., et al., Paclitaxel causes degeneration of both central and peripheral axon branches of dorsal root ganglia in mice. BMC Neurosci, 2016. **17**(1): p. 47.

172 Torres, K.C., et al., Expression of neuronal calcium sensor-1 (NCS-1) is decreased in leukocytes of schizophrenia and bipolar disorder patients. Prog Neuropsychopharmacol Biol Psychiatry, 2009. **33**(2): p. 229-34.

173 Treloar, H.B., et al., Expression of the neuronal calcium sensor protein NCS-1 in the developing mouse olfactory pathway. J Comp Neurol, 2005. **482**(2): p. 201-16.

174 Tsujimoto, T., et al., Neuronal calcium sensor 1 and activity-dependent facilitation of P/Q-type calcium currents at presynaptic nerve terminals. Science, 2002. **295**(5563): p. 2276-9.

175 Tsvetkov, P.O., et al., Functional Status of Neuronal Calcium Sensor-1 Is Modulated by Zinc Binding. Front Mol Neurosci, 2018. **11**: p. 459.

176 Uhlen, M., et al., Proteomics. Tissue-based map of the human proteome. Science, 2015. **347**(6220): p. 1260419.

177 Urbano, F.J., et al., Pedunculopontine Nucleus Gamma Band Activity-Preconscious Awareness, Waking, and REM Sleep. Front Neurol, 2014. **5**: p. 210.

178 Valls-Sole, J., J. Leote, and P. Pereira, Antidromic vs orthodromic sensory median nerve conduction studies. Clin Neurophysiol Pract, 2016. **1**: p. 18-25.

179 Vaziri, C. and C.P. Downes, G-protein-mediated activation of turkey erythrocyte phospholipase C by beta-adrenergic and P2y-purinergic receptors. Biochem J, 1992. **284 (Pt 3)**: p. 917-22.

180 Walser, M., Ion association. VI. Interactions between calcium, magnesium, inorganic phosphate, citrate and protein in normal human plasma. J Clin Invest, 1961. **40**: p. 723-30.

181 Walsh, M.E., et al., Use of Nerve Conduction Velocity to Assess Peripheral Nerve Health in Aging Mice. J Gerontol A Biol Sci Med Sci, 2015. **70**(11): p. 1312-9.

182 Wang, B., et al., Neuronal Calcium Sensor 1 Has Two Variants with Distinct Calcium Binding Characteristics. PLoS One, 2016. **11**(8): p. e0161414.

183 Wang, L., et al., Phosphodiesterase-5 is a therapeutic target for peripheral neuropathy in diabetic mice. Neuroscience, 2011. **193**: p. 399-410.

184 Wang, M., et al., Role of Ca(2)(+) and ion channels in the regulation of apoptosis under hypoxia. Histol Histopathol, 2018. **33**(3): p. 237-246.

185 Wang, M.S., et al., Calpain inhibition protects against Taxol-induced sensory neuropathy. Brain, 2004. **127**(Pt 3): p. 671-9.

186 Weaver, B.A., How Taxol/paclitaxel kills cancer cells. Mol Biol Cell, 2014. **25**(18): p. 2677-81.

187 Weiss, J.L., H. Hui, and R.D. Burgoyne, Neuronal calcium sensor-1 regulation of calcium channels, secretion, and neuronal outgrowth. Cell Mol Neurobiol, 2010. **30**(8): p. 1283-92.

188 Wickham, N.W., et al., Measurement of intracellular calcium concentration in intact monolayers of human endothelial cells. J Lab Clin Med, 1988. **112**(2): p. 157-67.

189 Xu, L., et al., Two EF-hand motifs in ryanodine receptor calcium release channels contribute to isoform-specific regulation by calmodulin. Cell Calcium, 2017. **66**: p. 62-70.

190 Yanez, M., J. Gil-Longo, and M. Campos-Toimil, *Calcium binding proteins.* Adv Exp Med Biol, 2012. **740**: p. 461-82.

191 Ye, J., et al., Primer-BLAST: a tool to design target-specific primers for polymerase chain reaction. BMC Bioinformatics, 2012. **13**: p. 134.

192 Yip, P.K., et al., Cortical overexpression of neuronal calcium sensor-1 induces functional plasticity in spinal cord following unilateral pyramidal tract injury in rat. PLoS Biol, 2010. **8**(6): p. e1000399.

193 Zhang, K., et al., Paclitaxel accelerates spontaneous calcium oscillations in cardiomyocytes by interacting with NCS-1 and the InsP3R. J Mol Cell Cardiol, 2010. **49**(5): p. 829-35.

194 Zhu, Y., et al., R102Q mutation shifts the salt-bridge network and reduces the structural flexibility of human neuronal calcium sensor-1 protein. J Phys Chem B, 2014. **118**(46): p. 13112-22.

6.2 Internet & Software Sources

[I 1] Leitlinienprogramm Onkologie (Deutsche Krebsgesellschaft, Deutsche Krebshilfe, AWMF): Supportive Therapie bei onkologischen PatientInnen - Langversion 1.0, 2016, AWMF Registernummer: 032/054OL, https://www.leitlinienprogramm-onkologie.de/fileadmin/user_upload/Downloads/Leitlinien/Supportivtherapie/LL_Supportiv_Langversion_1.1.pdf (zuletzt eingesehen 16.05.2019) — pp. 13 & 65

[I 2] Super West Dura, INSTRUCTIONS https://assets.thermofisher.com/TFS-Assets/LSG/manuals/MAN0011307_SupSig_West_Dura_Extend_Dur_Subs_UG.pdf (zuletzt eingesehen 16.05.2019) — pp. 19 & 34

[I 3] UV-Vis Spectrophotometer user manual https://mlz-garching.de/files/nanodrop_2000_user_manual.pdf (zuletzt eingesehen 16.05.2019) — pp.19 & 23

[I 4] 7500 Fast & 7500 Real-Time PCR System, user manual https://assets.thermofisher.com/TFS-Assets/LSG/manuals/cms_050330.pdf (zuletzt eingesehen 16.05.2019) — pp.19, 22, 32, 40&41

[I 5] QIAprep® Miniprep/Midiprep Kit Handbook PROM-1206-1095533-HB-QIAprep-Miniprep-0615-WW-1.pdf (zuletzt eingesehen 22.02.2019) — pp. 19 & 31

[I 6]	RNeasy® Mini Handbook https://www.qiagen.com/ch/resources/resourcedetail?id=14e7cf6e-521a-4cf7-8cbc-bf9f6fa33e24&lang=en & http://www.bea.ki.se/documents/EN-RNeasy%20handbook.pdf (zuletzt eingesehen 16.05.2019)	pp. 19, 25, 95 & 101
[I 7]	For Research Use Only. Not for use in diagnostic procedures.High Capacity cDNA Reverse Transcription KitUSER GUIDE https://assets.thermofisher.com/TFS-Assets/LSG/manuals/MAN0017977_highcap_cDNA_RT_UG.pdf (zuletzt eingesehen 16.05.2019)	pp. 19 & 26
[I 8]	TOPO® TA Cloning® Kit User guide https://tools.thermofisher.com/content/sfs/manuals/topota_man.pdf (zuletzt eingesehen 16.05.2019)	pp. 19, 29, 95 & 102
[I 9]	REDExtract-N-Amp Tissue PCR Kit, protocol https://www.sigmaaldrich.com/technical-documents/protocols/biology/redextract-n-amp.html (zuletzt eingesehen 16.05.2019)	pp. 19 & 35
[I 10]	1 Kb Plus DNA Ladder https://www.thermofisher.com/order/catalog/product/10787018 (zuletzt eingesehen 16.05.2019)	pp. 20, 95 & 97
[I 11]	SYBR Select Master Mix, QUICK REFERENCE https://assets.thermofisher.com/TFS-Assets/LSG/manuals/4472919_4473368_SYBR_Select_MasterMix_QR.pdf (zuletzt eingesehen 16.05.2019)	pp. 20 & 32
[I 12]	IncuCyte incubator, Users Manual https://sydney.edu.au/medicine/bosch/facilities/molecular-biology/live-cell/ZOOM%20Manual%202013A.pdf (zuletzt eingesehen 16.05.2019)	pp. 20 & 34
[I 13]	Paclitaxel, PRODUCT INFORMATION SHEET https://www.sigmaaldrich.com/content/dam/sigma-aldrich/docs/Sigma/Product_Information_Sheet/t7402pis.pdf (zuletzt eingesehen 16.05.2019)	pp. 20 & 38
[I 14]	Neurodiagnostic Instruments Service Manual: https://cdn.shopify.com/s/files/1/1046/1086/files/Viasys-Neurodiagnostic-Instruments-Service-Manual.pdf (zuletzt eingesehen 16.05.2019)	pp. 20 & 35
[I 15]	Anesthesia System, User Guide andOperating Manual http://www.vetequip.com/pdfs/LAAS%20Manual.pdf (zuletzt eingesehen 16.05.2019)	pp. 20 & 36
[I 16]	Genotyping primers, (2.1.3.1) https://tspace.library.utoronto.ca/bitstream/1807/73080/1/Ng_Enoch_201606_PhD_thesis.pdf (zuletzt eingesehen 16.05.2019)	p.21 & p.35
[I 17]	NetPrimer, primer analysis algorithm software http://www.premierbiosoft.com/netprimer/ (zuletzt eingesehen 16.05.2019)	pp. 22 & 23
[I 18]	Conversion software for DNA sequences http://www.bioinformatics.org/sms/rev_comp.html (zuletzt eingesehen 16.05.2019)	pp. 22 & 24
[I 19]	Prism version 6.00-8.00 for Mac, GraphPad Software www.graphpad.com (zuletzt eingesehen 16.05.2019)	pp. 22 & 40
[I 20]	Citation manager, Endnote X7.7.1 https://endnote.com/ (zuletzt eingesehen 16.05.2019)	p. 22

[I 21] iWork, Pages Version 7.3 (5989), Numbers Version 5.3 (5989), Version 8.3 (5989) p. 22
apple.com/mac/pages, https://www.apple.com/numbers/, https://www.apple.com/keynote/
(zuletzt eingesehen 16.05.2019)

[I 22] DNA sequence file analysis tool pp. 22
https://www.nucleobytes.com/ & 31
(zuletzt eingesehen 16.05.2019)

[I 23] DNA Sequencing, Yale School of Medicine, W.M. Keck Foundation p. 31
https://medicine.yale.edu/keck/dna/protocols/template.aspx
(zuletzt eingesehen 16.05.2019)

[I 24] Flurkey, K; Currer, J M.; and Harrison, D E., "Mouse models in aging research." (2007). Faculty p. 67
Research 2000 - 2009. 1685.
https://mouseion.jax.org/stfb2000_2009/1685
https://www.jax.org/research-and-faculty/research-labs/the-harrison-lab/gerontology/life-span-as-a-biomarker
(zuletzt eingesehen 16.05.2019)

[I 25] Schematic chamber of a hemocytometer with Neubauer ruling. pp. 95
https://biocyclopedia.com/index/cell_biology_methods/counting_cells.php & 101
(zuletzt eingesehen 16.05.2019)

[I 26] Theoretical concepts of primers used for reverse transcription pp. 95
https://www.thermofisher.com/de/en/home/life-science/cloning/cloning-learning-center/ &103
invitrogen-school-of-molecular-biology/rt-education/reverse-transcription-setup.html
(zuletzt eingesehen 16.05.2019)

[I 27] mouse tagging utensils pp. 95
https://www.rarc.wisc.edu/animal_health/experimental_techniques/rodent_methods_of_id.html & 106
(zuletzt eingesehen 16.05.2019)

7. Appendix

7.1 Table of Figures

Appendix Figures

7.2 Table of Tables

7.3 Electrophoresis Pictures

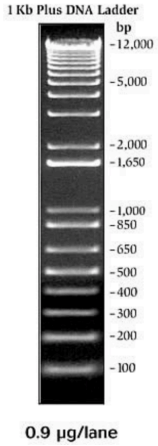

Apx-Fig. 4 **1 kb Plus DNA Ladder** [I 10]

7.3.1 qPCR

Apx-Fig. 6 **Touchdown PCR product gel**
cDNA of SHSY5Y cells was used as template. Lane 1 Ladder; Lane 2 no template control V2F + V2R; Lane 3 no template control V2FPC+ V2R no template control; lanes 4 & 5 V2FPC+V2R; lanes 6 & 7 V2F + V2R. Agarose: 2.67%; Voltage: 100V; running time: 40mins

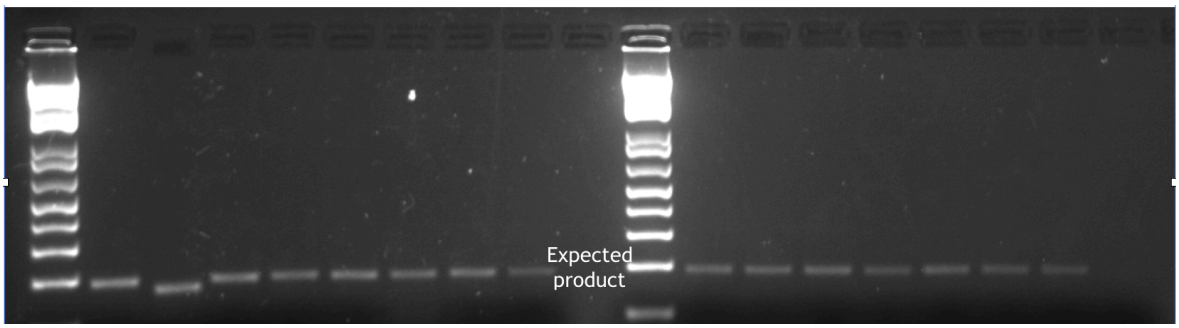

Apx-Fig. 7 **Gradient PCR to determine an ideal annealing temperature**
The experiment was conducted using cDNA of HEK293 cells (left) and SH-SY5Y cells (right). Lanes 1 and 10 show DNA ladders. Lane 9 is not filled. Gradient ranges from 52°C (lane 2 and 11) to 65°C (lane 8 and 17). Note that due to a broken comb lane 3 is not perfectly aligned with the other lanes. For each cDNA library the 3rd reaction setup (lane 4

and 13) is brighter than the rest. So that an ideal annealing temperature of 55°C was assumed. Difference is only marginal as all lane show the expected product.
Agarose: 2.5%; Voltage: 100V; running time: 40mins

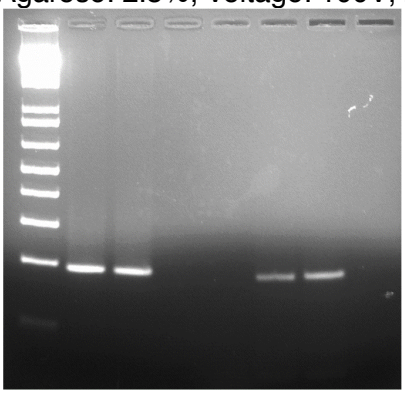

Apx-Fig. 8 **PCR product amplification for primer pairs V1F & V1R and V2F & V2R**
lane 1 ladder; lane 2 and 3 V1F & V1R in cDNA SH-SY5Y; lane 4 no template control V1F & V1R; lane 5 left blank; lane 6 and 7 V2F & V2R in cDNA SH-SY5Y; lane 8 no template control V2F & V2R; band just below 200bp as expected
Agarose: 2.5%; Voltage: 100V; running time: 40 mins

7.3.2 Genotyping

7.3.2.1 NCV

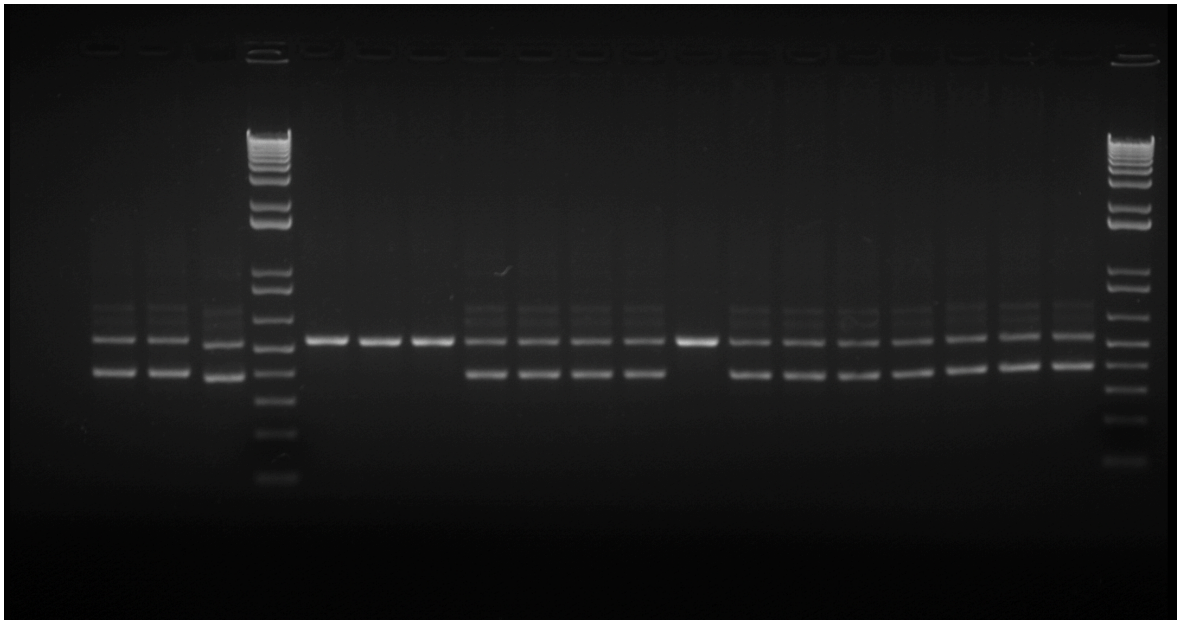

Apx-Fig. 11 Genotyping 1 , Agarose 1%

Lane 1	not related to this work	Lane 11	1432 — Het
Lane 2	not related to this work	Lane 12	1433 — KO
Lane 3	not related to this work	Lane 13	1362 — Het
Lane 4	DNA ladder	Lane 14	1138 — Het
Lane 5	1122 — KO	Lane 15	1449 — Het
Lane 6	1140 — KO	Lane 16	1450 — Het
Lane 7	1141 — KO	Lane 17	1451 — Het
Lane 8	1146 — Het	Lane 18	1452 — Het

Lane 9	1361 — Het
Lane 10	1431 — Het
Lane 19	1408 — Het
Lane 20	DNA ladder

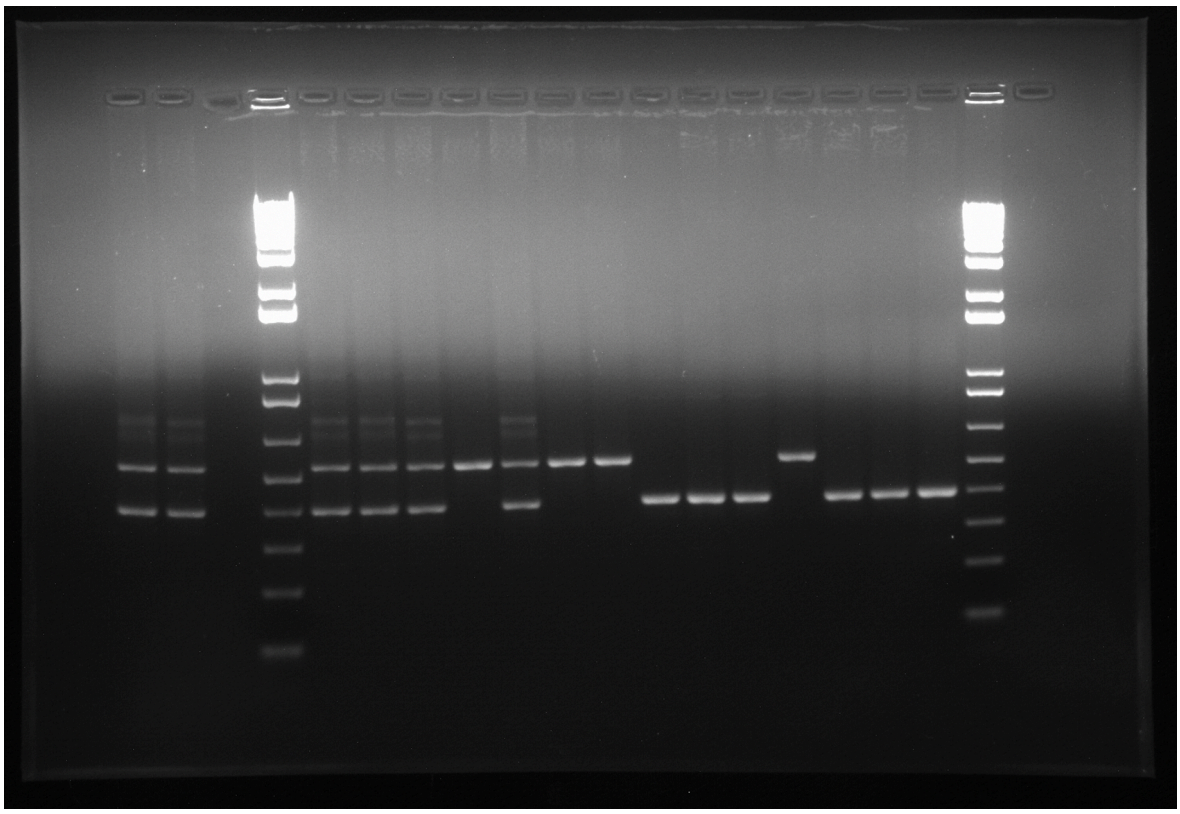

Apx-Fig. 12 Genotyping 2 , Agarose 1%

Lane 1	not related to this work
Lane 2	not related to this work
Lane 3	left blank
Lane 4	DNA ladder
Lane 5	1409 — Het
Lane 6	1410 — Het
Lane 7	1411 — Het
Lane 8	1402 — KO
Lane 9	1417 — Het
Lane 10	1352 — KO
Lane 11	1366 — KO
Lane 12	1316 — WT
Lane 13	1348 — WT
Lane 14	1310 — WT
Lane 15	1325 — KO
Lane 16	1329 — WT
Lane 17	1441 — WT
Lane 18	U — WT
Lane 19	DNA ladder
Lane 20	left blank

7.3.2.2 Genotyping (EM picture mice)

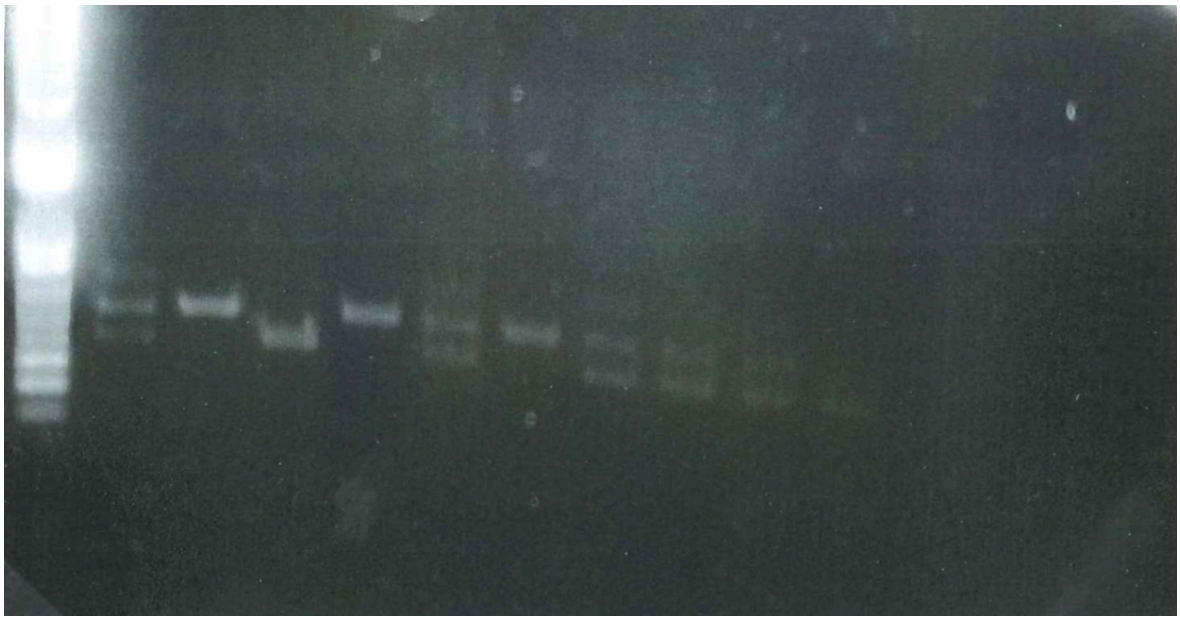

Apx-Fig. 13 Genotyping 3 , Agarose 1%

Lane 1	DNA ladder
Lane 2	not related to this work
Lane 3	not related to this work
Lane 4	1343 — WT
Lane 5	1344 — KO
Lane 6	not related to this work
Lane 7	1345 — KO
Lane 8	not related to this work
Lane 9	not related to this work
Lane 10	not related to this work
Lane 11	1346 — WT
Lane 12	left blank
Lane 13	left blank
Lane 14	left blank
Lane 15	left blank

7.4 Supplementary Figures and Tables

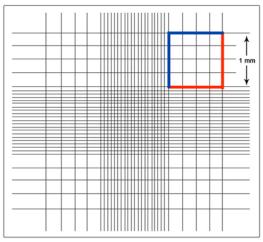

Apx-Fig. 1 **Schematic chamber of a hemocytometer with Neubauer ruling.** [I 25]
All cells within the colored 1x1mm² squares were included in the counting. Cells touching the edge were included into the counting if they were on the red edge and not included if on the blue. 1x1mm² squares of the other corners were counted accordingly and the arithmetic mean was calculated.

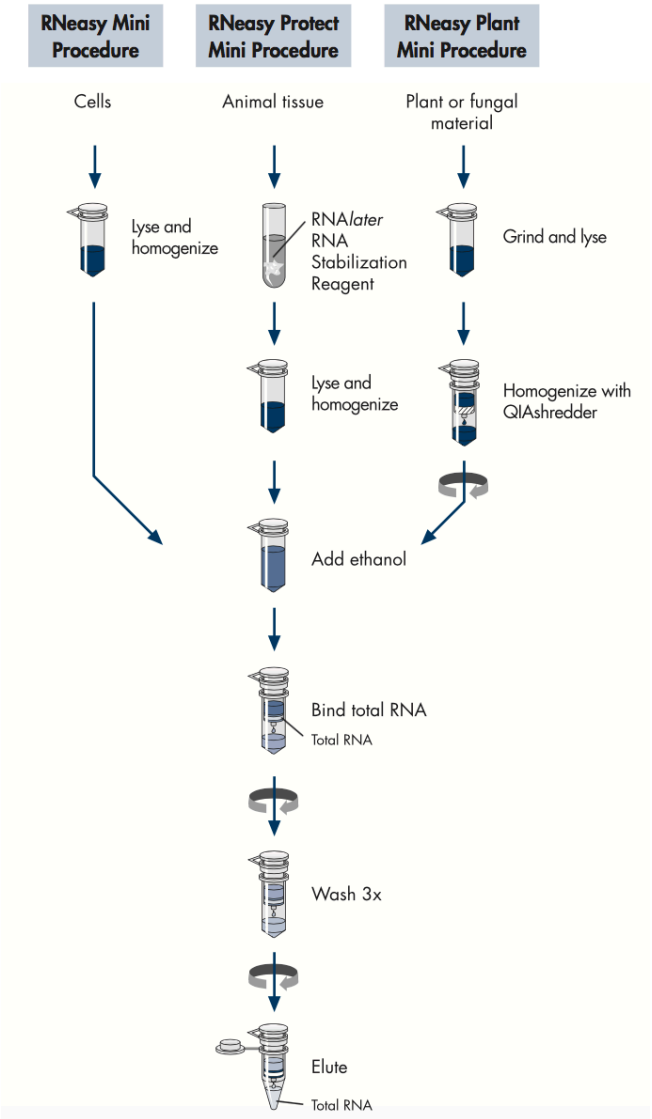

Apx-Fig. 2 Schematic procedure of RNA Extraction using RNeasy Mini Kit [I 6]

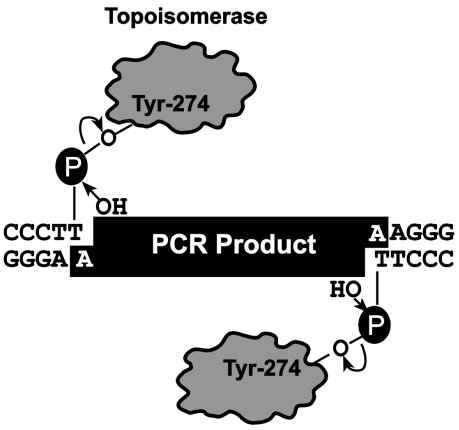

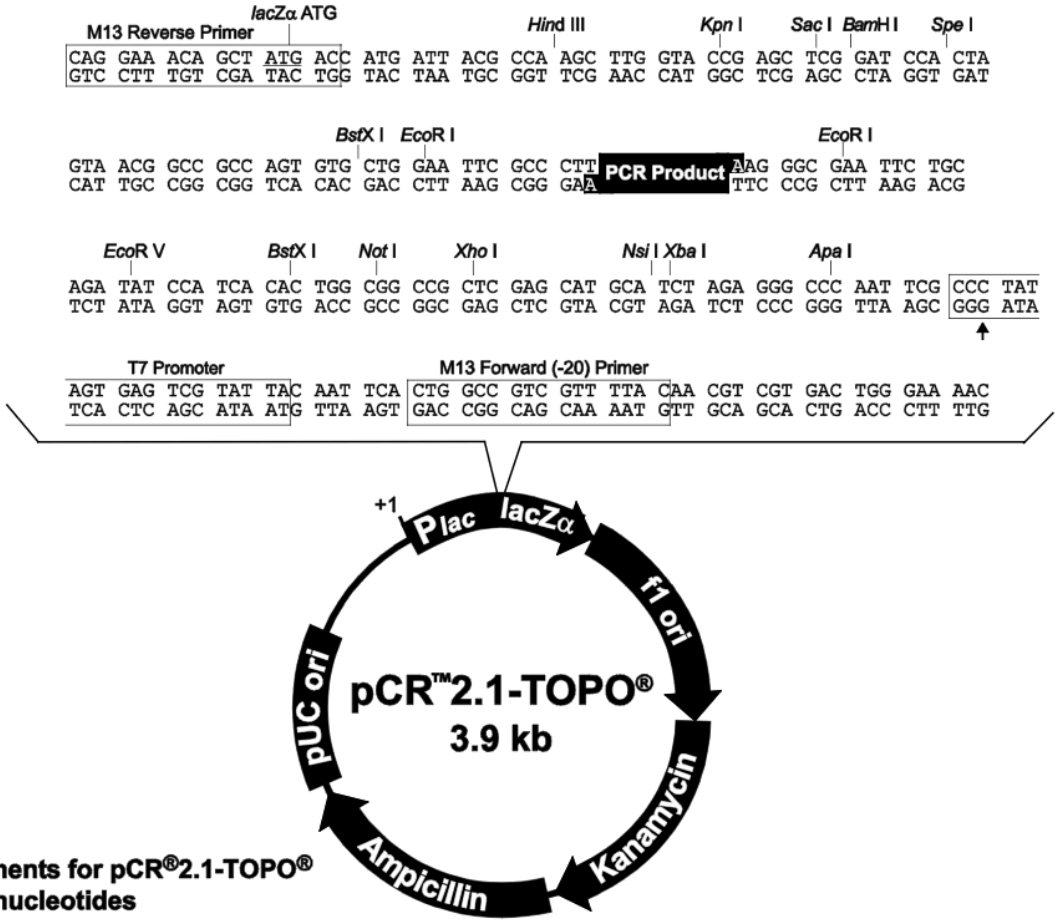

Comments for pCR®2.1-TOPO®
3931 nucleotides

LacZα fragment: bases 1-547
M13 reverse priming site: bases 205-221
Multiple cloning site: bases 234-357
T7 promoter/priming site: bases 364-383
M13 Forward (-20) priming site: bases 391-406
f1 origin: bases 548-985
Kanamycin resistance ORF: bases 1319-2113
Ampicillin resistance ORF: bases 2131-2991
pUC origin: bases 3136-3809

Apx-Fig. 3 **Cloning concept using Topoisomerase I in TOPO TA Cloning Kit and Map of pCR™2.1-TOPO ® [I 8]**

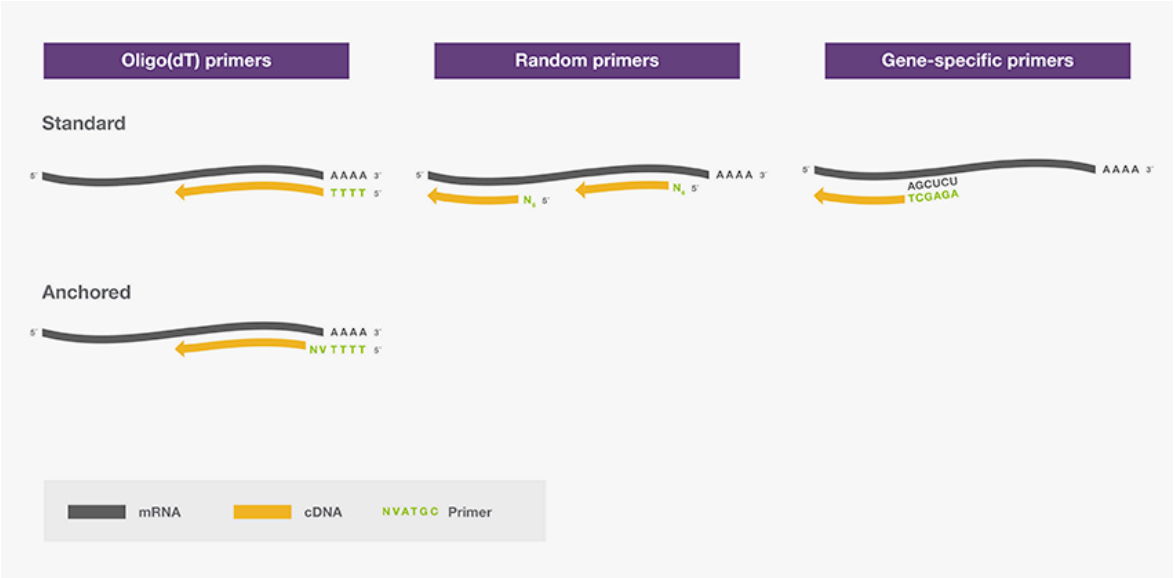

Apx-Fig. 5 **Theoretical concepts of primers used for reverse transcription** [I 26]

Component for single reaction	Volume/20 µL reaction
10× RT Buffer	2.0 µL
25× dNTP Mix (100 mM)	0.8 µL
10× RT Random Primers	2.0 µL
MultiScribe Reverse Transcriptase	1.0 µL
RNase Inhibitor	1.0 µL
Nuclease-free H_2O	3.2 µL
Total per Reaction	10.0 µL

Apx-Tab. 1 **Master mix setup for single reverse transcription reaction**

RT Step	Temperature	Time
Step 1	25 °C	10 min
Step 2	37 °C	120 min
Step 3	85 °C	5 min
Step 4	4 °C	Hold

Apx-Tab. 2 **Thermal cycler setting for reverse transcription reaction**

TD-PCR reaction (final concentration/sample)	25 µl Reaction
Autoclaved distilled water	18.15 µL
10X PCR buffer (1x)	2.50 µL
50 mM $MgCl_2$ (1.5mM)	0.75 µL
10 mM dNTP mix (0.2mM)	0.50 µL

Taq DNA Polymerase (1.0 U)	0.10 µL
10 uM Forward primer (0.5 μM)	1.25 µL
10 uM Reverse primer (0.5 μM)	1.25 µL
Template DNA (<1μg)	0.50 µL

Apx-Tab. 3 **Reaction setup for touchdown PCR**

PCR Cycle			Temperature	Time min:sec
Step 1:	Initial denaturation		94 °C	3:00
Step 2:	Denaturation		94 °C	0:45
Step 3:	Annealing	Touch down 13 cycles 1°C/ cycle	60-48 °C	0:30
		22 Cycles	48°C	0:30
Step 4:	Elongation		72 °C	0:15
Step 5:	Final Elongation		72 °C	10:00
Step 6:	Cooling		4 °C	Hold

Apx-Tab. 4 **Thermal cycler settings for touchdown PCR**

PCR Cycle			Temperature	Time min:sec
Step 1:	Initial denaturation		94 °C	3:00
Step 2:	Denaturation		94 °C	0:45
Step 3:	Annealing	Gradient	52-65 °C	0:30
Step 4:	Elongation		72 °C	0:15
Go to Step 2 and repeat 35 X				
Step 5:	Final Elongation		72 °C	10:00
Step 6:	Cooling		4 °C	Hold

Apx-Tab. 5 **Gradient PCR cycling conditions**

qPCR reaction (final concentration/sample)	20 μL Reaction
2x SYBR Select Master Mix	10.0 µL
Forward primer (100nM)	0.2 µL
Reverse primer (100nM)	0.2 µL
Sample/Control in H_2O	9.6 µL

Apx-Tab. 6 **Reaction setup for qPCR**

qPCR Cycle		Temperature	Time min:sec
Step 0:	Initiation	50 °C	2:00
Step 1:	Initial denaturation	95 °C	15:00
Step 2:	Denaturation	94 °C	0:30
Step 3:	Annealing	59 °C	0:40
Step 4:	Elongation	72 °C	0:40
Go to Step 2 and repeat 40 X			
Step 5:	Cooling	4 °C	Hold

Apx-Tab. 7 **qPCR thermocycling conditions**

Var1 1	Var1 2	Var1 3	Var1 4
Var1 5	Var1 6	Var2 1	Var2 6
SH-SY5Y high	MB 231 high	HEK 293 high	H_2O
SH-SY5Y low	MB 231 low	HEK 293 low	SH-high nPP / MB high nPP / HEK high nPP
Var2 1	Var2 2	Var2 3	Var2 4
Var2 5	Var2 6	Var1 1	Var1 6
SH-SY5Y high	MB 231 high	HEK 293 high	H_2O
SH-SY5Y low	MB 231 low	HEK 293 low	SH-low nPP / MB low nPP / HEK low nPP

Apx-Fig. 9 **qPCR 96-well plate layout**
Each sample was tested in triplicates. The background colors indicate the primer pair that was used in the well: blue - V1F & V1R; green - V2F & V2R; white - no primer pair (nPP) control. The letters within a group of three squares indicate the well content aside from the primer pair: Either a sample of a human cell line cDNA library with high (5000ng/well) or low (200ng/well) DNA concentration; H_2O - a water and primer only control; Var1- Plasmid containing NCS1 Variant 1; Var2- Plasmid containing NCS1 Variant 2. The number within a Var1/Var2 triplicate indicates dilution factor (1:5), e.g. “Var1 1“ means 1,600 copies/well of Variant 1 or “Var2 6“ means 5000000 copies/well of Variant 2.

Apx-Fig. 10 **Mouse tagging utensils** [I 27]

PCR Reaction (per sample)	**Volume**
Red Extract	10.0 µL
MS66 Primers (10 µM)	0.8 µL
MS67 Primers (10 µM)	0.4 µL
JH32 Primers (10 µM)	0.4 µL
H2O	6.4 µL
Genotyping master mix	**18.0 µL**
DNA extracted from ear	+ 2.0 µL
Total reaction volume:	**20.0 µL**

Apx-Tab. 8 **Genotyping PCR reaction sample setup for single reaction**

PCR Cycle		Temperature	Time min:sec
Step 1:	Initial denaturation	94 °C	3:00
Step 2:	Denaturation	94 °C	0:30
Step 3:	Annealing	59 °C	0:40
Step 4:	Elongation	72 °C	0:40
Go to Step 2 and repeat 35 X			
Step 5:	Final Elongation	72 °C	5:00
Step 6:	Cooling	4 °C	Hold

Apx-Tab. 9 **Thermal cycler settings for genotyping amplification reaction**

	1343	**1344**	**1345**	**1346**	**Σ**
DRG	82	51	329	394	856
Sciatic nerve	66	115	229	363	773
Tibial nerve	141	90	192	319	742
Σ	289	256	750	1076	2371

Apx-Tab. 10 **Analyzed nerve fibers/axons per mouse and area**

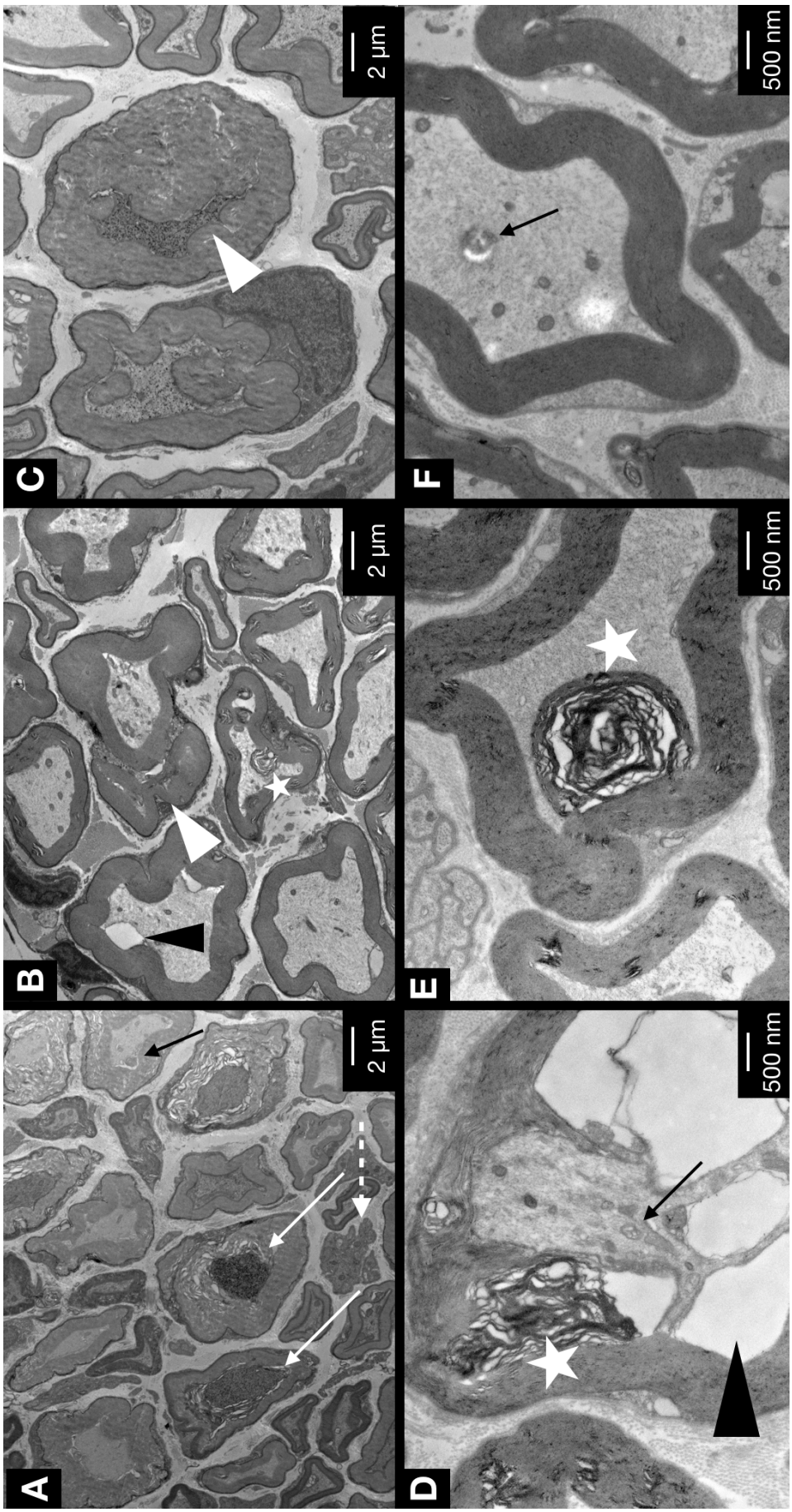

Fig. 26 **Morphologies of PTX induced neuronal degeneration (sciatic nerve) (enlarged),** see p.57

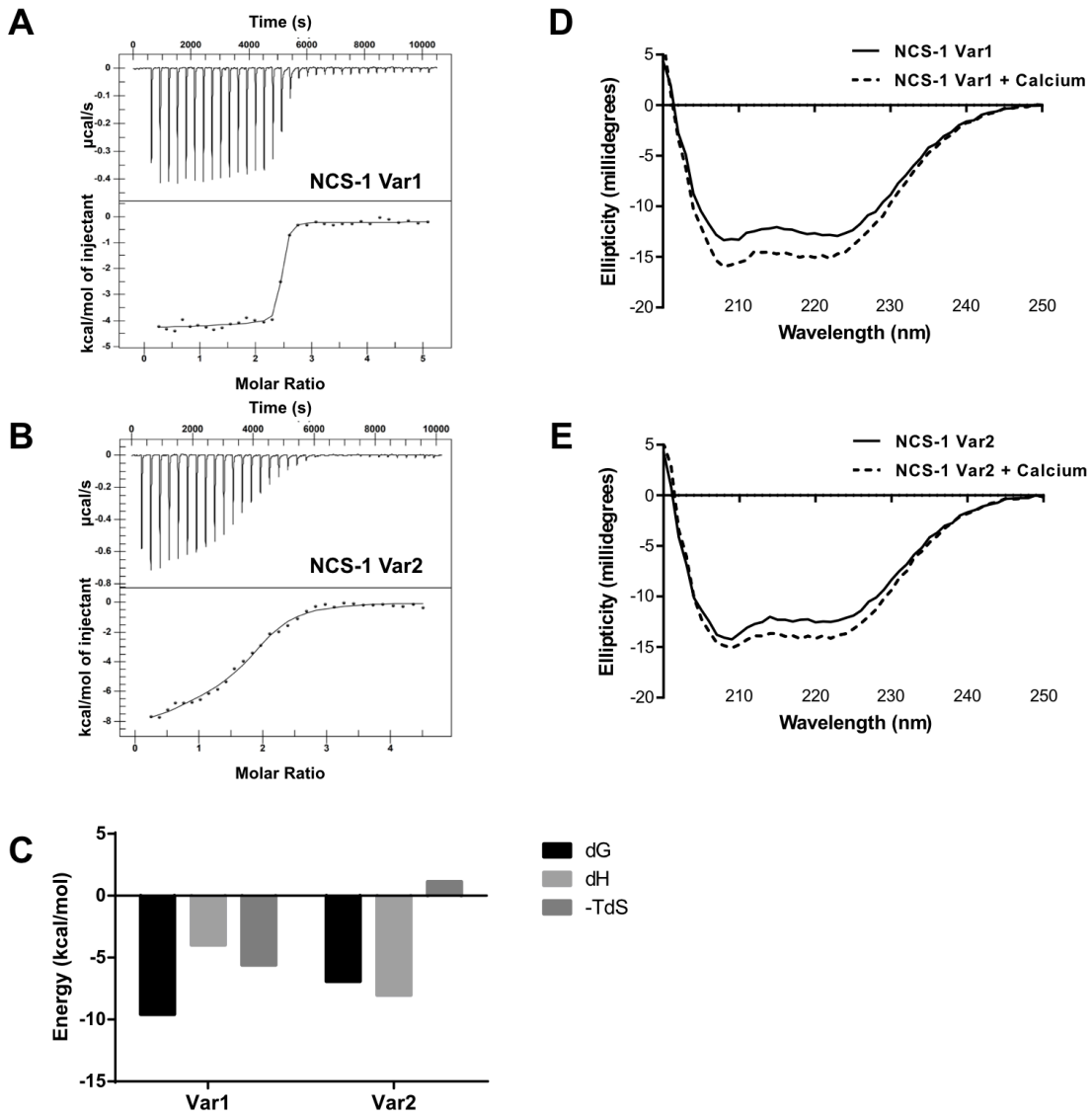

Apx-Fig. 14 **Ca^{2+} binding to NCS-1 variants assessed by ITC and CD** (adapted from [182]) **A-B)** The top plots of the panels depict the raw heat measurements of titrating 1.5 µL of 1.5mM Ca^{2+} into 100µM NCS-1 Var1 and NCS-1 Var2, respectively, a result of isothermal titration calorimetry (ITC). The corresponding bottom plots show the fitted binding isotherms of the same experiment. **C)** The graph shows the observed free energy change associated with Ca^{2+} binding to each NCS-1 variant as well as their entropic and enthalpic contributions. **D-E**) The effects of Ca^{2+} binding on the conformational states of NCS-1 Var1 and NCS-1 Var2 are shown by the far UV circular dichroism spectra in panels D and E. The final protein concentration in each measurement was 2µM, and the final Ca^{2+} concentration in the ligand binding experiments was 600µM. (adapted from [182])

NCS-1	Dissociation constant, Kd (nM)	Number of Binding Sites, n	Enthalpy, ΔH (kcal/mol)	Entropy Term, -TΔS (kcal/mol)	Gibbs Free Energy, ΔG (kcal/mol)
Var1	96 ± 48	2,4 ± 0,02	-4,0 ± 0.1	-5,6	-9,6
Var2	8600 ± 3200	1,8 ± 0,05	-8,0 ± 0.6	1,1	-6,9

Apx-Tab. 11 **ITC Thermodynamic Parameters of Calcium Binding to NCS-1 Variants.** (adapted from [182])

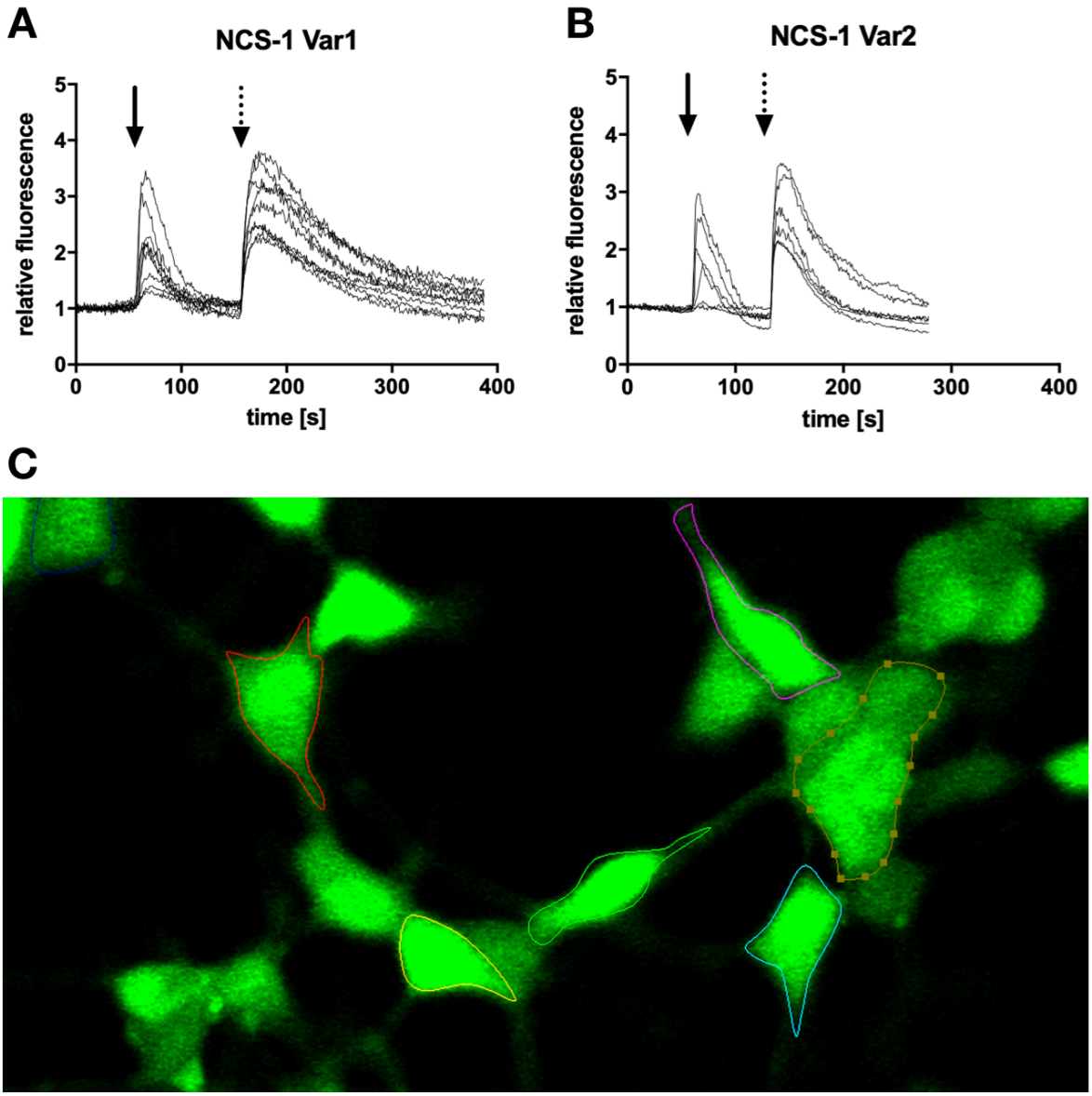

Apx-Fig. 15 **Live cell Ca^{2+}-imaging on SH-SY5Y cells overexpressing NCS-1 Var1 or Var2**

A & B) Presented is the relative fluorescence over time in SH-SY5Y cells transfected with NCS-1 Var1 plasmid (A) or NCS-1 Var2 plasmid (B). Each recorded value divided by the mean of the first 30 seconds of the corresponding area. Full arrow indicates stimulation with ATP (5μM). ATP activates $InsP_3$-dependent Ca^{2+} release from the ER. Dotted arrow indicates addition of ionomycin an ionophore that was used as positive control. As done by previous studies, whole-cell fluorescence was measured by defining each cell as one region of interest (colored lines around the cells) [24]. **C)** Representative photo of ATP stimulated SH-SY5Y cells with calcium indicator Fluo-4, AM, excitation wavelength 488nm.

Despite variation of several parameter (transfection reagents; indicator application time; coverslip coating; cell line etc.) no consistent response was gather to produce reliable results. The represented plots (A&B) show “ideal“ experiments that were not reliably reproduced. In these selected experiments no significant difference between the two variants was observed.

8. Statement of Authorship and Acknowledgements

8.1 Statement of Authorship

I hereby declare that I am the sole author of this thesis and that I have not used any sources other than those listed in the bibliography and identified as references. I further declare that I have not submitted this thesis at any other institution in order to obtain a degree.

_____ _____

(place, date) (signature)

8.2 Acknowledgments

Firstly, I am grateful to my *doctor parents* Prof. Barbara Ehrlich & Prof. Cor de Wit. Thank you, Barbara, for offering me this great chance of a research position in your laboratory and for helping with these first steps in science. Thank you for the project and your relentless optimism. I have learned so much during my year at Yale University. Thank you for providing context and larger scale perspectives when failed experiments frustrated me and thank you for joining in my cheers when I successfully troubleshooted them. Thank you for constantly reminding me of a balanced *work hard—play hard* attitude and for teaching me lessons beyond the bench! You have influenced and coined the lives of so many students and I can proudly count myself to be one of them. You cannot imagine in how many ways you have changed my world.

As for Prof. de Wit, not only were you the first person to teach me about calcium and the beauty of channels, transporters and *what holds the world together in the innermost*, you were also open to the idea of supporting me with a project on the other side of the Atlantic Ocean. Thank you, for all the critical input, the spontaneous discussions, the feedback and the motivation.

Special thanks go to the Studienstiftung des deutschen Volkes for ideological and financial support throughout my studies at the Universität zu Lübeck and especially during my time at Yale University. I would like to thank Prof. Thomas Peters and Prof. Stefan Anemüller for supporting my application and my preparation before my research year in the U.S.

I am also inexpressibly grateful to the medical department of the *Universität zu Lübeck* that has been my alma mater since 2011 and prepared me for the upcoming challenges of being a doctor.

Concerning this work and the amazing time in the United States, I would like to thank all my co-worker, fellow-lab mates and friends. Lien Nguyen, Caitlin Wright, Sophie Duong, Fernanda Lemos, Ivana Kuo, Yifei Yang, Edward Kaftan, Florian Gatzke, Ahmed Lawan, Lauren Moore, Michael Sierant, Daniel Ehrlich, and Daniel Schütte you guys are incredible.

Three people deserve a special mention: Larry Huynh, Baisheng (Victor) Wang, and Lily Nguyen, all of you helped me learn such a broad variety of techniques in such a short period of time with enormous patience. Aside from huge scientific and medical success I wish for you to keep up this amazing teaching attitude.

Larry, thank you, for letting me live with you in Walter Boron's old house! You are truly a great friend; I will never forget our talks!
Cristina Cruz-Uribe and Sushant Sachdeva, you guys have been great roommates during my time in the U.S. and it was important to have you for so many interesting conversations and perspectives outside the box of biomedical research, thank you.
Stefanie, Eva and Jan, I am grateful for your constant support throughout the experimental and post-experimental phase of this work. You always had cheerful words for me and supported me like a second family.
My dearest Marie, I can only insufficiently express how grateful I am to have your support. Despite the time and geographic distance I felt your presence throughout the time of this work. You made an invaluable gift of listening, comforting and encouraging me in a way that is beyond comparison. I always know you have my back and I am so very lucky to have you in my life.
To my siblings, Lina Boeckel and Sebastian Boeckel, thank you for your support. Sebastian, I am grateful for your patience and willingness to argue with me about statistics and to help me understand the beauty behind the tests and analyses.
Last but not least, I am forever grateful to my parents who not only supported me throughout the time of this thesis, but enabled an education without which I would not be where I am today. I cannot imagine what an immense sacrifice it must have been for you to let your son leave for boarding school at such a young age, yet, undoubtedly the training, the work ethic, the education and people I met throughout my journey are the roots and the foundation of all my later achievements. Thank you for believing in me, even in times of doubt. Without your sacrifices and support I would not be here today.

Editorial input

Writing a thesis in a nonnative language is not easy. Therefore, I thank Barbara Ehrlich, Lily Nguyen & Larry Huynh for editorial input and comments concerning grammar and nuances of the English language.

9. Curriculum Vitae

10. Publications related to this Work

Publications

Neuronal Calcium Sensor 1 Has Two Variants with Distinct Calcium Binding Characteristics.

Wang B, **Boeckel GR**, Huynh L, Nguyen L, Cao W, De La Cruz EM, Kaftan EJ, Ehrlich BE.PLoS One. 2016 Aug 30;11(8):e0161414.

NCS-1 is a regulator of calcium signaling in health and disease.

Boeckel GR, Ehrlich BE. Biochim Biophys Acta. 2018 May 8. pii: S0167-4889(18)30089-2. doi: 10.1016/j.bbamcr.2018.05.005. Review.